MODELING THE TRANSPORT AND FATE OF OIL-PARTICLE AGGREGATES AFTER AN OIL SPILL IN INLAND WATERWAYS

BY

ZHENDUO ZHU

DISSERTATION

Submitted in partial fulfillment of the requirements
for the degree of Doctor of Philosophy in Civil Engineering
in the Graduate College of the
University of Illinois at Urbana-Champaign, 2015

Urbana, Illinois

Doctoral Committee:

Professor Marcelo H. García
Professor Gary Parker
Professor Bruce L. Rhoads
Dr. David Soong
Professor Albert J. Valocchi

ABSTRACT

This dissertation was motivated by a study of the July 2010 Kalamazoo River oil spill. The spill occurred due to a pipeline rupture, releasing approximately 1.1 million US gallons of diluted bitumen into Talmadge Creek, which is a tributary of the Kalamazoo River, located in the state of Michigan, United States. It was even more unfortunate that a 50-year flood event occurred in the Kalamazoo River at the same time, which significantly transported and spread the released heavy crude oil. It is considered the largest inland oil spill and one of the costliest (1.2 billion US dollars as of 2014 for cleanup) spills in U.S. history.

After tremendous cleanup efforts of floating oil and oil contaminated soil on river banks and floodplain areas within one year following the spill, substantial residual deposits from the oil spill were found remaining in the waterway system, mostly due to the formation of oil-particle aggregates (OPAs). OPAs are a mixture of oil droplets and solid particles (e.g. suspended sediment) under turbulent flow conditions. Their density can be heavier than water and they sink onto river bed, especially in the areas where flow velocity is low. The recovery of OPAs lasted for more than three years after the spill. There are many unknowns about OPAs, such as how oil droplets and particles interact, where they deposit, when they can be entrained into water and transported, what are their impacts on aquatic life. Thus the understanding of the fate and transport of OPAs is very important for recovery efforts and future management. It is believed that this study is not only useful for the Kalamazoo River oil spill, but also a good reference for other potential oil spills in freshwater environments. Subjected to increasing demand of crude oil transport, the ageing pipelines all over the country are running the risks of rupture at a higher possibility, especially for those located around inland waterways where there's a closer interaction between water environment and people. Therefore, oil spills in inland waterways should attract more atten-

tion and researches. Moreover, the lessons, tools, and knowledge we learned from oil spills in freshwater environment could be helpful for studying the oil residue in marine environments. Also, the tools developed in this study have the potential to be applied to contaminated sediment in general, including those polluted by other contaminates such as hazardous industrial chemicals.

Numerical models were developed for this study, with the help of laboratory experiments and field surveys for model calibration and validation. A particle tracking algorithm for OPAs was developed and coupled with a 3D hydrodynamic for Morrow Lake, where the effects of wind and dam operation cannot be neglected. The three-dimensional Eulerian/Lagrangian model was used to locate where OPAs would deposit in Morrow Lake and when OPAs could be resuspended under different scenarios. Selected sediment traps in the Kalamazoo River were studied with 2D shallow water models to understand where and when OPAs deposit. A new parallelized 2D hydrodynamic, sediment transport, and bed morphology model was also developed. The new model was parallelized with the domain decomposition method using MPI. A $k - \varepsilon$ turbulence model was also implemented into the model. Any OPAs flowing downstream of Morrow Lake have the potential to reach Lake Michigan.

To my family, for their consistent understanding and support.

ACKNOWLEDGMENTS

I would like to thank my supervisor, Prof. Marcelo H. Garcia, for bringing me into such a wonderful place and guiding me through the fantastic journey of doctoral graduate life. Supervised by Prof. Garcia, I have got opportunities to learn different interesting topics and cooperate with outstanding experts and colleagues.

I gratefully acknowledge my Ph.D. committee members, Prof. Gary Parker, Prof. Bruce L. Rhoads, Dr. David Soong, and Prof. Albert J. Valocchi, for their time and support with my dissertation. Many thanks to David Waterman of University of Illinois, Dr. Faith Fitzpatrick of the USGS Wisconsin Water Science Center and Rex Johnson of Global Remediation Technologies, Inc. for their help in the Kalamazoo River project. Jessica Zinger of University of Illinois is acknowledged for providing laboratory experiment measurements to validate the new model, HydroSedFoam. All their comments about this dissertation are acknowledged.

I greatly value the friendship with my outstanding colleagues and friends at the Ven Te Chow Hydrosystems Laboratory, especially my officemates. They have made this journey much easier and more enjoyable for me with my work and personal life. I would like to thank my roommates and basketball teammates who have made my daily life always happy. I have benefited so much from being together with them.

I would also like to take this chance to thank my guides in college who led me to the Ph.D. life, Dr. Jiahua Wei, Prof. Zhaoyin Wang, Prof. Chunbo Jiang, and Prof. Keqin Zhu.

I cannot imagine where I am without the continuous and unchanged understanding and support from my family. Although my parents have no idea about my research, they have always been there for me to support. I dedicate my dissertation to the memory of my grandfather who was and has been always being my hero. The last acknowledgement is to my wife. I would like

to thank her for the encouragement, caring and being the first reader of my dissertation with our two-month old baby. Wish happiness to all of us.

TABLE OF CONTENTS

CHAPTER 1

INTRODUCTION

The petroleum industry is absolutely critical for global production and people's living. However, many oil spills have been occurring due to human activities of oil exploitation and transport. Although oil spills in the marine environment are more publicized and studied, such as the 2010 Deepwater Horizon spill, there are actually more serious oil spills in inland waterways, which result in severer impact on both human health and ecological environment.

The 2010 Kalamazoo River oil spill in the state of Michigan is the largest inland oil spill in U.S. history, where approximately 1.1 million US gallons of heavy crude oil due to a pipeline rupture were released. The cleanup work took about 1.2 billion dollars as of 2014. Although most of the spilled oil was collected, the spill is believed to have long-term impacts on the environment. One main reason is the formation and transport of oil-particle aggregates (OPAs), which are the mixture of oil droplets and sediment particles. Figure 1.1 shows a simplified diagram of the processes associated with OPA formation. First, oil droplets are formed at the interface between surface floating oil and water body. Those droplets can be entrained into water body due to turbulence and mixing energy, where they can interact with particles such as suspended sediment particles. Due to the negative buoyancy of OPAs, they deposit on the river bed and can be resuspended and transported under different hydrodynamics scenarios. To understand the fate and transport of OPAs is very important for the cleanup work and future management during accidents.

To the author's knowledge, studies about oil spills in inland waterways are still very limited, especially for the fate and transport of OPAs. This provided the motivation for this dissertation. Numerical models were developed in this study. Two-dimensional (2D) shallow water models were developed for selected sediment traps in the Kalamazoo River to study where and when

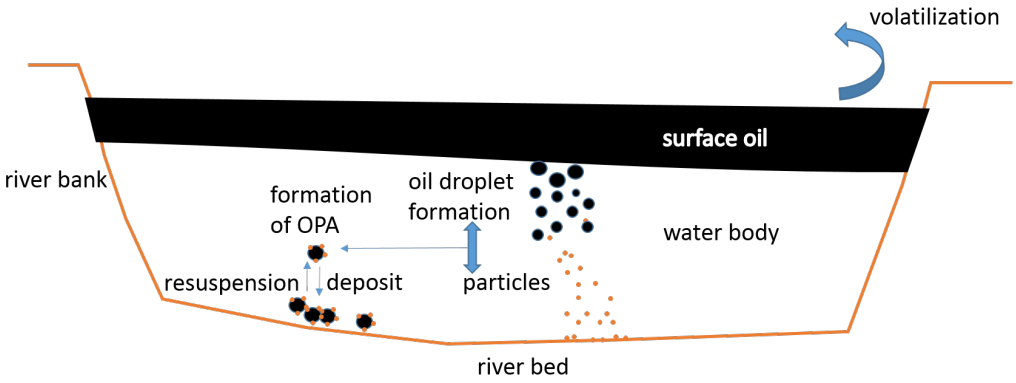

Figure 1.1: Simplified diagram of the OPAs formation processes in a freshwater environment

OPAs deposit. A three-dimensional hydrodynamics model was implemented for Morrow Lake, which is the final barrier position before OPAs can migrate into Lake Michigan. A Lagrangian particle tracking model was developed and coupled with the hydrodynamics model in order to simulate the transport, deposition, and resuspension of OPAs in the lake. Sediment traps, such as bifurcation channels and cutoff channels, in the river system affect the transport of OPAs tremendously, which is one of the unique characteristic of oil spill in rivers. Fine mesh grids and high-performance computation are needed for modeling these effects in a 65 km long river-lake system. A new parallelized 2D shallow water solver with both turbulence model and sediment transport models were developed using OpenFOAM, which can take advantage of computer clusters and workstations to speed up simulations.

1.1 Background

Many human activities can result in oil spilled into the inland waterways and marine environment, including oil well blowouts, oil tankers accidents, and oil pipeline ruptures. Although Etkin (2001) concludes that the numbers of oil spills, as well as the amount spilled, have decreased significantly from 1985 to 1999, disasters caused by oil spills have never stopped occurring. The 2010 Deepwater Horizon (DWH) oil spill released approximately 5 million barrels of crude oil into the Gulf of Mexico ([1]), which is the largest marine oil spill in U.S. history. Again in 2010, the Enbridge Line 6B Kalamazoo River oil

spill due to a pipeline rupture resulted in the largest release of heavy crude oil into an inland waterways in U.S. history (see Figure 1.2).

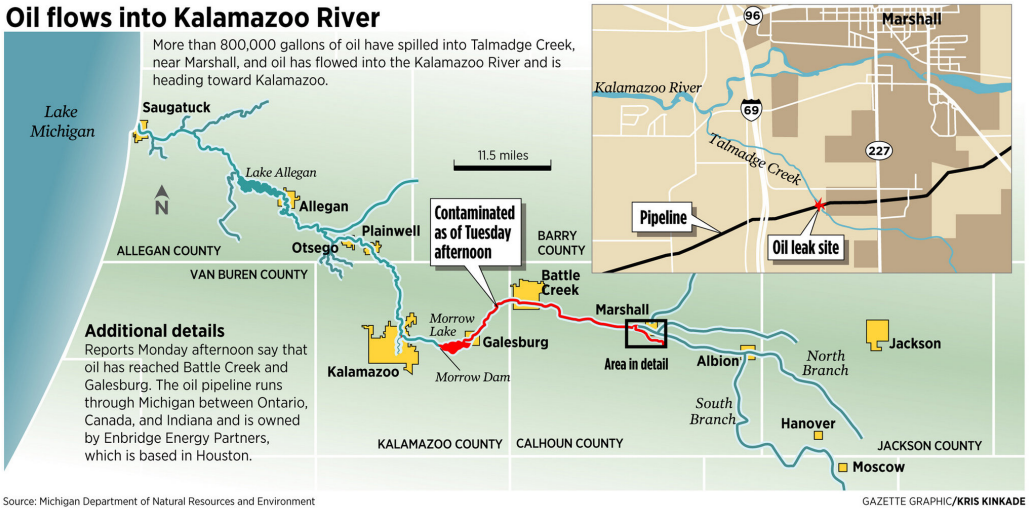

Figure 1.2: Map of the 2010 Kalamazoo Oil Spill (source: Michigan Department of Natural Resources and Environment)

Regardless of the high cost of cleanup work ([2]), oil spills cause tremendous environmental and human health problems in both short and long terms ([3]). Although coastal oil spills seem better known by the public, e.g. 2010 DWH spill and 1989 Exxon Valdez spill, larger spills actually are more likely to occur in inland environment and those spills can cause more severe public health problems since the inland environment is usually more interactive with human beings ([4]). However, unlike the coastal spills where extensive researches have been performed on, the transport and fate of oil spills in inland waterways has not been studied much ([5, 6, 7]).

Following the oil spill at Kalamazoo River waterways system in 2010, extensive oil cleanup and environmental remediation efforts have taken place. However, substantial residual deposits from the oil spill remain in the river system due to the formation of oil-particle aggregates (OPAs) and their negative buoyancy. One of the biggest concerns is to understand the conditions under which the OPAs become resuspended, transported and re-deposited. Once OPAs pass through Morrow Lake, they will continue to migrate toward Lake Michigan. Many complex physical, chemical, and biological changes take place after oil is spilled into the water, including spreading, drifting, dispersion, stranding, and weathering ([8]). Oil droplets may be formed and

entrained into the water body where they can interact with suspended particles and form OPAs. Once OPAs are formed, its density can be larger than the density of water so it may deposit and become practically impossible to clean completely. The formation of OPAs can greatly affect the fate of oil in the environment. Thus, the study of the fate and transport of OPAs may help the long-term cleanup work as well as the monitoring and management in the future.

Although the formation of OPAs and their deposition were reported many years ago by Poirier and Thiel ([9]), most of the oil spill models developed to date do not consider it because the interaction of oil droplets and suspended particles is very complicated ([8, 10]). Niu et al. ([11]) specifically modeled the transport and fate of oil-mineral aggregates (OMA) for short time periods after an initial spill in a marine environment using a Lagrangian particle-tracking technique. Bandara et al. ([12]) simulated the oil-sediment interaction and transport in near-shore waters and found that up to 65% of released oil may be removed from the water body and deposit as oil-sediment aggregates. Pando et al. ([13]) studied the transport of organo-mineral aggregates within the Nazare submarine canyon using also a Lagrangian transport model.

The unique character of the riverine hydrodynamics and the residual oil-sediment deposits in the Kalamazoo River system has to be treated differently from the ones in marine systems ([14]). One main difference between inland and marine oil spills is the application of oil dispersants. Dispersants, which are mixtures of solvents, additives, and surfactants, are used widely in the marine oil spills in order to break oil slicks into oil droplets and accelerate their dispersal and biological degradation in the water body. The properties of the OPA particles, such as specific gravity and diameter, will have a major effect on the particle settling velocity. A recent study by Khelifa et al. ([15]) evaluated settling velocities of OPAs and effects of dispersants. However, oil dispersants are not suitable for inland oil spills because of the limited natural purification capacity of inland waterways systems and their closer interaction with people's living. Moreover, the types of oil and properties of suspended sediment are also critical impact factors of the OPA formation, so they also greatly affect the settling velocity and the critical shear stress for resuspension. Therefore, the properties of OPAs in the Kalamazoo River must be evaluated and implemented into the computational models.

Another main difference between coastal/marine environment and inland waterways is the existence of various sediment traps in rivers, such as cut-off channels, meandering, and bifurcation channels. Floodplains can also be important sediment traps. The sediment traps significantly affect the hydrodynamics and sediment transport in rivers. However, to the authors knowledge, the impact of both artificial and natural sediment traps on the fate of OPAs has not been studied.

It is worth mentioning that due to increasing demand of crude oil transport, aging pipeline infrastructure all over the world will probably run into more risks of rupture. This study is not only useful for the Kalamazoo River oil spill, but should also be helpful when other inland oil spills occur in the future.

1.2 Thesis Outline

This thesis is organized as follows:

Chapter 2 describes the modeling of the fate of OPAs in Morrow Lake, where a 3D model is necessary especially when the effects of wind and dam operation can not be neglected. An OPAs particle tracking model is developed and coupled with a 3D hydrodynamic model. The objective of this study is to locate where OPAs deposit in Morrow Lake and when OPAs can be resuspended under different scenarios. Two applications of the model are also shown in the end of this chapter.

Chapter 3 describes 2D shallow water models developed for studying selected sediment traps in the Kalamazoo River. The objective is to understand where and when OPAs deposit. The models provide useful information for managers. Also, the issue of computation time for a big waterway system arises and indicates the need of a new parallelized river model.

Chapter 4 describes the development of a new parallelized 2D hydrodynamic, sediment transport, and bed morphology model. The new model is parallelized with the domain decomposition method using MPI. A $k-\varepsilon$ turbulence model is also implemented into the model. The hydrodynamic model is validated by comparing with a laboratory experiment of sine-shape meandering flume. Also, a case study of movable bed is performed to validate the bed morphology model by comparing with analytical solution. In the end,

the parallel performance is evaluated.

Chapter 5 presents a summary of the main findings and conclusions. Also, potential future work is discussed.

CHAPTER 2

MODELING THE TRANSPORT AND FATE OF OIL-PARTICLE AGGREGATES IN MORROW LAKE

Transport of oil through pipelines is at all-time high and so is the risk of oil spill accidents. The July 2010 spill of diluted bitumen into the Kalamazoo River was the largest release of heavy crude into an inland waterway in U.S. history. After extensive cleanup and recovery efforts, substantial residual deposits from the oil spill remained in the river system, mainly due to formation of oil-particle aggregates (OPAs). It is important to understand the conditions under which OPAs can be suspended, transported and deposited. Concerns about OPAs reaching Lake Michigan motivated this work. A three-dimensional Eulerian/Lagrangian model for OPA transport was developed for Morrow Lake in the Kalamazoo River. The three-dimensional model enabled consideration of the Morrow Lake dam operational rules as well as wind effects, which might increase the risk of resuspension and transport of OPA downstream. Compared to field surveys for locating heavily oil-contaminated areas, the numerical model could save considerable time and efforts.

2.1 Introduction

The petroleum industry is absolutely critical for global production and people's living. However, oil spills have been occurring due to human activities of oil exploitation and transport. Many of the human activities can result in oil spilled into the inland waterways and marine environment, including oil well blowout, oil tankers accidents, and oil pipeline rupture. Although reports have shown that the frequency of oil spills, as well as the annual amount spilled, have decreased significantly since late 1900s [16], disasters caused by oil spills have never stopped occurring. The well-known 2010 Deepwater Horizon (DWH) spill released approximately 5 million barrels of crude oil into the Gulf of Mexico [1], which is the largest marine oil spill

in U.S. history; while the 2010 Enbridge Line 6B Kalamazoo River oil spill due to pipeline rupture resulted in the largest release of heavy crude oil into an inland waterway in U.S. history [17]. Although oil spills in the marine environment are more publicized and studied, e.g. the DWH spill and the 1989 Exxon Valdez spill, there are actually more serious oil spills in inland areas than those in the marine environment [4]. Besides the extremely high cost of cleanup work [2], oil spills can cause tremendous environmental and human health problems in both the short and long term [3].

Following the oil spill at Kalamazoo River waterways system in 2010, extensive oil cleanup and environmental remediation efforts have taken place. Although the floating oil was collected in the first few months, it took a long time for the remaining submerged oil to be recovered [17]. One main reason is the formation and transport of oil-particle aggregates (OPAs), which are a mixture of oil droplets and particles such as suspended sediment and organic matter. Due to the negative buoyancy of OPAs, they deposit on a river bed and can be transported under different hydrodynamics scenarios. Considering the recurrences of oil sheen and other ecological problems due to submerged diluted bitumen oil [18], one of the biggest concerns was to understand the conditions under which the remaining submerged OPAs could become re-suspended, transported and re-deposited along the river.

To the author's knowledge, studies about oil spills in inland waterways are still very limited, especially for the fate and transport of submerged oil [7, 6, 5]. Although the deposition of oil by sediments was found in 1941 [9], most of the existing oil spill models failed to take this process into account. One important reason was that the properties and fate of OPAs were not well known [8]. While several modeling studies in marine systems had been done [11, 12], the characteristics of riverine hydrodynamics as well as the properties of residual OPAs are quite different from the ones found in marine systems. Motivated by the need to know the fate of the OPAs in Morrow Lake, a three-dimensional hydrodynamic model was developed and coupled with a Lagrangian particle tracking model, implemented to model the transport of OPAs. The developed model was then applied to Morrow Lake and its delta in Kalamazoo River waterways to study the fate of OPAs and predict the depositional areas where most of the residual oil could be found.

2.2 Model Development

2.2.1 Three-dimensional Hydrodynamic Model

Environmental Fluid Dynamics Code (EFDC) is a public domain code which can be used to model both hydrodynamics and water quality for surface water systems [19]. The model solves the three-dimensional vertically hydrostatic equations of motions with the Boussinesq approximation. It uses sigma vertical coordinates and curvilinear orthogonal horizontal coordinates. The modified Mellor-Yamada turbulence closure [20, 21] is implemented for solving vertical turbulence viscosity. The Smagorinsky's formula [22] is applied to compute horizontal turbulence viscosity. The governing equations of continuity and horizontal momentum are as follows.

$$\frac{\partial \xi}{\partial t} + \frac{\partial (Hu)}{\partial x} + \frac{\partial (Hv)}{\partial y} + \frac{\partial w}{\partial z} = 0 \tag{2.1}$$

$$\begin{aligned} &\frac{\partial (Hu)}{\partial t} + \frac{\partial (Huu)}{\partial x} + \frac{\partial (Huv)}{\partial y} + \frac{\partial (uw)}{\partial z} - fHv \\ &= -H\frac{\partial (g\xi + p)}{\partial x} - \left(\frac{\partial h}{\partial x} - z\frac{\partial H}{\partial x}\right)\frac{\partial p}{\partial z} + \frac{\partial}{\partial z}\left(\frac{A_v}{H}\frac{\partial u}{\partial z}\right) + Q_u \end{aligned} \tag{2.2}$$

$$\begin{aligned} &\frac{\partial (Hv)}{\partial t} + \frac{\partial (Huv)}{\partial x} + \frac{\partial (Hvv)}{\partial y} + \frac{\partial (vw)}{\partial z} + fHu \\ &= -H\frac{\partial (g\xi + p)}{\partial y} - \left(\frac{\partial h}{\partial y} - z\frac{\partial H}{\partial y}\right)\frac{\partial p}{\partial z} + \frac{\partial}{\partial z}\left(\frac{A_v}{H}\frac{\partial v}{\partial z}\right) + Q_v \end{aligned} \tag{2.3}$$

where ξ is the surface elevation above or below datum; the total depth H is the sum of water depth below the undisturbed free surface datum, h, and ξ, which is $H = h + \xi$; u and v are the horizontal velocity components in the curvilinear orthogonal coordinates x and y; w is the vertical velocity; f is the Coriolis parameter; g is gravitational acceleration; and p represents the excess water hydrostatic pressure, which can be expressed as:

$$\frac{\partial p}{\partial z} = -gH\frac{\rho - \rho_0}{\rho_0} \tag{2.4}$$

where ρ is density, and ρ_0 is the reference density.

A_v is the vertical turbulent or eddy viscosity, which is solved by implementing the second moment turbulent closure Mellor-Yamada model. The model relates A_v to turbulent intensity q, a turbulent length scale l and a Richardson number R_q as follows:

$$A_v = 0.4(l + 36R_q)^{-1}(1 + 6R_q)^{-1}(1 + 8R_q)ql \tag{2.5}$$

$$R_q = \frac{gh\partial_z b}{q^2}\frac{l^2}{H^2} \tag{2.6}$$

$$\begin{aligned}\frac{\partial(Hq^2)}{\partial t} + \frac{\partial(Huq^2)}{\partial x} + \frac{\partial(Hvq^2)}{\partial y} + \frac{\partial(wq^2)}{\partial z} = \frac{\partial H^{-1}A_q\partial_z q^2}{\partial z} \\ +Q_q + 2H^{-1}A_v((\partial_z u)^2 + (\partial_z v)^2) + 2gA_b\frac{\partial b}{\partial z} - 2H(B_1 l)^{-1}q^3\end{aligned} \tag{2.7}$$

$$\begin{aligned}\frac{\partial(Hq^2l)}{\partial t} + \frac{\partial(Huq^2l)}{\partial x} + \frac{\partial(Hvq^2l)}{\partial y} + \frac{\partial(wq^2)}{\partial z} = \frac{\partial H^{-1}A_q\partial_z q^2 l}{\partial z} + Q_l \\ +H^{-1}E_1 lA_v((\partial_z u)^2 + (\partial_z v)^2) + gE_1E_3lA_b\frac{\partial b}{\partial z} - H(B_1 l)^{-1}q^3(1 + E_2(\kappa L)^{-2}l^2)\end{aligned} \tag{2.8}$$

where $L^{-1} = H^{-1}(z^{-1} + (1 - z)^{-1})$; $B_1 = 16.6$, $E_1 = 1.8$, $E_2 = 1.0$, and $E_3 = 1.8$ are empirical constants. Q_l and Q_q are source and/or sink terms for turbulent length scale and energy. The vertical diffusivity, A_q, is generally taken as equal to the vertical turbulent viscosity, A_v. Q_u and Q_v are horizontal momentum diffusion terms and expressed by the following formulas:

$$Q_u = \frac{\partial}{\partial x}\left(HA_H\left(\frac{\partial u}{\partial x} - \frac{\partial v}{\partial y}\right)\right) + \frac{\partial}{\partial y}\left(HA_H\left(\frac{\partial u}{\partial y} + \frac{\partial v}{\partial x}\right)\right) \tag{2.9}$$

$$Q_v = \frac{\partial}{\partial x}\left(HA_H\left(\frac{\partial u}{\partial y} + \frac{\partial v}{\partial x}\right)\right) - \frac{\partial}{\partial y}\left(HA_H\left(\frac{\partial u}{\partial x} - \frac{\partial v}{\partial y}\right)\right) \tag{2.10}$$

The horizontal diffusion coefficient, A_H, can be modeled by the following formula:

$$A_H = A_{H_D}\Delta x\Delta y\left(\left(\frac{\partial u}{\partial x}-\frac{\partial v}{\partial y}\right)^2+\left(\frac{\partial u}{\partial y}+\frac{\partial v}{\partial x}\right)^2\right)^{1/2} \tag{2.11}$$

where A_{H_D} is a dimensionless parameter; Δx and Δy are the grid sizes.

The model uses the staggered arrangement of variables in a structured grid format. The velocity components are located on the faces of the control volume, while the depth, buoyancy and concentration of the transported variables are stored at the center of the control volume. The temporal integration of the governing equations is carried out with either two time level trapezoidal scheme or a semi-implicit three time level, leap frog trapezoidal scheme. The detailed numerical scheme is presented in [19].

2.2.2 A Lagrangian Particle Tracking Model for OPAs

Formation of OPAs is due to mixture of oil and suspended particles in turbulent water [23, 24, 25, 26, 8]. The formation mainly depends on properties of spilled oil, suspended particles, and aquatic environment such as temperature, salinity, and turbulence. Due to various properties of OPAs, a Lagrangian particle tracking model is implemented and coupled with the three-dimensional Eulerian hydrodynamics model described above. Lagrangian models have been widely used in ecological and environmental models [27, 28, 13]. Random walk is used to simulate the movement of OPAs caused by turbulent diffusion. The movement of any particle is described by the following formulas:

$$x^{t+\Delta t} = x^t + \left(u+\frac{\partial A_H}{\partial x}\right)\Delta t + R\sqrt{2A_H\Delta t} \tag{2.12}$$

$$y^{t+\Delta t} = y^t + \left(v+\frac{\partial A_H}{\partial y}\right)\Delta t + R\sqrt{2A_H\Delta t} \tag{2.13}$$

$$z^{t+\Delta t} = z^t + \left(w-w_s+\frac{\partial A_q}{\partial z}\right)\Delta t + R\sqrt{2A_q\Delta t} \tag{2.14}$$

where (x, y, z) is the coordinates of a particle; (u, v, w) represents flow velocities in x, y, z directions and A_H and A_q are the horizontal and vertical diffusion coefficients, which are computed by the hydrodynamic model; w_s is settling velocity of a particle, R is a random number between -1 and 1 by a

uniformly distributed random variable generator with a mean of 0.

Settling and Resuspension

Due to the negative buoyancy of a particle, it may settle with falling velocity w_s. Regarding oil-particle aggregates, the settling velocity depends on properties of fluid, oil droplet and solid particle, as well as how they interact and constitute [15]. Therefore, knowledge and study about OPAs' properties for each specific case is required. The properties of OPAs remaining in the Kalamazoo River waterways were studied in related efforts [29, 30, 31, 32]. OPAs were formed with a laboratory shaker and examined with an ultraviolet epifluorescence microscope. The most common OPA types were found to be single and multiple droplet aggregates [31]. Their settling velocity was found to be in the range between 1.0 mm/s and 3.0 mm/s, and the critical bed shear stress for resuspension was found to be around 0.1 Pa. If a particle hits river bed, it is treated as deposited/settled on the bed. A deposited particle can be entrained into water body if turbulent bed shear stress exceeds critical bed shear stress for resuspension.

Reflective Boundary Condition

Reflective boundary condition is applied for wall and water surface boundaries. If the computed position of a particle at the next time step crosses a wall or water surface boundary, it is reflected back into the computation domain as Figure 2.1 shows. The hydrodynamic model handles wetting and drying. The boundaries between a wet computational cell and a dry one are treated the same as wall boundaries.

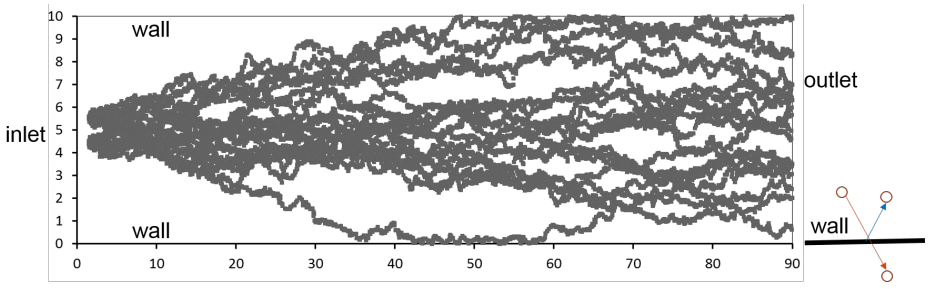

Figure 2.1: A schematic of random walk and reflective boundary condition

2.3 Study of the Kalamazoo River Oil Spill

2.3.1 Study Domain

The 2010 Kalamazoo River oil spill, in the state of Michigan, is the largest inland heavy crude oil spill in U.S. history. It released approximately four million liters of diluted bitumen (dilbit) due to Enbridge pipeline rupture. It cost 1.2 billion U.S. dollars to clean up until the end of 2014, four years after the spill. The contaminated waterway was closed for 21 months. In this study, the research domain is Morrow Lake and its delta (see Figure 2.2). Morrow Dam is located at the downstream of the domain, which is the last structure to prevent spilled oil from flowing into Lake Michigan. The domain is approximately 5.6 kilometers long.

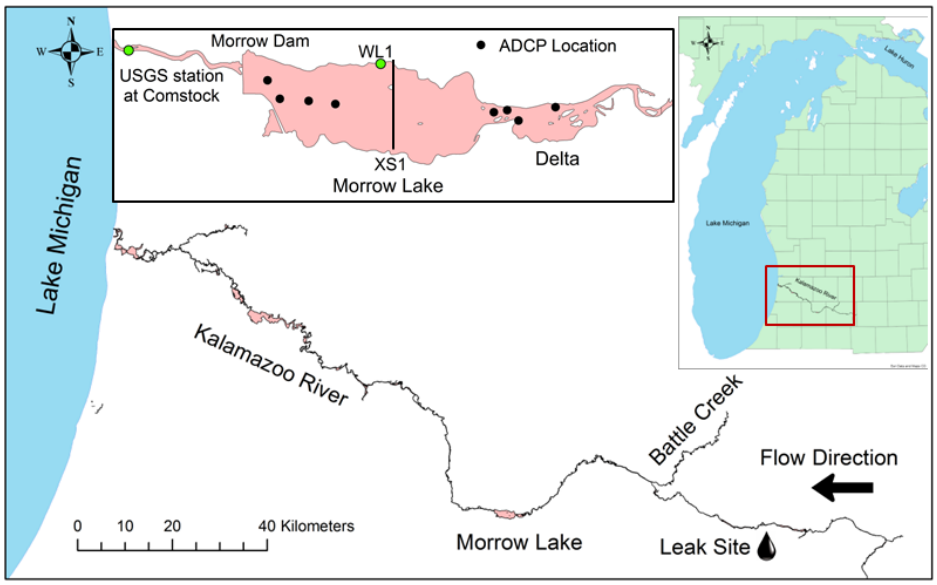

Figure 2.2: Study domain and location of U.S. Geological Survey stations

The Morrow Lake model uses curvilinear orthogonal grids, which consist of 16,206 horizontal cells and eight vertical layers. The size of the horizontal cells is 20 meters by 20 meters.

Two flow scenarios were simulated to represent high inflow and low inflow fluxes, respectively. The peak of the April 9-29, 2013 flow is higher than the 95th percentile of daily mean value for the same dates in the last 80 years, while July 9-19, 2013 flow is slightly lower than the median daily mean value of July, one of the periods with lowest flow discharge within a year.

These two flow events were selected because field measurement data for model calibration and validation is readily available. Also, they are representative for high and low flow scenarios in this waterway system.

2.3.2 Computational Meshes and Bathymetry

The Morrow Lake model used curvilinear orthogonal grids, which consisted of 16,206 cells in the (x, y) plane (figure 2.3) and 8 vertical layers (figure 2.4). The size of the horizontal cells was approximately 60 feet by 60 feet. The bathymetry data was provided by Weston Solutions, Inc. The bed elevation was interpolated to the center of each grid cell with the help of an in-house FORTRAN code (figure 2.5).

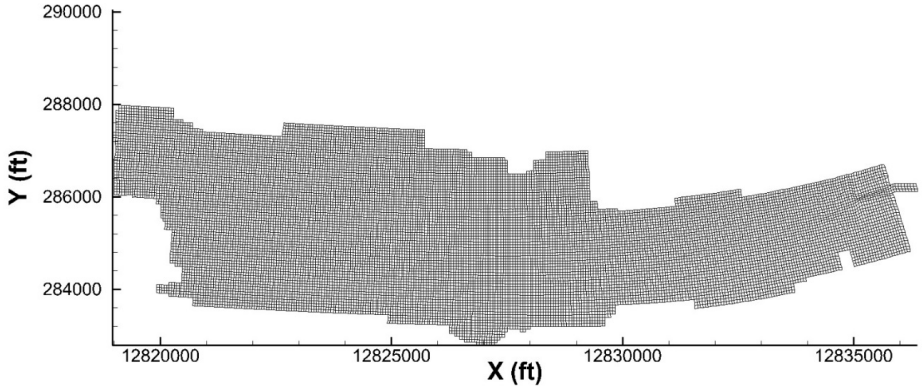

Figure 2.3: Plan View of the Computational Meshes

2.3.3 Model Simulation Scenarios

Figure 2.6 shows the historical flow record (1933-2013) at the USGS gauging station 04106000, located downstream of Morrow Lake (see Figure 12.2). The daily mean discharge of April and July 2013 events is shown by blue and red circles, separately. It indicates that the peak of the April 2013 flow is higher than the 95th percentile of daily mean value for those dates in the last 80 years. A July 2013 flow event is slightly under the median daily mean value in July, one of the lowest flow period within a year. These two flow events (April 9 29, 2013 and July 9 - 19, 2013) were selected because of

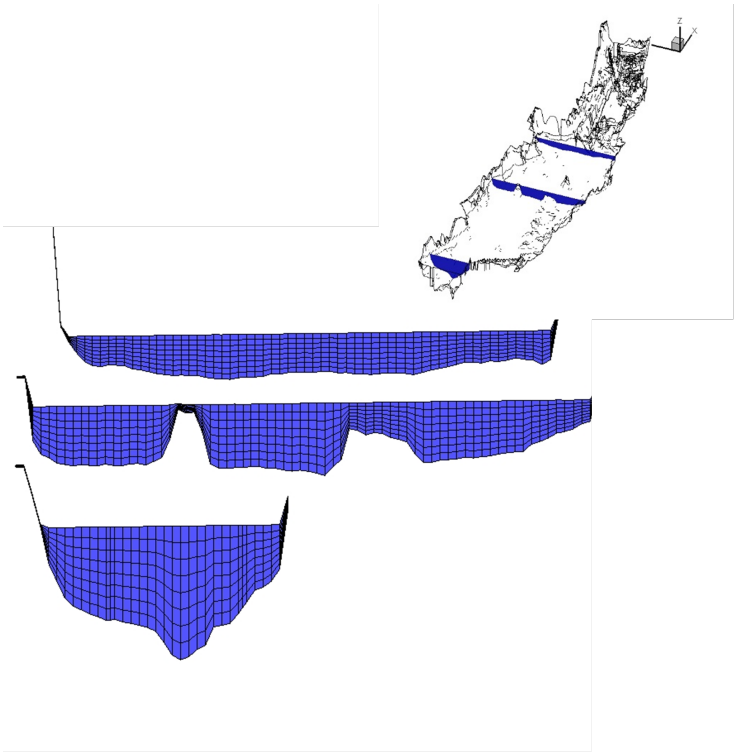

Figure 2.4: Sectional View of Computational Meshes at Three Cross Sections

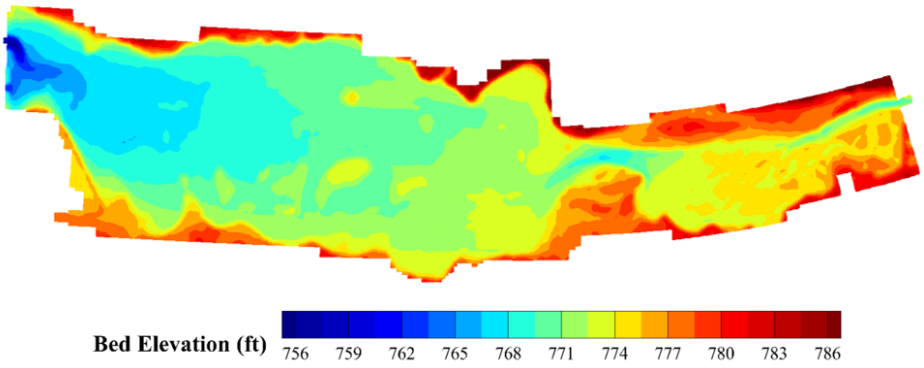

Figure 2.5: Bed Elevation of Morrow Lake and Delta (NAVD88)

the availability of ADCP and stage recorder data for model calibration and validation.

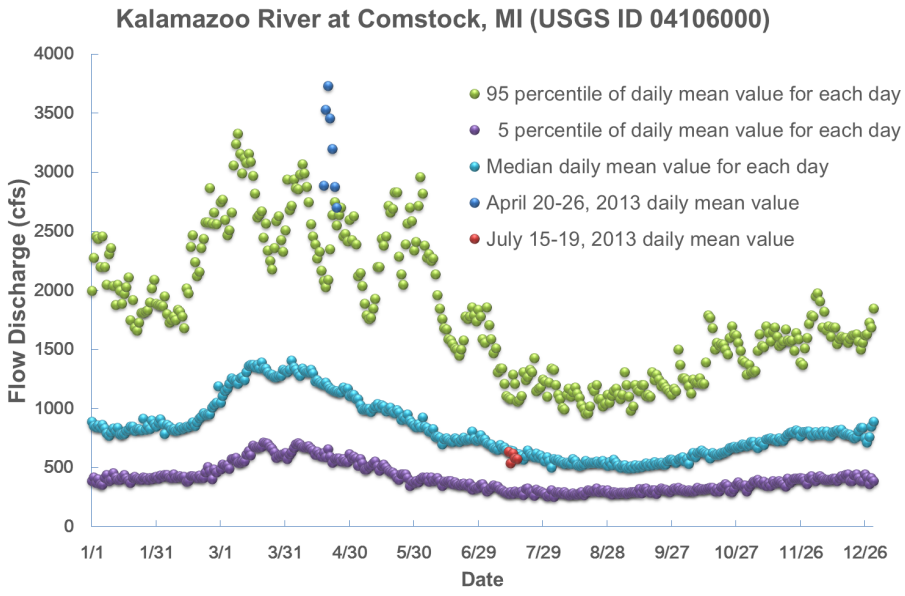

Figure 2.6: Historical Flow Record at USGS Comstock Station

2.3.4 Boundary Conditions

There exist two USGS gauging stations (see Figure 2.2) for providing continuous flow discharge measurement to the study reach, one upstream near Battle Creek (USGS04105500) and the other one downstream at Comstock (USGS04106000). The downstream gauge at Comstock is located roughly 1 mile downstream of Morrow Lake Dam so that it indicates outflow discharge from Morrow Dam. Conversely, there are several tributaries in the reach between the upstream station (near Battle Creek) and the upstream boundary of the numerical domain, MP 36.5. Therefore the flow discharge measured at the upstream station near Battle Creek may differ substantially from the inflow discharge of the study domain. The difference can be clearly seen in Figure 2.7. In other words, for the model domain the outflow discharge was known quite well while the inflow discharge was not. However, with the installation of a stage level recorder at MP 36.5 (discussed later, give reference), the recorded water levels were used as upstream boundary conditions for both April and July 2013 simulation events.

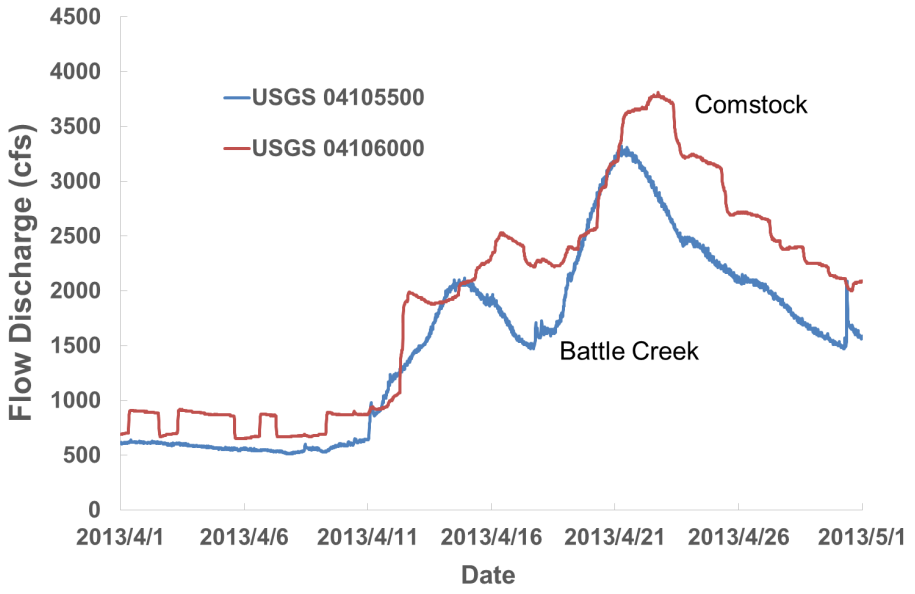

Figure 2.7: Discharge of April 2013 High Flow Scenario Measured at USGS Gauging Stations

Morrow Dam is owned by a STS Hydropower Ltd (STS) who controls the stage level of Morrow Lake for electricity generation and other purposes. There are two outflow sections at the dam (see Figure 2.8; The glass building to the right (looking upstream) contains the power generators and four turbines underneath. To the left of the glass building are two tainter gates with flap gates on top.): one is the powerhouse with four turbines (250 cfs capacity each) and the other section is two tainter gates with flap gates on top of each. In general, the operator of the dam follows operational rules and estimated inflow (use USGS gauge station 04105500, Kalamazoo River near Battle Creek for reference) to maintain the lake level at 776 feet (NGVD). STS recorded lake level and provided several sets of recorded lake stage to assist the study. From the comparison of STS stage records and counterpart discharge at Kalamazoo River at Comstock station, it can be expected that from time to time the released discharges deviated from the operational rules. Therefore, although Comstock gauge station provided the outflow discharge, the discharge itself was not sufficient to estimate the stage level solely based on outflow. Figure 2.9 shows available data of the stage level near the dam against outflow discharge. For a given stage level, the outflow rate can vary from 0 cfs to 4000 cfs. On the other hand, with a given outflow discharge, stage level can vary up to 1 foot.

Figure 2.8: Structures at the Morrow Dam

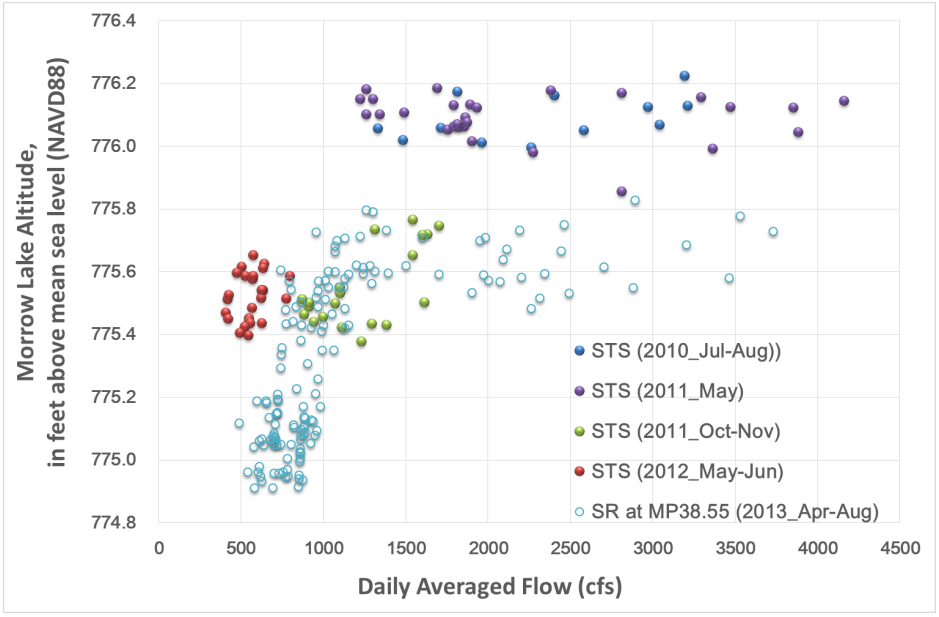

Figure 2.9: Comparison of Measured Outflow Discharge at Kalamazoo River at Comstock and Measured Lake Level at Upstream of Morrow Dam

For model simulations, it was decided that the most suitable boundary condition to use was the flow discharge at downstream (Morrow Dam) and the stage level at the upstream (MP 36.5, Figure 2.10). The effect of operations at Morrow Dam that controls the OPA movement was one of the study objectives. Applying the flow boundary condition at the downstream end allowed the inclusion of dam operation rules. A model can be set up to estimate how much flow passes through turbines, flap gates, and tainter gates, respectively (Figure 2.11). The importance of treating each outflow mode independently was that the turbines' inlet was near the bottom while the flap gates' outflow was located at the lake's surface, which yielded different hydrodynamic conditions in the water column. Instead of assuming a vertically uniform outflow distribution throughout the water depth, more accurate hydrodynamics were achieved by specifying outflow through the top or bottom layers under different conditions (see Figure 2.11). For example, discharging from the top or the bottom would have different effects on the bottom shear stress near the dam. It can be expected that bottom discharge would result in higher bottom shear stress than surface discharge.

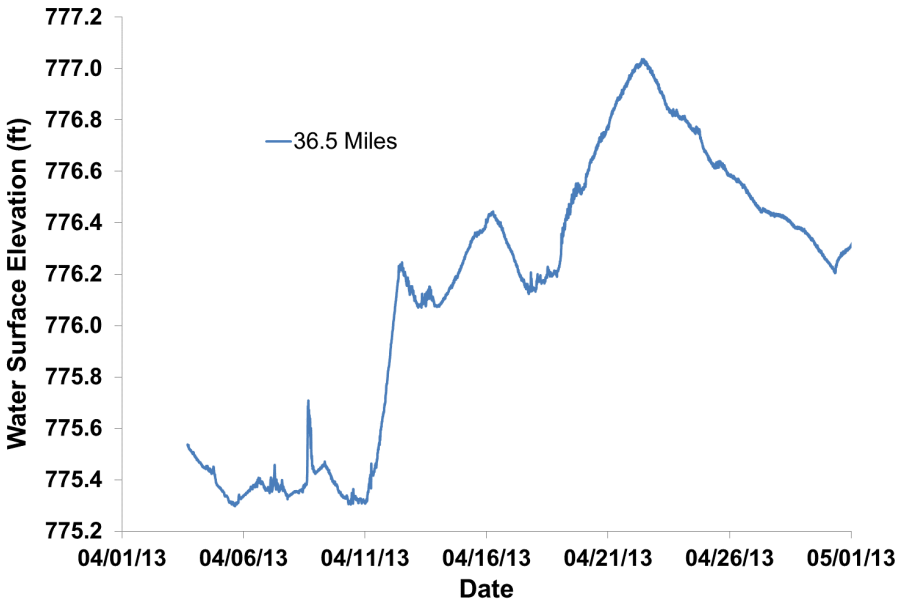

Figure 2.10: Upstream Stage Level of April 2013 High Flow Scenario at MP 36.5

Discharge from flap gate (overflow) and from tainter gates (underflow) were computed using rating curve equations provided by the STS operator. In conjunction with reference to the operation rules regarding which control(s)

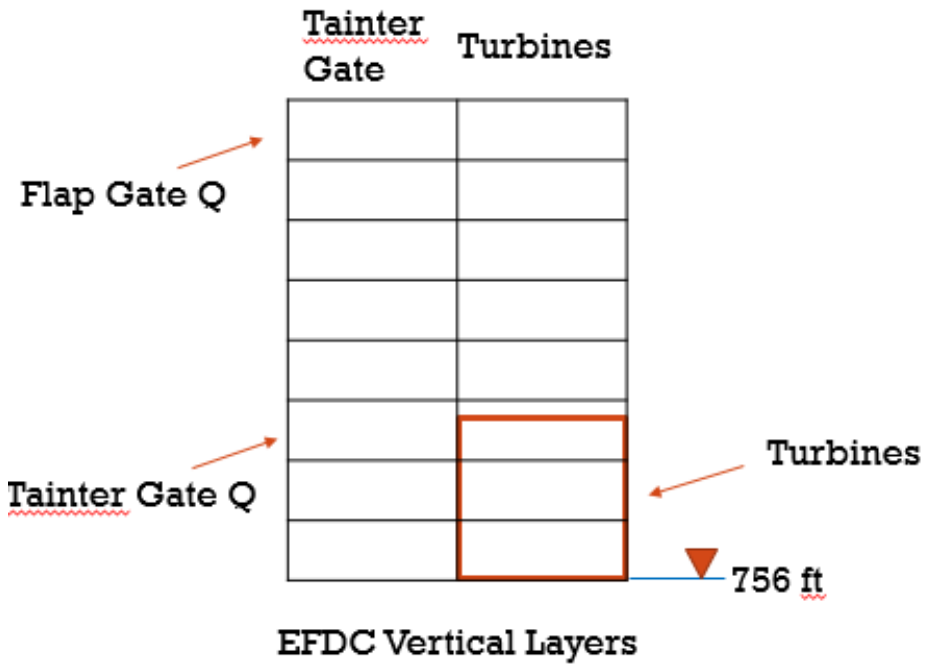

Figure 2.11: Sectional View of Grids Representing Morrow Dam

were in operation under given incoming discharge amount, the discharge time history from the flap gages, tainter gates, and turbines can be estimated. As an example, the total discharge at Comstock station for the April 2013 event was partitioned (Figure 2.12) using the technique mentioned above.

Wind effect was also considered in the modeling. Wind speed and direction data was measured hourly at Kalamazoo/Battle Creek International Airport (see Figure 2.13) that was approximately 4.4 miles from Morrow Lake (`http://www.ncdc.noaa.gov/cdo-web/`; station 94815).

2.3.5 Three-dimensional Hydrodynamic Model

Morrow Dam

Morrow Dam is owned by STS Hydropower Ltd (STS) and controls the stage level of Morrow Lake for electricity generation and other purposes. There are two outflow sections at the dam: one is the powerhouse with four turbines and the other one is two tainter gates. Total outflow discharge is recorded by U.S. Geological Survey station at Comstock (see Figure 2.2). With the rating curves and water level provided by STS, outflow through turbines and

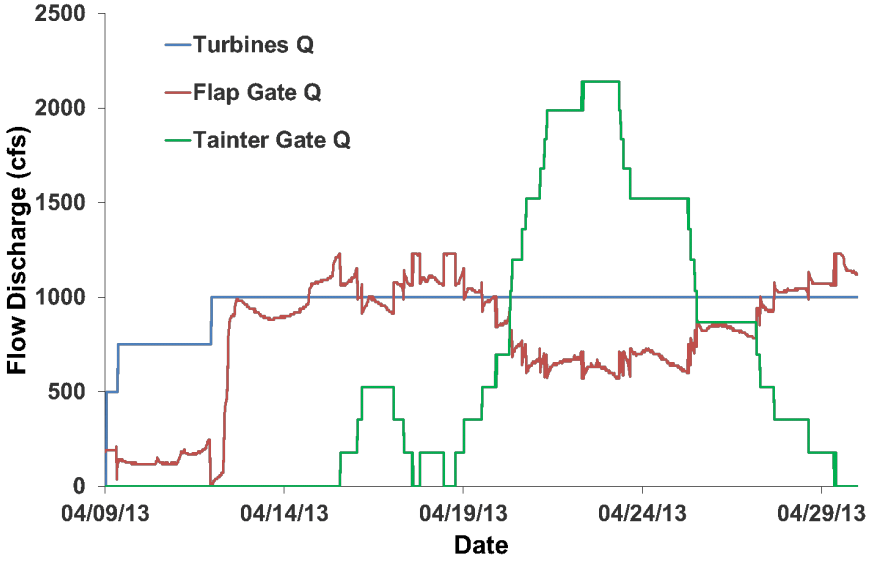

Figure 2.12: Outflow Distribution at Morrow Dam during April 2013 High Flows

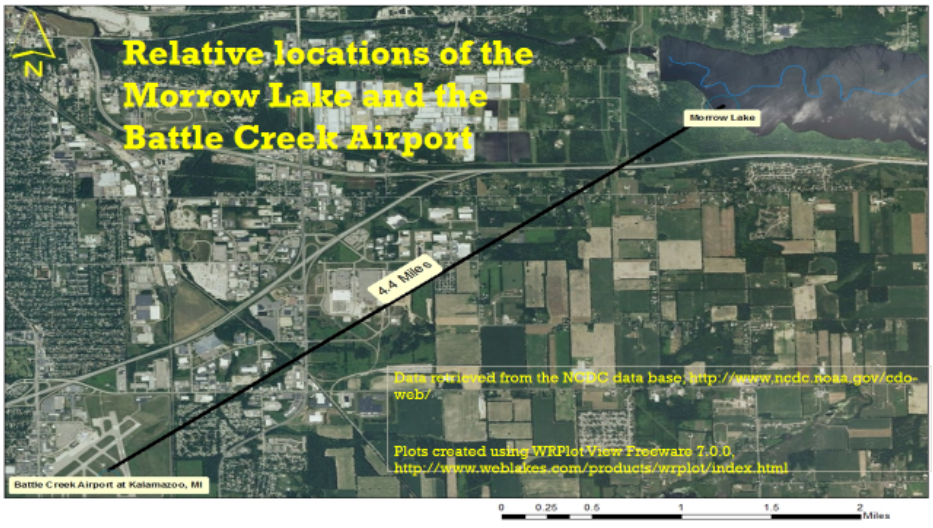

Figure 2.13: Location of Kalamazoo/Battle Creek Intl. Airport (wind data)

tainter gates was computed and applied as downstream boundary condition. At upstream, the measured water surface elevation was used for boundary condition.

Figure 2.14, 2.15, and 2.16 show the distribution of velocity magnitude and bed shear stress near the Morrow Dam with different flow discharge resulting from dam operations. The velocity and bed shear stress increase as outflow discharge increases. However, the increase is obvious near the dam but not obvious far away from the vicinity of the dam.

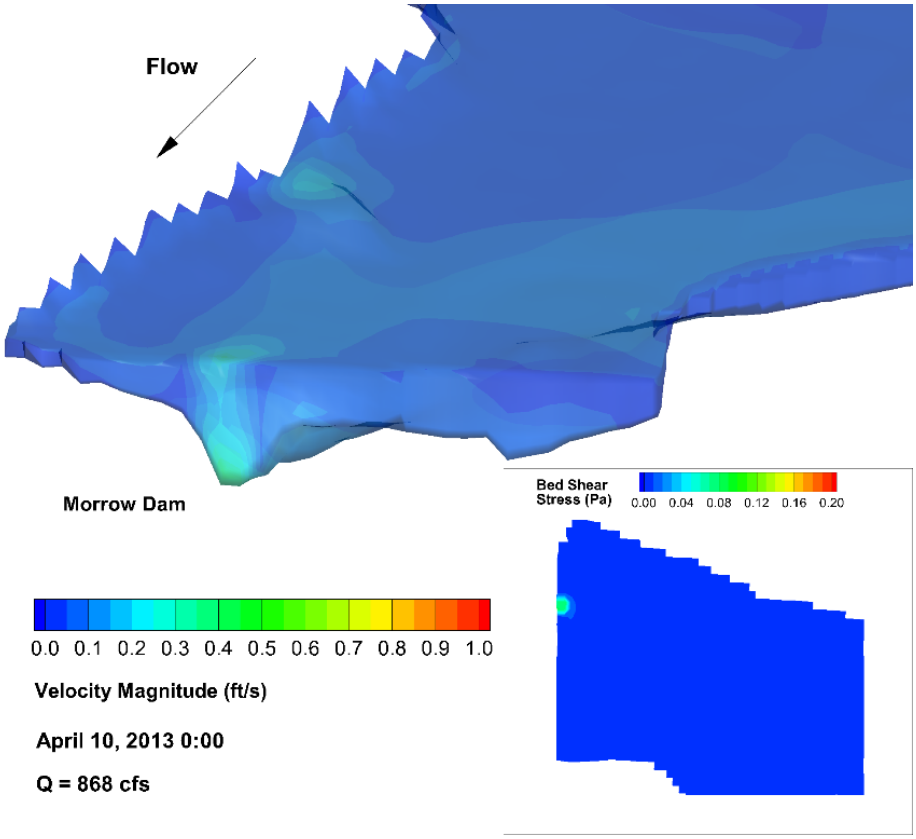

Figure 2.14: Velocity and Bed Shear Stress Distribution near Morrow Dam (Q = 868 cfs, three turbines in operation)

Wind Effect

Wind effect is important for flow patterns in a lake. Wind speed and direction data were measured hourly at Kalamazoo/Battle Creek International Airport, located at approximately seven kilometers from Morrow Lake. An example of wind effect is shown in Figure 2.17 by comparing velocity distri-

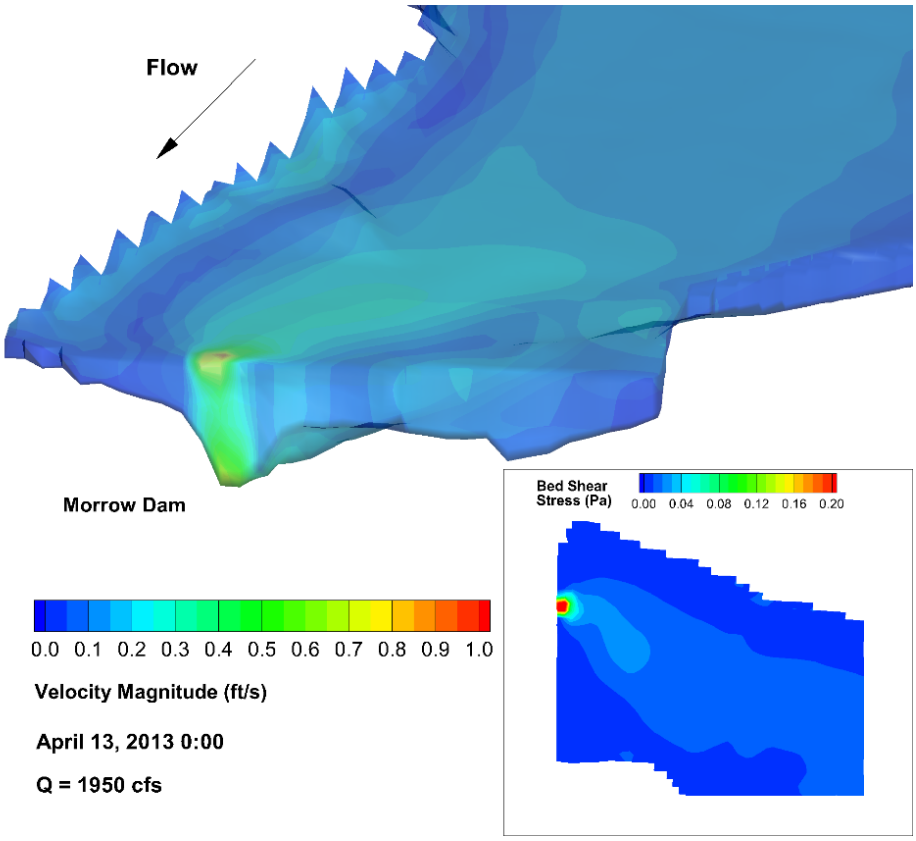

Figure 2.15: Velocity and Bed Shear Stress Distribution near Morrow Dam (Q = 1950 cfs, four turbines and flap gate in operation)

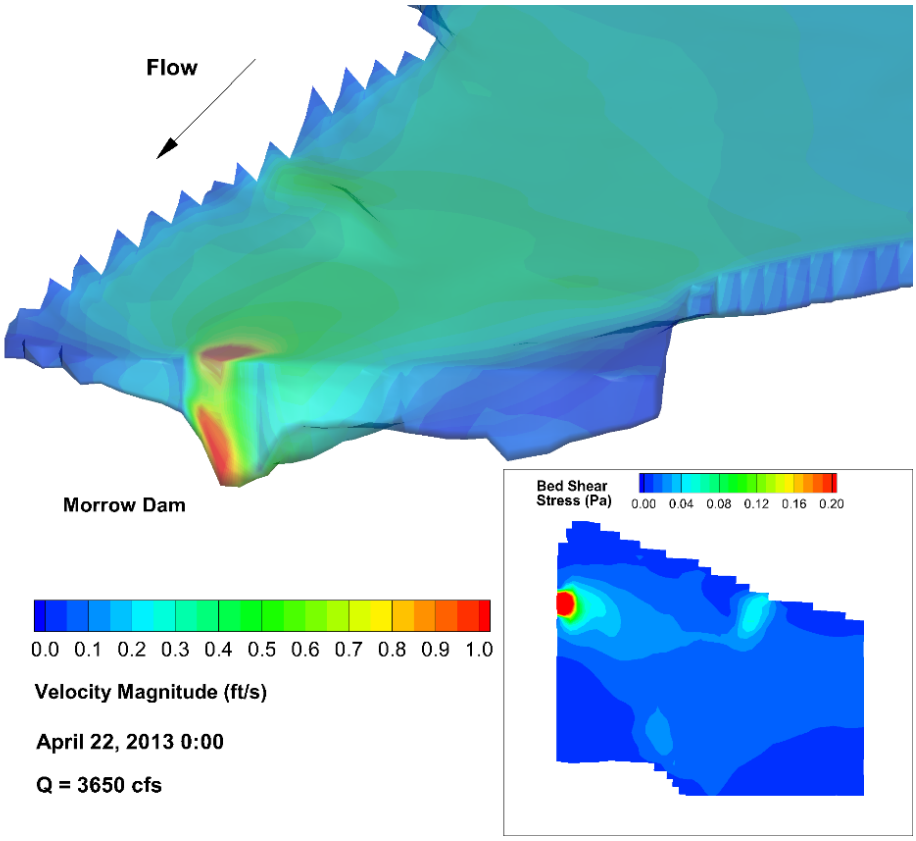

Figure 2.16: Velocity and Bed Shear Stress Distribution near Morrow Dam (Q = 3650 cfs, four turbines, flap gate, and tainter gate in operation)

bution at a cross section in the middle of the lake (see XS1 in Figure 2.2) with and without wind effect. Color represents the magnitude of velocity (looking downstream), while vectors represent velocities in the transverse plane. The results were exported when the wind speed was 10 kilometers per hour and wind direction was south to north (i.e. left to right in the sectional view). It is shown that wind obviously changes flow pattern and can enhance secondary flows and near-bed velocities depending on wind direction.

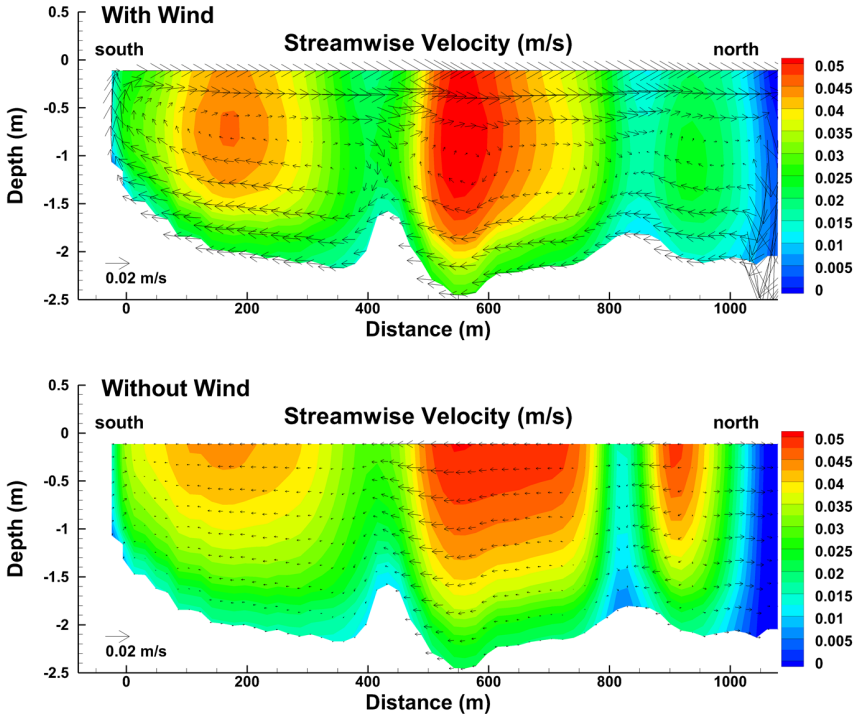

Figure 2.17: Sectional View of Velocity Distribution at XS1

Model Calibration and Validation

Model calibration was accomplished primarily by matching the water surface elevation measurement through adjustment of the roughness height at the bed. The April 2013 high flow scenario was used for calibration. The comparison of water stage level at WL1 (see Figure 2.2) between field measurement and numerical results is shown in Figure 2.18. The bed roughness height within the floodplain is different from those in riverine and lake areas. It was found that the roughness height values were 0.3 mm in lake and

riverine areas and 3 mm in floodplain areas. The July 2013 low flow scenario was used for the validation examination 2.18. The difference between measurement and simulation was less than 0.05 meter.

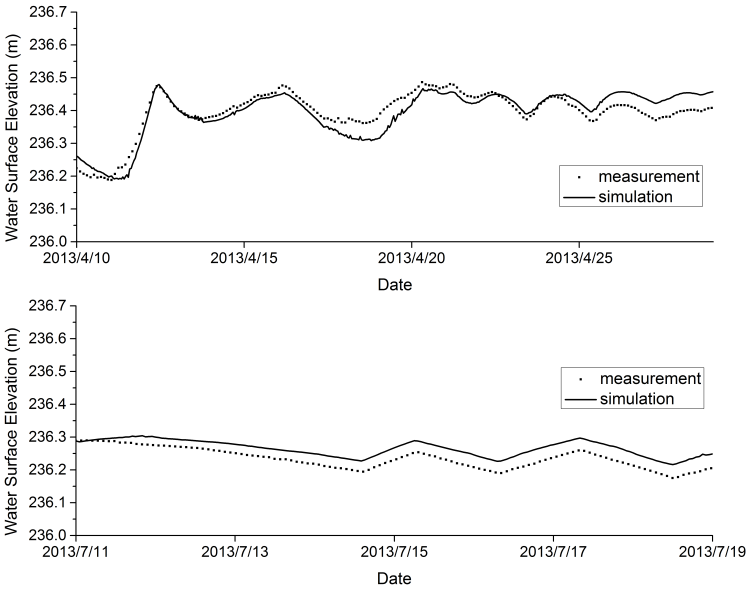

Figure 2.18: Model calibration and validation

Additional validation was performed using stationary Acoustic Doppler Current Profiler (ADCP) measurements. Locations of ADCP measurement is shown in Figure 2.2. The bed shear stresses can be estimated from the measured velocity profiles by fitting the data to the log law to calculate the shear velocity, which was then converted to the bed shear stress [33, 34]. Comparison of bed shear stresses between numerical simulation and estimation from ADCP data is shown in Figure 2.19. The model results of bed shear stress matched quite well with the estimation from ADCP measurement, especially when bed shear stress was higher than 0.01 Pa. At very low-velocity areas, ADCP measurement yielded higher bed shear stress than model results.

Effect of Inflow Flux on Bed Shear Stress Distribution

Bed shear stress distributions under high and low inflow scenarios are shown in Figure 2.20 and Figure 2.21. During low flows, the particles transported

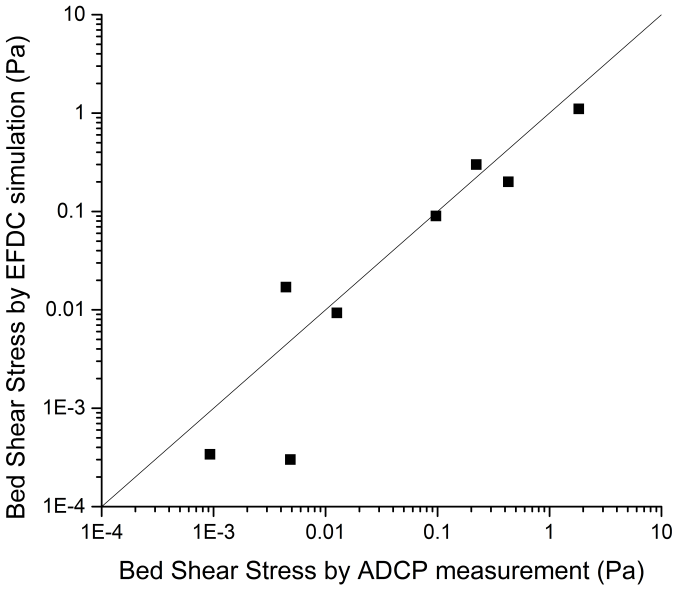

Figure 2.19: Comparison of bed shear stresses between simulation and estimation from ADCP data

from upstream would mostly deposit in the delta. It is expected that few particles may migrate beyond the neck at downstream of delta. On the other hand, in high flow scenario high bed shear stress extends to the lake. However, Figure 2.20 also shows that the bed shear stress decreases dramatically once the flow passes the neck area. Obviously higher flow has more capacity to transport particles.

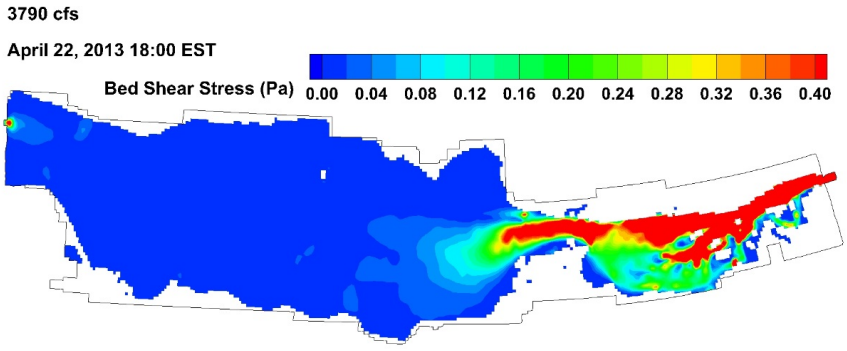

Figure 2.20: Bed Shear Stress Distribution at Discharge Q = 3790 cfs

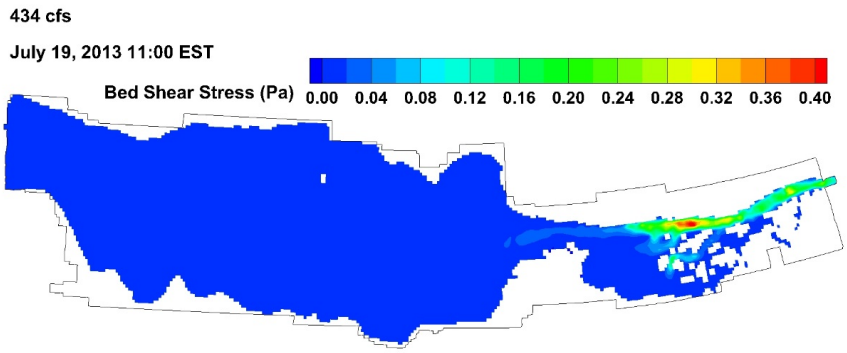

Figure 2.21: Bed Shear Stress Distribution at Discharge Q = 434 cfs

2.3.6 Transport of OPAs using Lagrangian Simulation

The Lagrangian particle tracking model allowed to specify different properties for each OPA particle, such as settling velocity and critical bed shear stress for resuspension. Studies on OPA formation mainly depend on laboratory experiments. It is important to understand OPA properties for a specific spill event, since conditions of aquatic environment and spilled oil may vary. The properties of OPAs remaining in the Kalamazoo River waterways were as follows: Their settling velocity was in the range between 1.0 mm/s and 3.0 mm/s, and the critical bed shear stress for resuspension was around 0.1 Pa. OPA with the settling velocity of 1.0 mm/s and the critical bed shear stress of 0.1 Pa was chosen as representative.

For April 2013 high flow scenario, 8000 particles were released at inlet entrance at the starting time. The location of all particles at several time is illustrated in Figure 2.22. Green dots represent deposited particles, while red dots represent OPAs in suspension. Almost all particles deposited after 2 days. However, with increase of flow fluxes, particles were entrained and transported further downstream into the lake. Although no particle was found passing through the downstream dam for given conditions, some were quite close. The same type of OPA was used for the July 2013 low flow scenario. More particles deposited in the delta and their travel time and distance were less (Figure 2.23). Using the numerical model, highly oil-contaminated areas can be identified given information of historical hydrodynamic conditions. An alternative is to do field survey and examine sediment samples, which is extremely time-consuming and costly. The model can be helpful and complement field efforts.

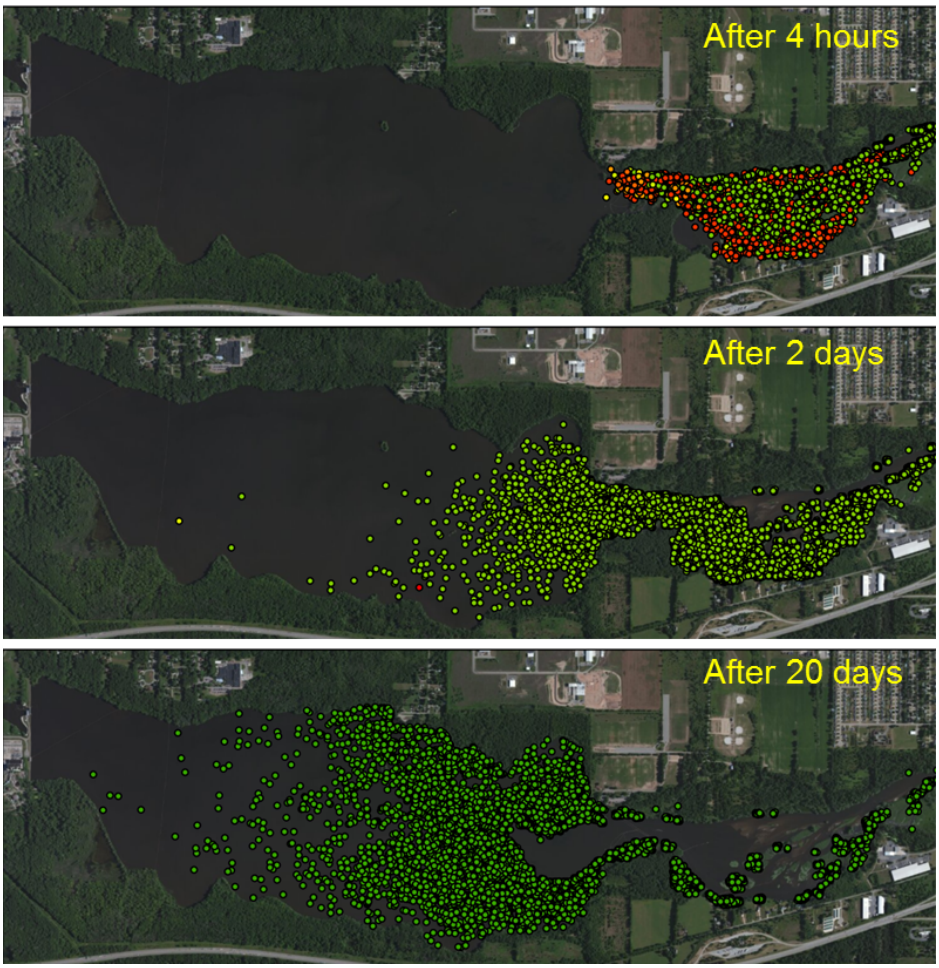

Figure 2.22: Transport of OPAs in April 2013 high flow scenario

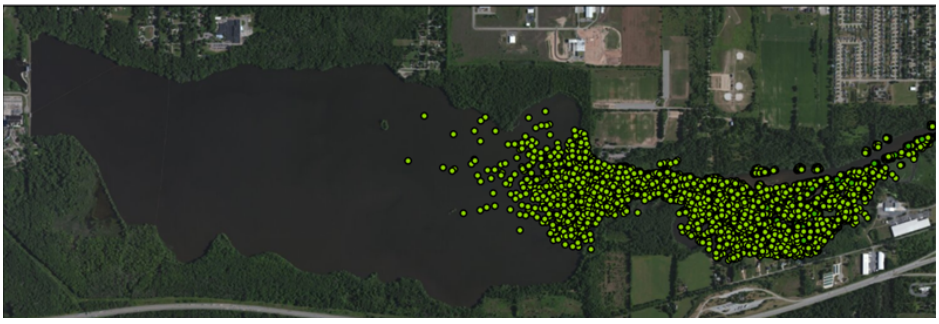

Figure 2.23: Transport of OPAs in July 2013 low flow scenario

April 2013 High Flow Scenario

Figure 2.24 to Figure 2.32 show plan views of particle locations in the April 2013 high flow scenario simulation. 8000 particles were released near the upstream inlet, which were uniformly distributed in the 8 vertical layers. The model allowed each particle to have individual properties. In this case it was assumed that all particles had the same properties. Typical OPA properties were assumed in this study. Settling velocity was specified as 1 mm/s and critical bed shear stress was assumed as 0.1 Pa. The results can be viewed by ArcGIS (for plan view) or Tecplot (for 3D view). The following figures were plotted with ArcGIS.

Figure 2.24: OPA Particle Locations at Time = 0 hour

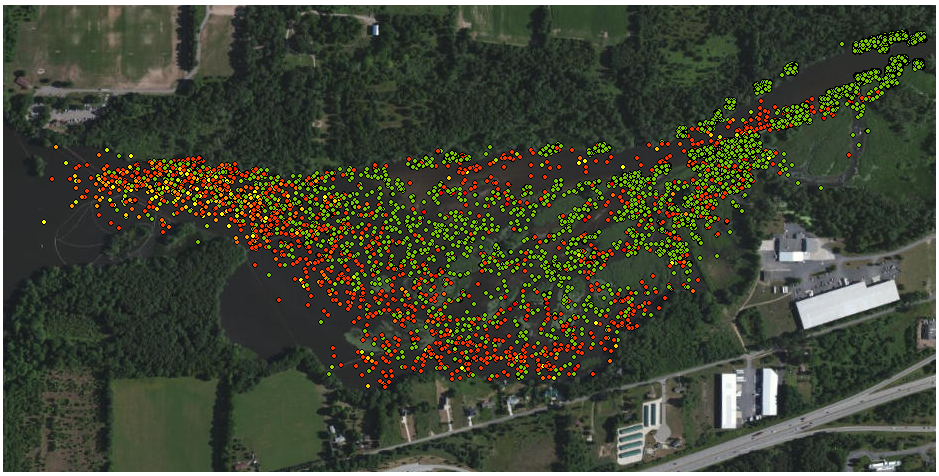

Figure 2.25: OPA Particle Locations at Time = 4 hour (Q = 690 cfs)

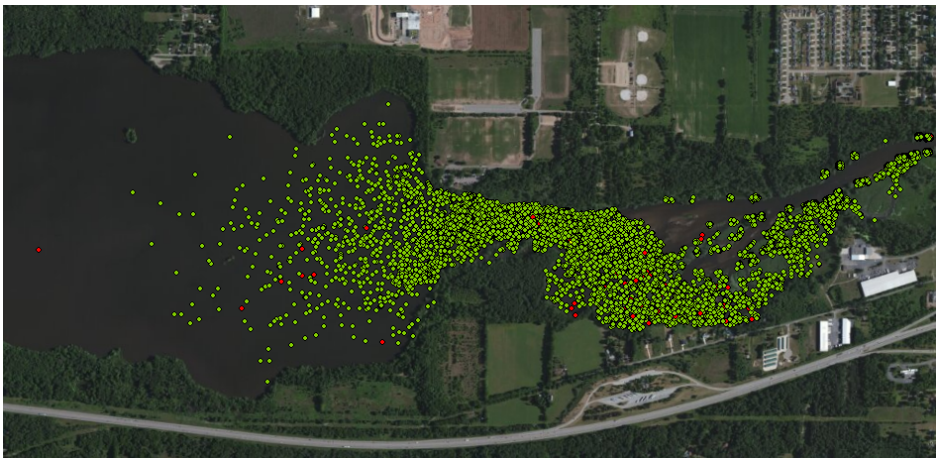

Figure 2.26: OPA Particle Locations at Time = 24 hour (Q = 868 cfs)

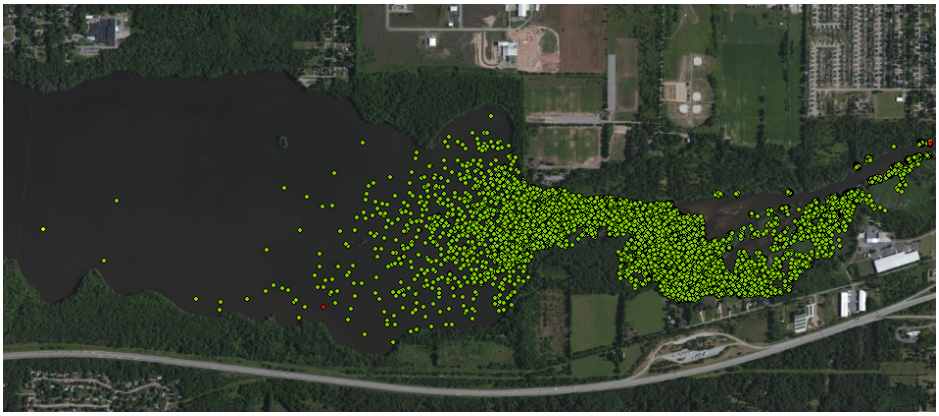

Figure 2.27: OPA Particle Locations at Time = 2 day (Q = 884 cfs)

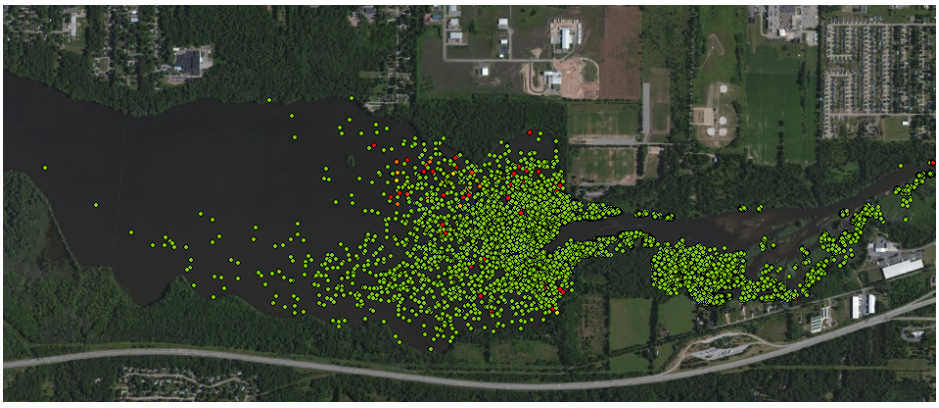

Figure 2.28: OPA Particle Locations at Time = 4 day (Q = 1940 cfs)

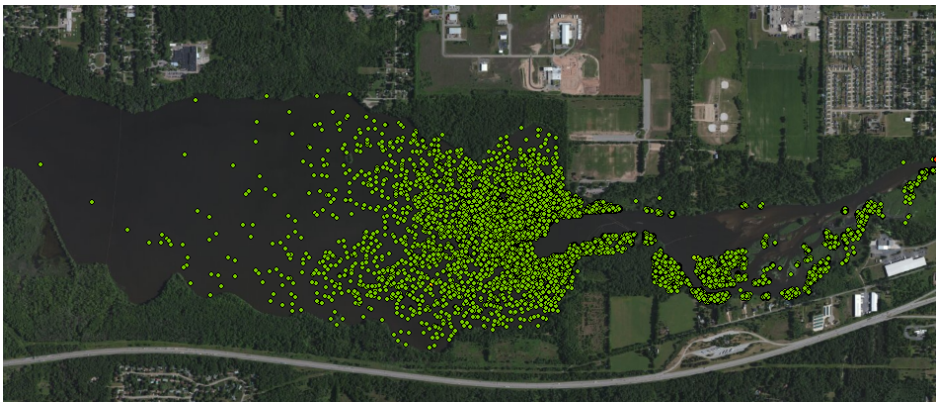

Figure 2.29: OPA Particle Locations at Time = 8 day (Q = 2440 cfs)

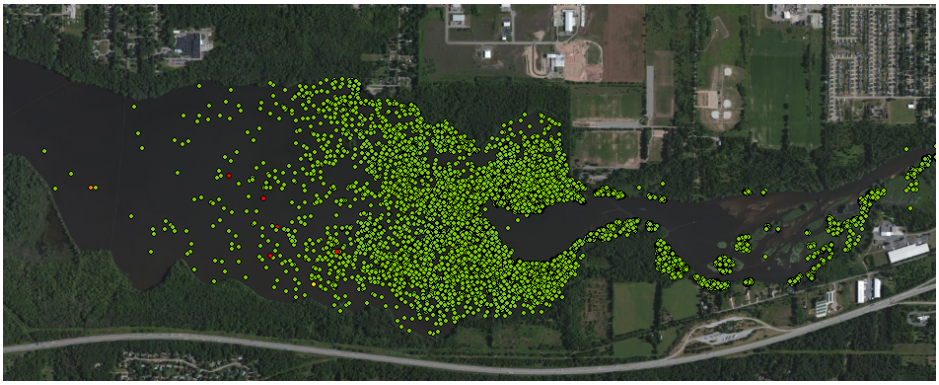

Figure 2.30: OPA Particle Locations at Time = 13 day (Q = 3660 cfs)

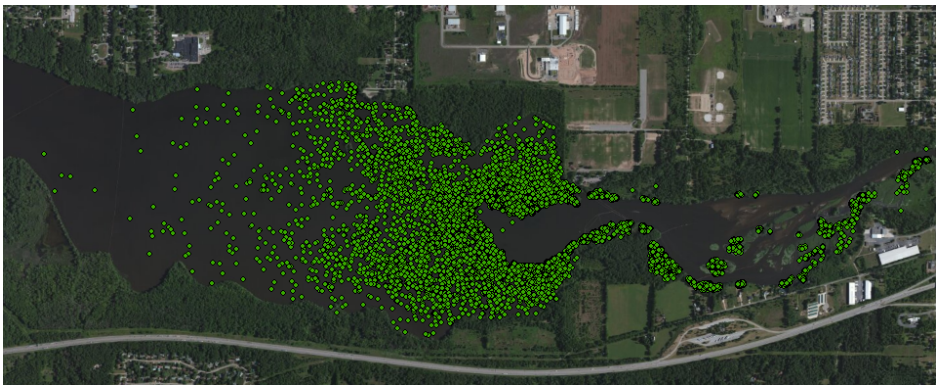

Figure 2.31: OPA Particle Locations at Time = 15 day (Q = 3230 cfs)

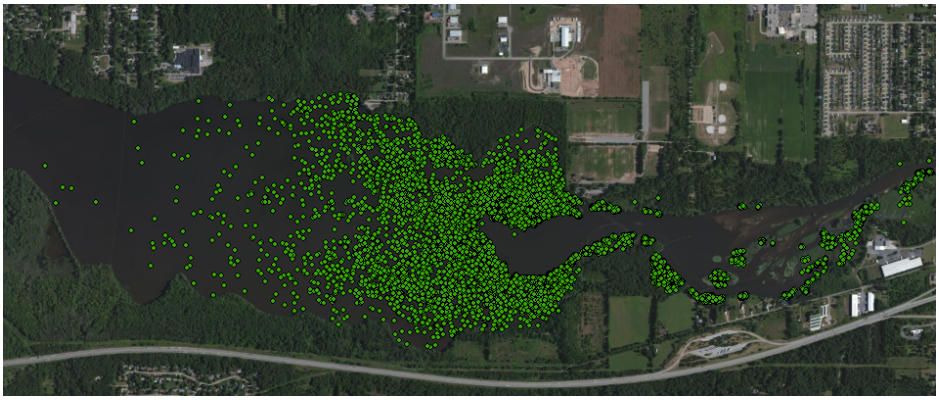

Figure 2.32: OPA Particle Locations at Time = 20 day (Q = 2250 cfs)

The color of particles indicates relative depth. Red dots mean particles are close to water surface while green ones mean they are close to bottom. At time = 4 hours, some particles already deposited, but many of them were still flowing downstream.

After 24 hours, simulation results inclined to show that most particles reached the bottom. Many particles deposited in the delta while some of them passed the delta and neck areas into the lake.

After 2 days almost all particles deposited. Because the flow discharge was in a relatively low range in the first two days, if bed shear stress was less than critical bed shear stress, particles that deposited would stay until flow increased such that bed shear stress sufficient to entrain them into water body was achieved.

At time = 4 days, flow discharge increased to 1940 cfs. As flow increased, bed shear stress increased and might exceed the critical bed shear stress for erosion of OPAs. OPAs were entrained and transported downstream. This phenomena was obvious in the upper part of the delta and channel portion of the neck areas.

Similar to Figure 2.28, flow discharge kept increasing so more particles were resuspended. The change happened mainly in the delta and neck areas because bed shear stress in the lake was still not sufficient to support particle resuspension. Particles entrained from the delta and neck areas all deposited in the lake.

After 13 days, inflow reached the maximum magnitude in this scenario. Deposition areas in the delta were much reduced. More particles can migrate into the lake.

After 15 days, all particles deposited and almost nothing changed from time = 15 days to time = 20 days because inflow discharge decreased. Some deposition areas were observed in the delta. Many particles were distributed in the lake but none passed the dam. However, some of them were already close to the downstream end.

The properties of OPA remaining in the Kalamazoo River waterways are studied (Waterman and Garcia, 2014; Hayter et al. 2015). Three different types of OPAs are characterized (figure 2.33): (A) single and multiple droplet aggregate; (B) solid aggregate of large, elongated oil mass with interior particles (dashed blue circles); (C) flake aggregate of thin membranes of clay aggregates that incorporate oil and fold up. Blue color represents particles and yellow represents oil. Their Stokes settling velocities are 75.54 (Type 1), 0.23 (Type 2), and 2.78 (Type 3) mm/s. The critical shear stress is assumed to be constant, 0.1 Pa, although the Lagrangian particle tracking model allows specifying each particle with different critical shear stress as well as other properties. The location of all particles at the end of the simulation is shown in figure 2.34.

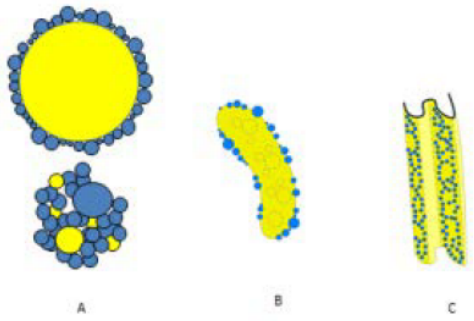

Figure 2.33: Types of OPA (from Fitzpatrick et al. 2015 [30])

All type 1 and type 3 OPAs were deposited at the end of simulation; while some of type 2 OPAs may migrate through the downstream dam. It is worth mentioning that most likely different types of OPAs have different critical bed shear stress. Also, armoring effect was not considered which meant all particles were assumed to be on the top of the river bed. They can be picked up by flow that provides larger bed shear stress than the critical bed shear stress.

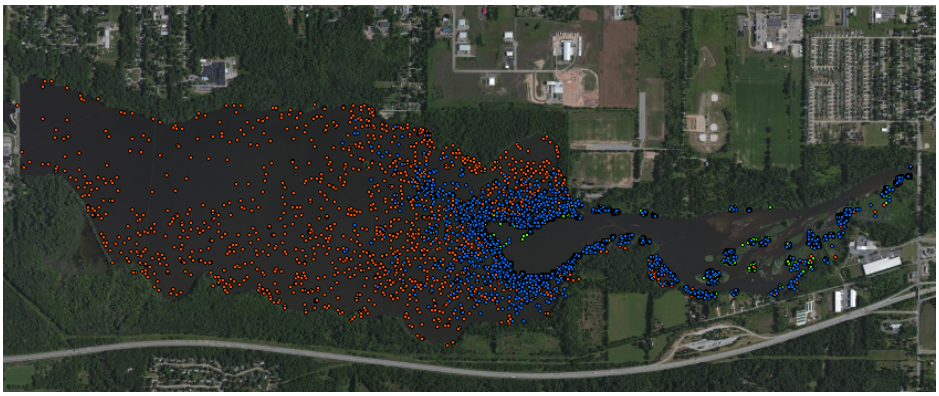

Figure 2.34: OPA Particle Locations at the end of simulation (Type 1 as green; Type 2 as red; Type 3 as blue)

July 2013 Low Flow Scenario

The same three types of OPAs as shown in the above were simulated for the July 9 -19, 2013 low flow scenario. 2000 particles of each type were released. All particles deposited in the end of the 10-day simulation. Their location is plotted in the following figures.

As shown from Figure 2.35 to Figure 2.37, more particles deposited in the delta and transport distance was less when settling velocity was bigger. Compared to the transport of OPAs in the April 2013 high flow scenario, OPAs deposited faster and more in the delta instead of migrating into the lake.

Figure 2.35: OPA Particle (Type 1) Locations at Time = 10 day (July 2013 Scenario)

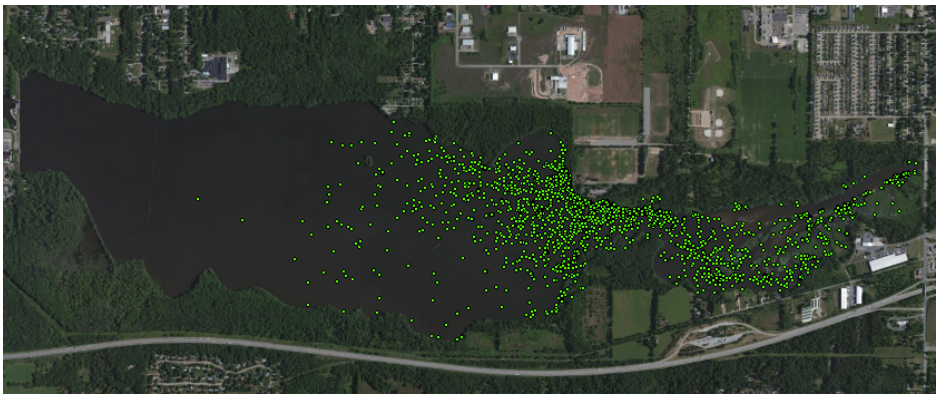

Figure 2.36: OPA Particle (Type 2) Locations at Time = 10 day (July 2013 Scenario)

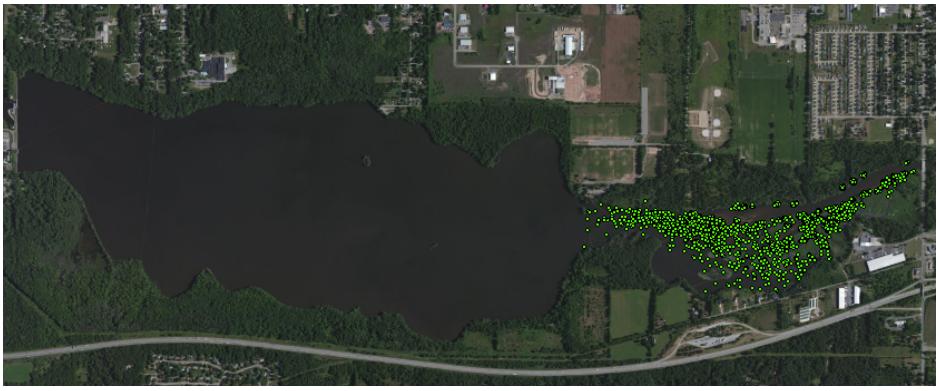

Figure 2.37: OPA Particle (Type 3) Locations at Time = 10 day (July 2013 Scenario)

2.3.7 Bed Shear Stress in a 100-yr Flood Scenario

In order to check the future risk of the mobilization of residual OPA deposits in the lake, a 100-yr flood scenario (flow discharge equals to 198 m^3/s) was tested. Given the assumption that the critical bed shear stress is 0.1 Pa, Figure 2.38 shows the distribution map of bed shear stress in Morrow Lake. With such an extreme flood event, bed shear stress in large areas of the lake exceeds 0.1 Pa, which means high possibility for residual OPAs to be re-entrained.

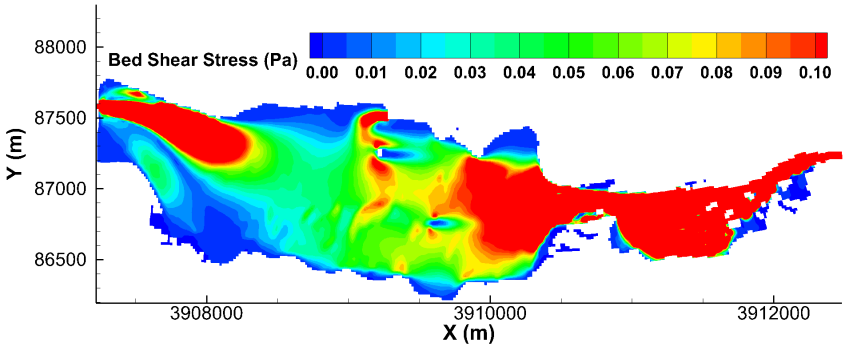

Figure 2.38: Distribution of bed shear stress in a 100-yr flood scenario

2.3.8 Discussion

OPA mostly deposited in delta during low flow events and could transport into lake when flow flux increased. This study focused on the residual deposits of oil after initial cleanup efforts so it considered only the transport of OPA, but not formation and breakup. The formation of oil droplet and interaction of oil and particles were also complicated and not taken into account. Laboratory studies have shown that OPA properties vary and each particle might have specific settling velocity and critical bed shear stress for resuspension. With the help of laboratory experiments, typical properties were chosen for this study. Also, potential armoring effects were not considered which meant all particles were assumed to be on the top of bed. They were not covered by sediment and can be entrained by turbulent flow once bed shear stress exceeded the critical bed shear stress.

Substantial residual deposits from an oil spill remain in inland waterway systems due to the formation of oil-particle aggregates. It is impor-

tant for cleanup efforts and management to understand the conditions under which the OPA becomes resuspended, transported and re-deposited. A three-dimensional Eulerian/Lagrangian model was developed for OPA transport. The 2010 Kalamazoo River oil spill was studied. The model enabled consideration of hydrodynamic effects of the dam operational rules and the wind effect. The April 2013 high flow scenario and the July 2013 low flow scenario were modeled. The model was calibrated and validated using field measurement data. The model can help to locate highly oil-contaminated areas. It is worth mentioning that subjected to increasing demand of crude oil transport, the ageing pipelines all over the world might probably run into more risks of rupture. Therefore, oil spills in inland waterways should attract more attention and researches.

2.4 Model Applications

2.4.1 Containment Scenario

The developed three-dimensional hydrodynamic model EFDC was used to simulate effects of containment on flow pattern, in particular in the Morrow Lake delta and neck areas. Containments were used to avoid oil passing downstream during dredging. Figure 2.39 shows the deployment of containments. A front view of the containment curtain in the water column is sketched in Figure 2.40. The bottom curtain is two feet high if the water depth is greater than four feet. Otherwise, it was assumed that the curtain height was half of the water depth. For describing the containment configurations, EFDC is able to simulate thin barriers which block the whole water depth. However, the curtain in this study only blocks the bottom layer. Also, the thin barrier option in EFDC can block U velocity (easting-direction velocity) and/or V velocity (northing-direction velocity). However, the directions of some containments were not parallel to either easting or northing direction. Therefore, the thin-barrier option was not suitable for this study. Further development of numerical code would be required if a half-blocking curtain with diagonal direction had to be modeled. An alternative approach was proposed herein and tested.

Although the curtain is very thin, it blocks flow in a certain direction (i.e.

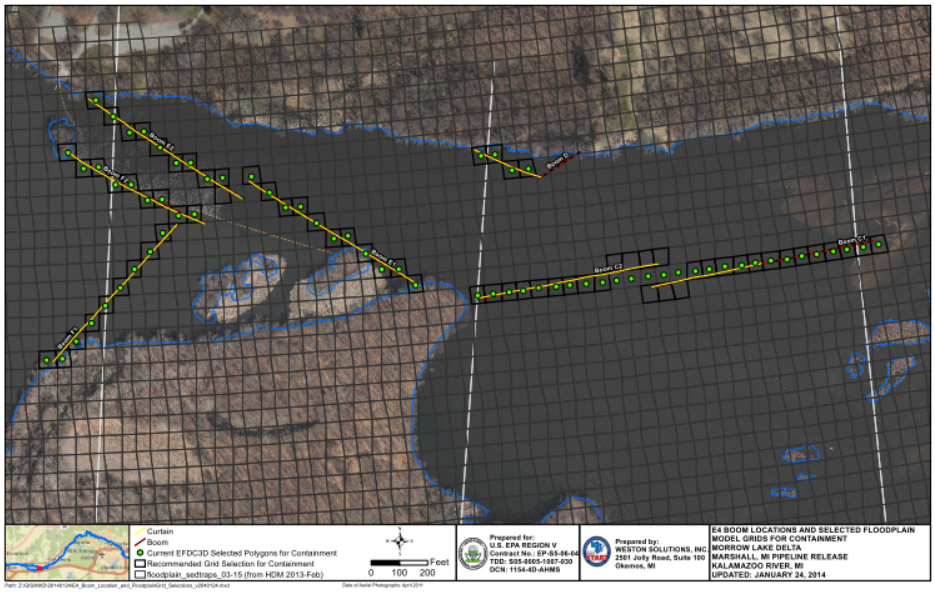

Figure 2.39: Location of Containment and Representative EFDC Grids

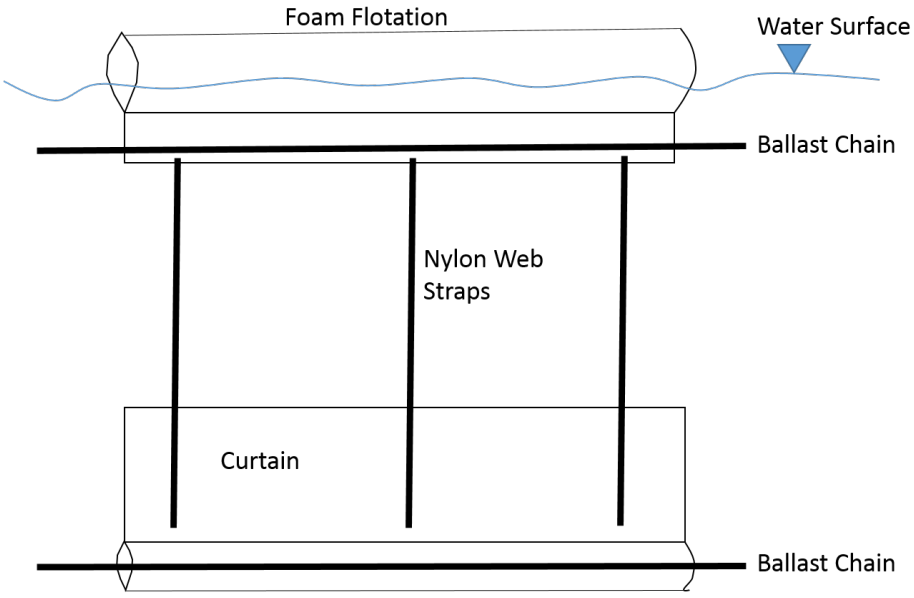

Figure 2.40: Curtain Vertical Detail

Figure 2.41: Containment Plan View

water cannot cross curtain) locally. In order to describe the curtain in EFDC, we assumed it could affect the distance of $\Delta x/2$ on both sides of the curtain where Δx was the grid size, which was around 60 feet in the current model. For example, in Figure 2.42 the blue line represents the real curtain which blocks flow crossing it. It was assumed that the effect of the curtain extends some distance away from it. In this affected area, velocity in the direction perpendicular to the curtain was negligible. Therefore those vertical cells covering the curtain from the bottom can be deleted and the upper cells can still be simulated. A drawback is that this approach does not allow results to be obtained very close to the curtain. However, from its neighbor grid cells we can at least better understand any flow pattern or bed shear stress change due to the curtain.

The curtain design was tested with a low flow of 500 cfs which corresponded to the August 27, 2012 flow when ADCP measurement data was available for comparison. Downstream water level was estimated as 775 ft. Compared to water stage level in June and July 2012, stage level in August was probably similar since outflow discharge was similar.

ADCP measurement was performed at eight cross sections (see Figure

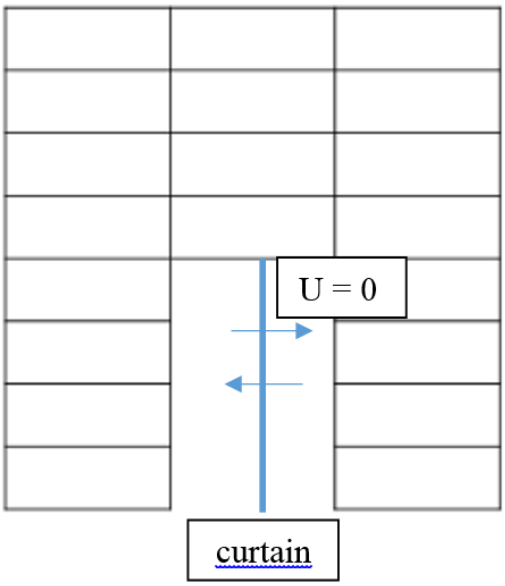

Figure 2.42: A Side View of Vertical Profile of EFDC Grids Representing Bottom Curtain

2.43). The comparison between flow discharge evaluated by ADCP and model results is summarized in Table 2.1. In general, the comparison shows good agreement at transect Dm-1, Dm-2, and Dm-3. However there is a relatively larger difference at Dm-4, Dm-7, and Dm-8 especially. The most likely reason is that the channel of Dm-8 is so narrow and was represented by only two grids in the (x, y) plane. Therefore, bathymetry and interpolation of bed elevation would highly affect the flow distribution. Similar effects by the interpolation might happen at Dm-4 and Dm-7. Possibly the estimated 500 cfs constant inflow rate and downstream stage level also somewhat affected the model results. In reality, the inflow may be different and changing in time.

The same boundary conditions were used for a simulation without containment so the difference caused by containment can be evaluated. The differences of velocity magnitude for with and without containment scenarios are presented in Figure 2.44. The comparison of model results between the scenarios with and without containment shows the effects of containment on flow distribution. Figure 2.44 shows the difference of velocity magnitude. It is worth mentioning that the judgment of whether the model approach is sufficient requires field measurement and experience. The ADCP measurement data was helpful, but there was no data for the non-containment

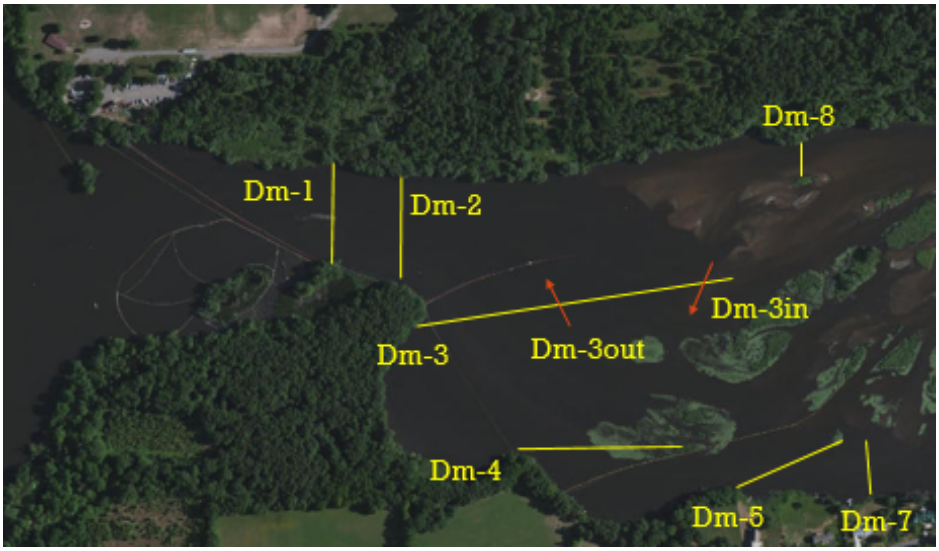

Figure 2.43: Cross-sections for Flow Discharge Check

Transect	ADCP (cfs)	Model (cfs)
Dm-1	502	500
Dm-2	517	500
Dm-3	189	172
Dm-3in		-12
Dm-3out		184
Dm-4	126	70
Dm-7	58	23
Dm-8	132	209

Table 2.1: Flow Discharge Distribution (ADCP Measurement vs. Model Results)

scenario so it was difficult to validate the effects of containment shown in the model.

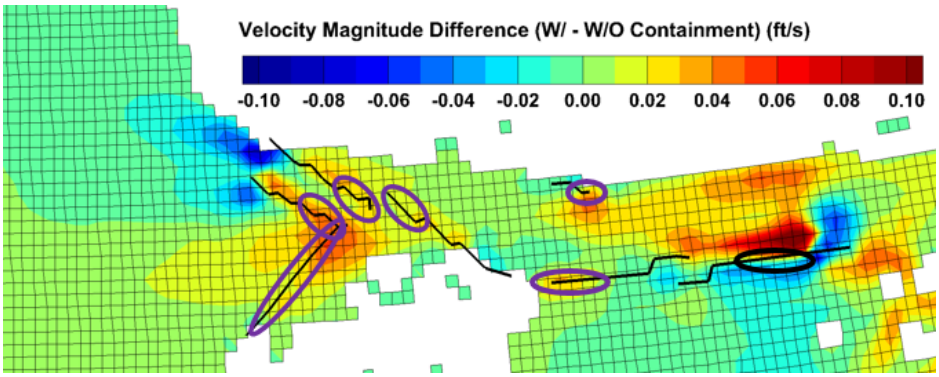

Figure 2.44: Deposition (black ellipse) and Erosion (purple ellipse) Areas with Velocity Difference between the scenarios with and without Containment

Other available data included 6 sets of bathymetry survey data on both sides of the curtains. The bathymetry survey indicated whether deposition or erosion happened on both sides of each containment. Figure 2.44 shows those areas with deposition as black ellipses and erosion areas with purple ellipses. Again it is worth pointing out that either deposition or erosion shown by the survey cannot simply be assumed to be directly caused by the containment curtains. Depending on the flow rate between survey periods, natural sediment deposition or erosion may have occurred regardless of the containment. However, according to model results, the existence of containment probably enhanced deposition or erosion by affecting velocity fields.

With the help of the numerical model, it was suggested that containment C1 and D (see Figure 2.45 for location) might be removed so that the effects on morphological change can be reduced and meanwhile the function of the containment system was not entirely eliminated. A set of simulations with inflow Q = 2320 cfs were provided. Figure 2.46 to figure 2.48 compare distributions of bed shear stress between different simulations, i.e. original containment, no D and half C1, and no C1.

2.4.2 Lake Drawdown Scenario

Another application of the developed model was to study possible drawdown scenarios of the Morrow Lake. Enbridge proposed the drawdown of the lake in

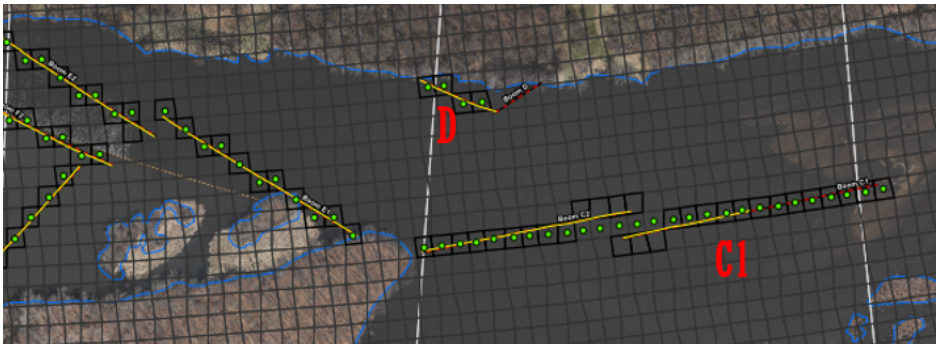

Figure 2.45: Location of Containment C1 and D

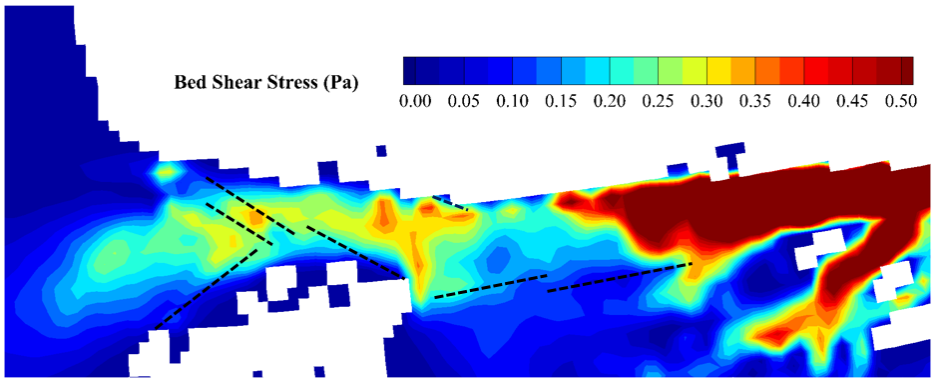

Figure 2.46: Distribution of Bed Shear Stress (with Original Containment Design)

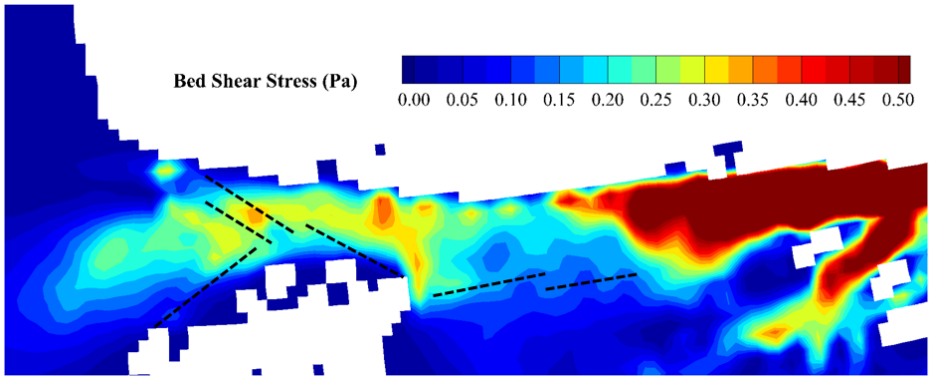

Figure 2.47: Distribution of Bed Shear Stress (without Containment D and Half C1)

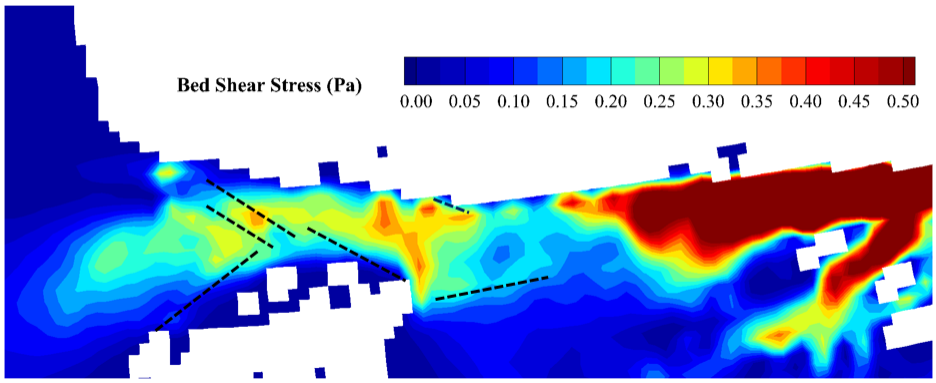

Figure 2.48: Distribution of Bed Shear Stress (without Containment C1)

order to make the excavation of the delta easier and cheaper. This model was used to evaluate how much drawdown was needed and which flow conditions were suitable for the drawdown.

According to historical flow measurement at USGS Comstock station (see Figure 2.6), the median daily mean flow between July 1st and October 31st is 585 cfs while that between November 1st and January 31st is 794 cfs. It was assumed that the initial lake level was 775.0 ft.

When flow discharge was 585 cfs, it was found that the downstream stage of 773 ft gave similar dry areas in delta to the stage of 771 ft. However, 771 ft resulted in much higher bed shear stress in lake. It was also noted that 773 ft would dramatically increase bed shear stress so the risk of OPA resuspension and transport have to be considered by decision makers.

When flow discharge increased to 794 cfs, drawdown of Morrow Lake would cause more substantial change to the bed shear stress distribution. The critical bed shear stress for OPA is around 0.1 Pa. Therefore, drawdown of Morrow Lake could highly increase the possibility of passing OPA through the downstream dam.

Finally, it should be noted that the numerical model can help to compute how much outflow discharge is needed in order to decrease lake stage level with a certain speed; the bed shear stresses in this transient drawdown condition could be readily determined.

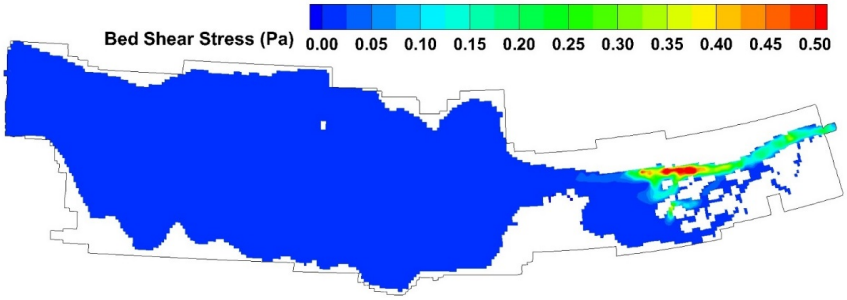

Figure 2.49: Distribution of Bed Shear Stress (Q = 585 cfs; DS Level = 775 ft)

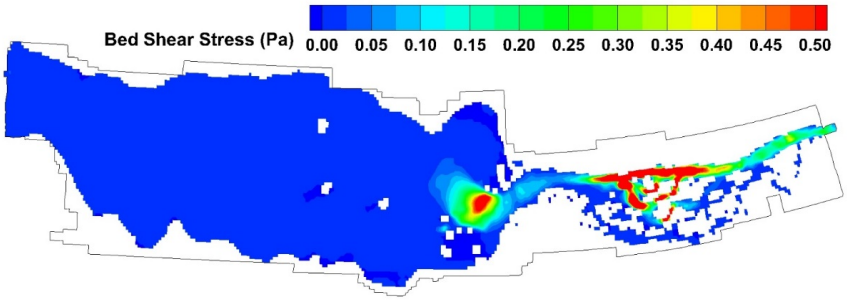

Figure 2.50: Distribution of Bed Shear Stress (Q = 585 cfs; DS Level = 773 ft)

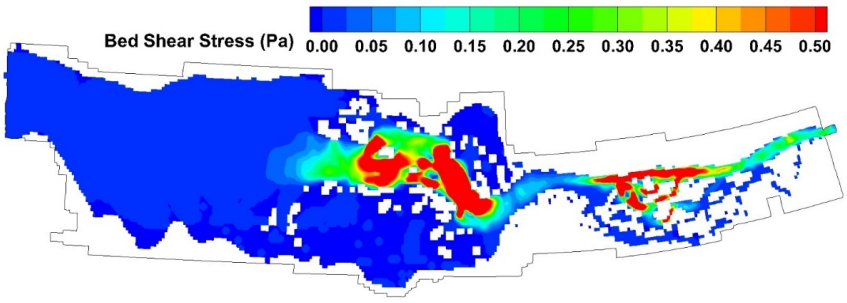

Figure 2.51: Distribution of Bed Shear Stress (Q = 585 cfs; DS Level = 771 ft)

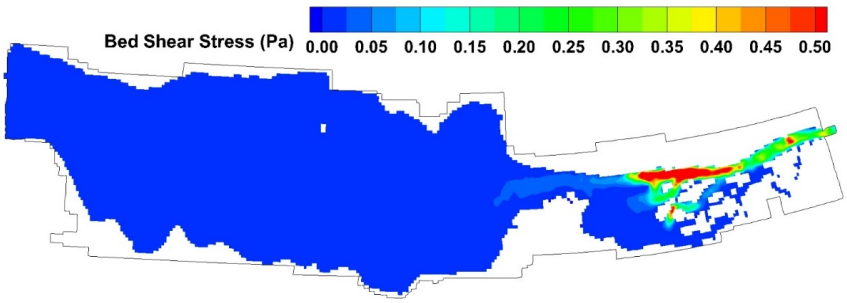

Figure 2.52: Distribution of Bed Shear Stress (Q = 794 cfs; DS Level = 775 ft)

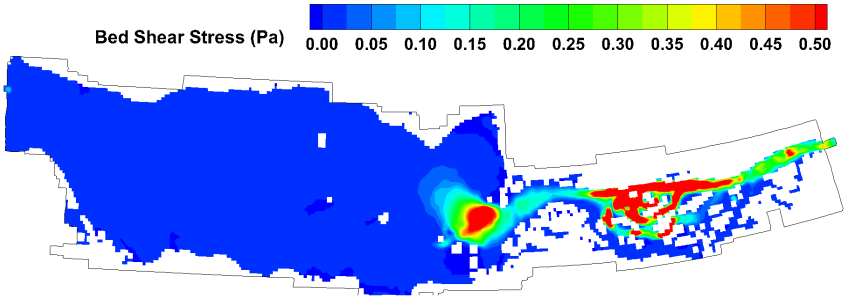

Figure 2.53: Distribution of Bed Shear Stress (Q = 794 cfs; DS Level = 773 ft)

CHAPTER 3

MODELING OF SELECTED SEDIMENT TRAPS IN KALAMAZOO RIVER, MICHIGAN

Following the oil spill at Kalamazoo River waterways system in 2010, extensive oil cleanup and environmental remediation efforts have taken place. Sediment traps, e.g. cutoff channel and meanders, are very critical areas for the cleanup work and future management because high concentrations of oil-particle aggregates (OPA) can be expected to deposit there.

Among many sediment traps in the waterways, three sediment traps were selected for modeling, namely MP10.4& 10.5, MP14.75, and MP21.5, because of their importance and representativeness. Figure 3.1 shows the location and geomorphic features of the sediment traps. MP10.5 has a backwater channel; MP14.75 has bifurcation and confluence channels; and MP21.5 is an oxbow.

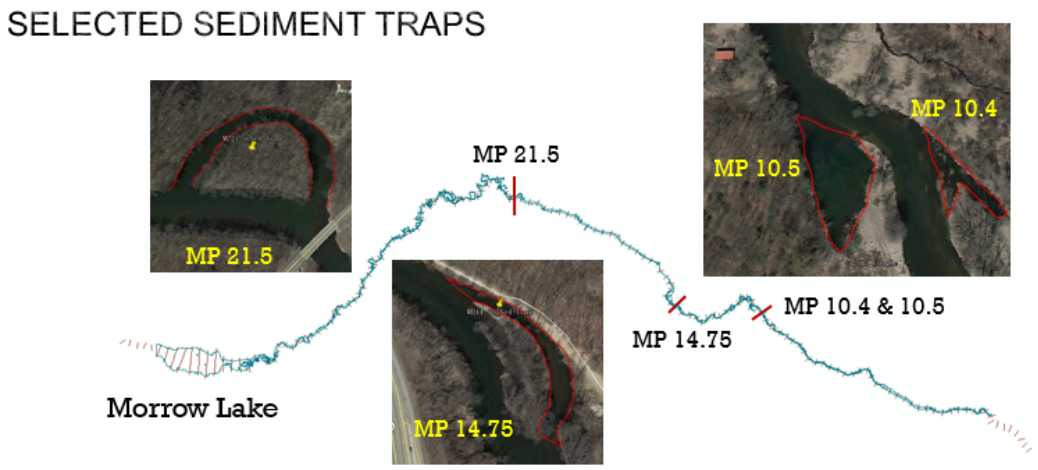

Figure 3.1: Location of Modeled Sediment Traps

Numerical models are built for covering the three river sections (numerical domains). The models facilitated our understanding of the physics of OPA transport in response to flow fields in different kinds of channels. The April 2013 high flow and July 2013 low flow scenarios were simulated. By comparing results obtained from the models to submerged oil survey data, good

agreement was revealed with respect to areas containing heavy amounts of submerged oil, indicating that the models are useful tools for future management and other purposes.

3.1 Description of the 2D Model HydroSed2D

An in-house code developed at Ven Te Chow Hydrosystems Laboratory, HydroSed2D, was used in this study. HydroSed2D was developed as a coupled two-dimensional shallow water model and bedload sediment transport model [35]. Zhu (2011) implemented suspended sediment transport into HydroSed2D [36]. The model has been tested and applied to many studies helping to understand sediment transport problems [37, 38, 39]. The continuity and momentum conservation equations are described in the following.

$$\frac{\partial h}{\partial t} + \frac{\partial (hU)}{\partial x} + \frac{\partial (hV)}{\partial y} = 0 \tag{3.1}$$

$$\frac{\partial (hU)}{\partial t} + \frac{\partial (hUU)}{\partial x} + \frac{\partial (hUV)}{\partial y} - \nu \left(\frac{\partial^2 (hU)}{\partial x^2} + \frac{\partial^2 (hU)}{\partial y^2} \right) = -gh\frac{\partial h}{\partial x} - \frac{\tau_b^1}{\rho} + hfV \tag{3.2}$$

$$\frac{\partial (hV)}{\partial t} + \frac{\partial (hVU)}{\partial x} + \frac{\partial (hVV)}{\partial y} - \nu \left(\frac{\partial^2 (hV)}{\partial x^2} + \frac{\partial^2 (hV)}{\partial y^2} \right) = -gh\frac{\partial h}{\partial y} - \frac{\tau_b^2}{\rho} - hfU \tag{3.3}$$

where h is water depth; (U, V) are depth-averaged velocities in x and y directions, respectively; ν is water viscosity; g is the gravitational acceleration; τ_b^1 and τ_b^2 are bed shear stresses in x and y directions, respectively; and f is the Coriolis parameter.

There are two methods existing in the model to compute bedload transport: Grass formula [40] and Meyer-Peter and Muller formula [41].

3.1.1 Bedload Transport Equations

Grass Formula

$$q_{sx} = AU\left(U^2 + V^2\right)^{\frac{m-1}{2}} \tag{3.4}$$

$$q_{sy} = AV\left(U^2 + V^2\right)^{\frac{m-1}{2}} \tag{3.5}$$

where q_{sx} and q_{sy} are bedload sediment fluxes in x and y directions, respectively; A and m are empirical parameters. For fine sand, $A = 0.001$ and $m = 3$ are recommended.

Advantage of the Grass method is that this method can be easily used in numerical models, because it directly links the bed transport rates to velocities by applying the parameters, A and m. Problems of this method may be the uncertainties and difficulties in the evaluation of the parameters A and m. Also, in this method, as long as the velocities are larger than zero, there will always be sediment bed load transport, thus, threshold condition for sediment movement cannot be considered using Grass method.

Meyer-Peter and Muller Formula

$$\frac{\mathbf{q_b}}{D\sqrt{gRD}} = 8\left(max\left(\frac{\tau_\mathbf{b}}{\rho gRD} - \tau_c^*, 0\right)\right)^{3/2} \tag{3.6}$$

where $\mathbf{q_b} = (\mathbf{q_{sx}}, \mathbf{q_{sy}})$ represents bedload sediment fluxes; D is the sediment grain size; $R = \rho_s/\rho - 1$; ρ_s and ρ are densities of sediment and fluid, respectively; $\tau_c^* = 0.047$ is non-dimensional critical shear stress.

3.1.2 Suspended Load Transport Equations

The 2D depth-averaged equation for suspended transport can be expressed as follows:

$$\begin{aligned}\frac{\partial(hC)}{\partial t} + \frac{\partial(hUC)}{\partial x} + \frac{\partial(hVC)}{\partial y} = \frac{\partial}{\partial x}\left(hD_{xx}\frac{\partial C}{\partial x}\right) + \frac{\partial}{\partial y}\left(hD_{yy}\frac{\partial C}{\partial y}\right) \\ + \frac{\partial}{\partial x}\left(hD_{xy}\frac{\partial C}{\partial y}\right) + \frac{\partial}{\partial y}\left(hD_{yx}\frac{\partial C}{\partial x}\right) + v_s\left(E_s - c_b\right) + Q_c\end{aligned} \tag{3.7}$$

where C is the depth-averaged concentration of suspended sediment; D_{xx}, D_{yy}, D_{xy} and D_{yx} are the components of generalized effective diffusion tensor; v_s is the sediment fall velocity which relates to the size of the sediment particles; Q_c is external source term; E_s represents entrainment rate; and C_b represents near-bed concentration of suspended sediment which relates to settling rates, $C_b = r_o C$. r_o is a parameter to relate near-bed concentration to depth-averaged concentration. It can be estimated as 2.0, or computed by the following expression [42]:

$$r_o = 1 + 31.5\left(\frac{u_*}{v_s}\right)^{-1.46} \tag{3.8}$$

where u_* is the shear velocity.

The sediment entrainment rate E_s can be estimated according to García and Parker [43, 44]:

$$E_s = \frac{\mathrm{A} Z_u^5}{1 + \frac{A}{0.3} Z_u^5} \tag{3.9}$$

where the empirical constant $A = 1.3 \times 10^{-7}$.

$$Z_u = \frac{u_{*s} R_{ep}^{0.6}}{v_s} \tag{3.10}$$

where u_{*s} is the shear velocity associated with skin friction; and for fine-grained non-cohesive sediments and $R_{ep} = \frac{D\sqrt{gRD}}{\nu} < 3.5$,

$$Z_u = 0.708 \frac{u_*}{v_s} R_{ep}^{0.6} \tag{3.11}$$

where u_* is shear velocity, $u_* = \sqrt{C_f \left(U^2 + V^2\right)}$; C_f is the dimensionless friction coefficient.

3.1.3 River Morphological Equation

The 2D Exner's equation is used herein to calculate the river morphological changes due to the sediment transport.

$$\left(1 - \lambda_p\right) \frac{\partial z}{\partial t} + \left(\frac{\partial q_{sx}}{\partial x} + \frac{\partial q_{sy}}{\partial y}\right) = v_s \left(c_b - E_s\right) \tag{3.12}$$

where λ_p is the bed porosity.

In this study, the scope of the Hydrosed2D/sediment trap modeling was limited to use of the model to simulate hydrodynamic conditions only for two of the sediment trap areas (e.g., MP10.5 and MP21.5), while the hydrodynamic and sediment transport simulations were performed for the third area (MP14.75). Mannings coefficient n = 0.03 was used as a constant for all three sediment traps.

3.2 Computational Meshes

The model used finite volume method and unstructured triangular meshes. Unlike structured meshes, unstructured triangular meshes allow modelers to deal with complex geometry. The computational meshes of the three sediment traps are shown in figures 3.2, 3.3, and 3.4. The number of computational grids is 1944, 23272, and 9606, respectively. The mesh size for all the three sediment traps is five meters. The boundaries of MP 10.4& 10.5 and MP 21.5 domains are the boundaries of bankful channel; while the boundary of MP 14.75 domain is the boundary of the 100-year floodplain.

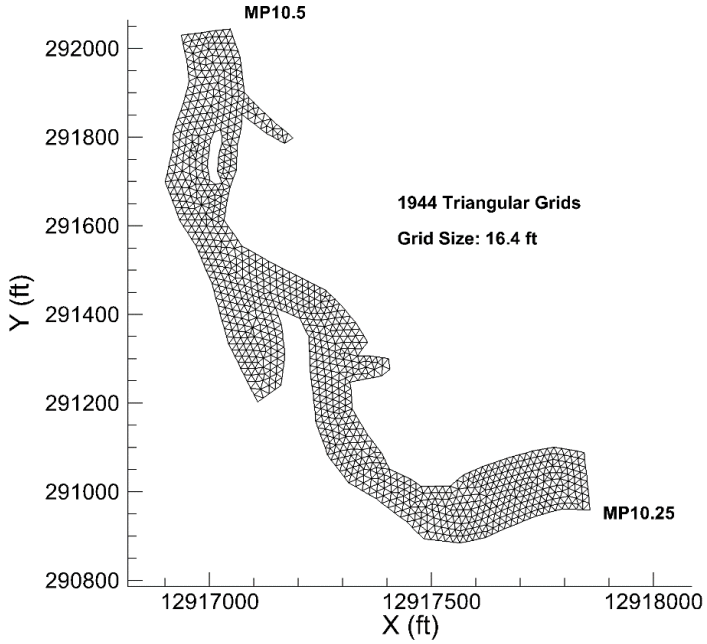

Figure 3.2: Computational Meshes of MP 10.4 & 10.5 Sediment Trap

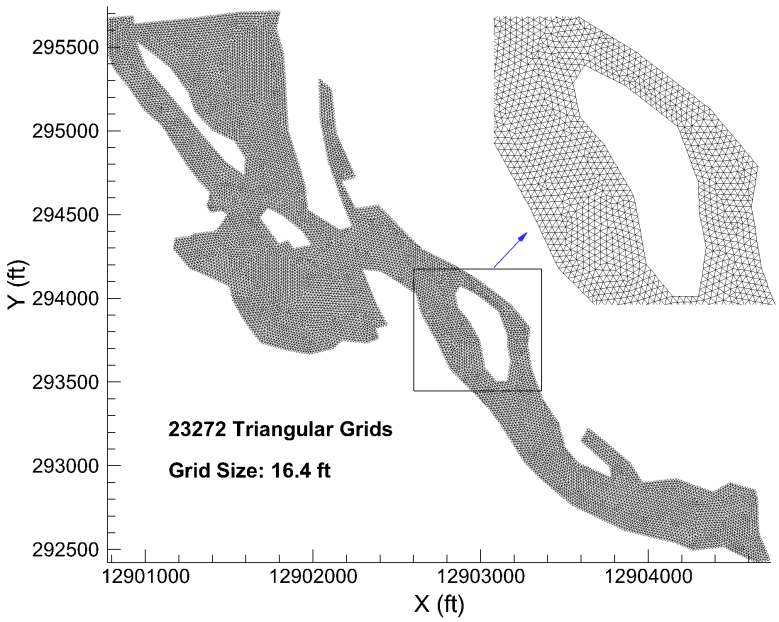

Figure 3.3: Computational Meshes of MP 14.75 Sediment Trap

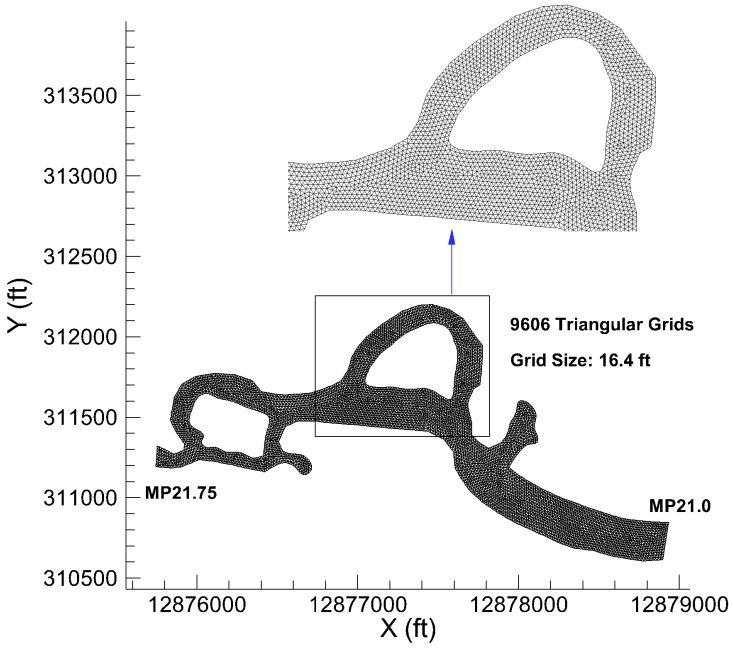

Figure 3.4: Computational Meshes of MP 21.5 Sediment Trap

3.3 Bathymetry

The bathymetry data of the three sediment traps was provided by Weston Solutions, Inc. River bed elevation was interpolated to the center of each grid. The interpolated bed elevation of three sediment traps is shown in figures 3.5, 3.6, and 3.7.

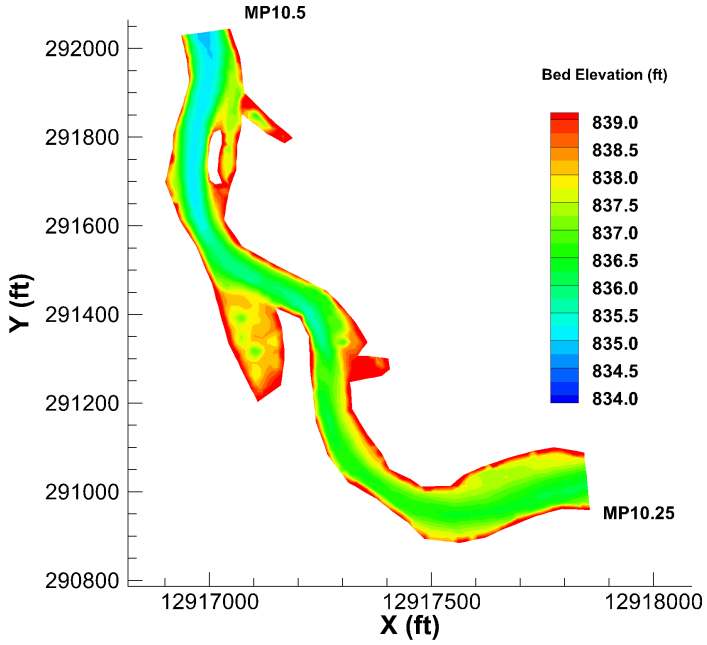

Figure 3.5: Bed Elevation of River and Floodplain at MP 10.4& 10.5 Sediment Trap

3.4 Model Scenarios and Boundary Conditions

Scenarios of April 2013 and July 2013 were simulated as representative scenarios of high flow and low flow, respectively. Figure 3.8 shows the historical flow record (1933-2013) at a USGS gauging station located downstream of Morrow Lake. It indicates that the peak of the April 2013 flow is higher than the 95th percentile of daily mean value for those dates in the last 80 years and the July 2013 flow is slightly under the median daily mean value in July, which is the period of the lowest flow discharge within a year. The April

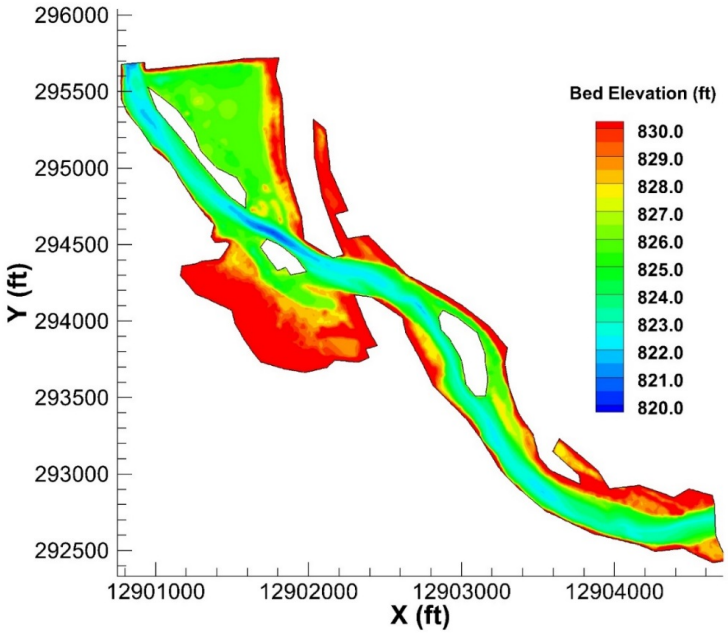

Figure 3.6: Bed Elevation of River and Floodplain at MP 14.75 Sediment Trap

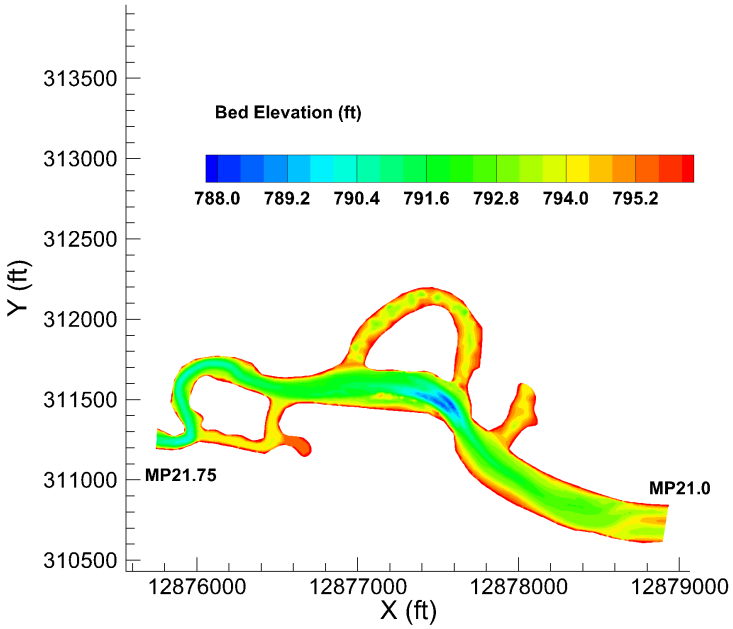

Figure 3.7: Bed Elevation of River and Floodplain at MP 21.5 Sediment Trap

2013 high flow has a flood exceedance probability of 4% (25-yr recurrence interval).

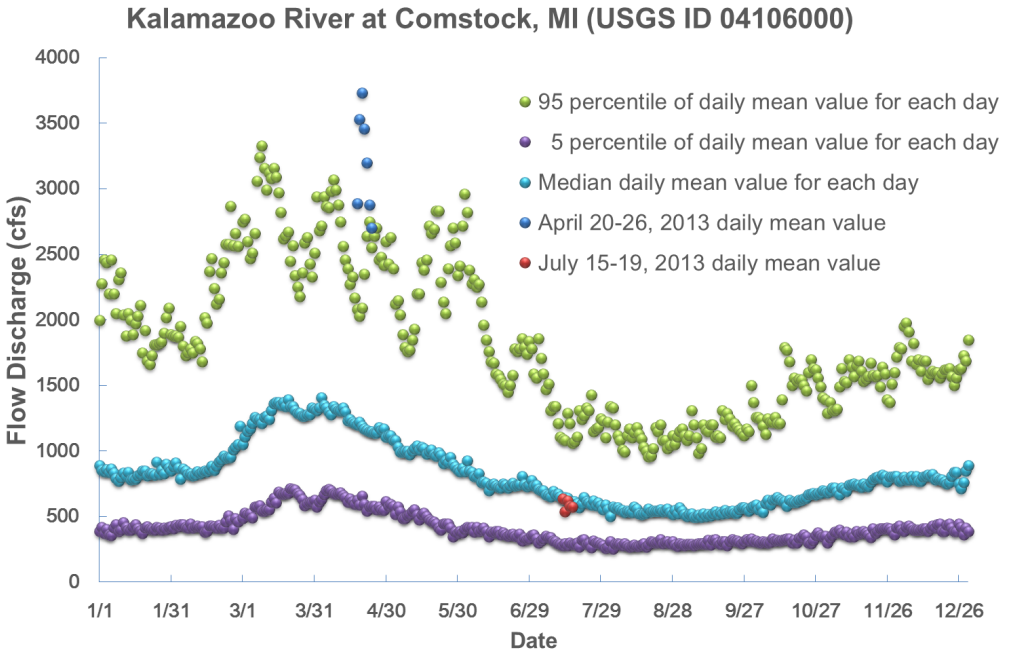

Figure 3.8: Flow Statistics for the Kalamazoo River at Comstock, MI (based on 1933-2013 data)

For each sediment trap simulation, upstream flow discharge and downstream water stage level were extracted from the LimnoTech-EFDC2D model [45] and used as boundary conditions. They are shown in Figure 3.9 to Figure 3.14.

3.5 Results of MP 10.4& 10.5 Sediment Trap Model

3.5.1 Distribution of Depth-Averaged Velocity Magnitude

Figure 3.15, Figure 3.16, and Figure 3.17 show examples of the depth-averaged velocity magnitude under high flow (April 2013) and low flow (July 2013) scenarios. There were two peaks in the April 2013 scenario (see Figure 3.9) and both of them are plotted. The dry water depth was defined as 0.1 meter, i.e. 0.33 ft. Under the high flow condition, it is shown that low velocities are present in sediment traps MP10.4 and MP10.5. Also, there is

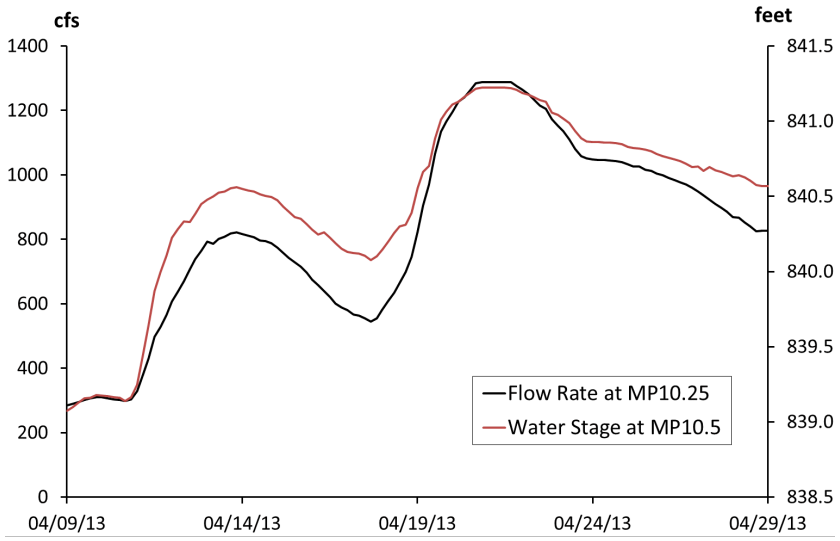

Figure 3.9: Boundary Conditions of April 9-29, 2013 at MP 10.4& 10.5 Sediment Trap

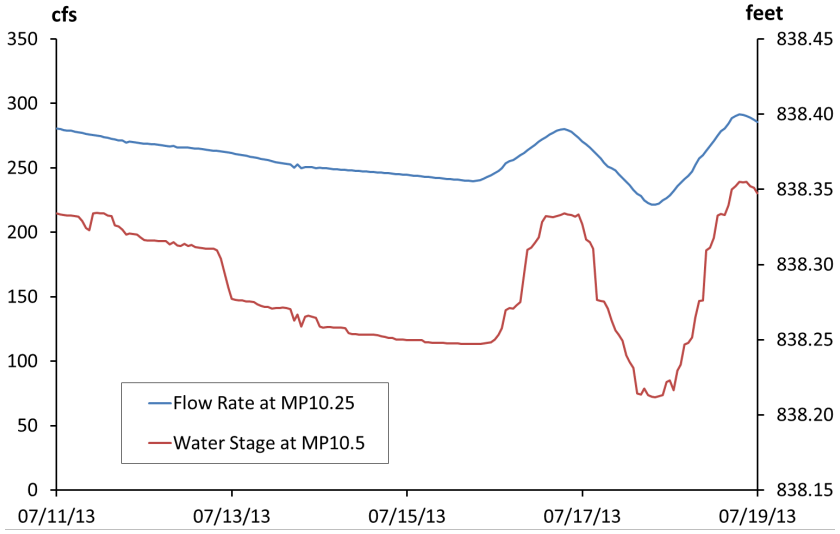

Figure 3.10: Boundary Conditions of July 11-19, 2013 at MP 10.4& 10.5 Sediment Trap

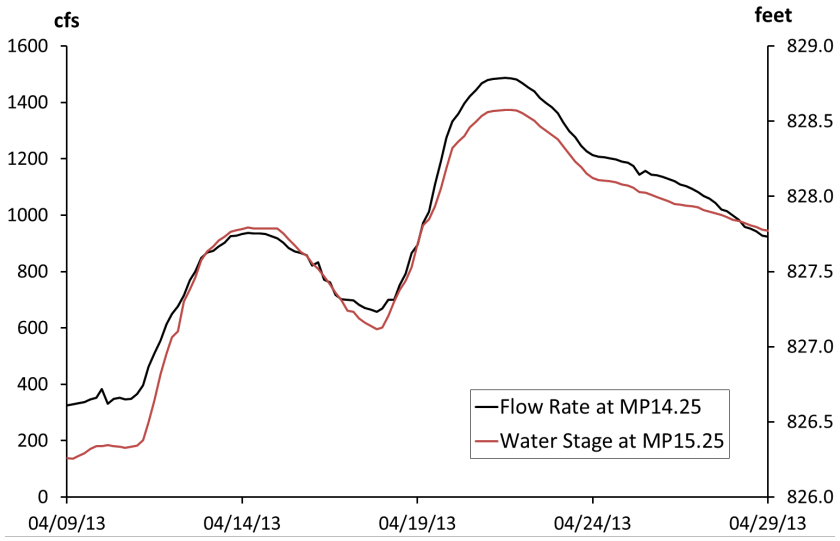

Figure 3.11: Boundary Conditions of April 9-29, 2013 at MP 14.75 Sediment Trap

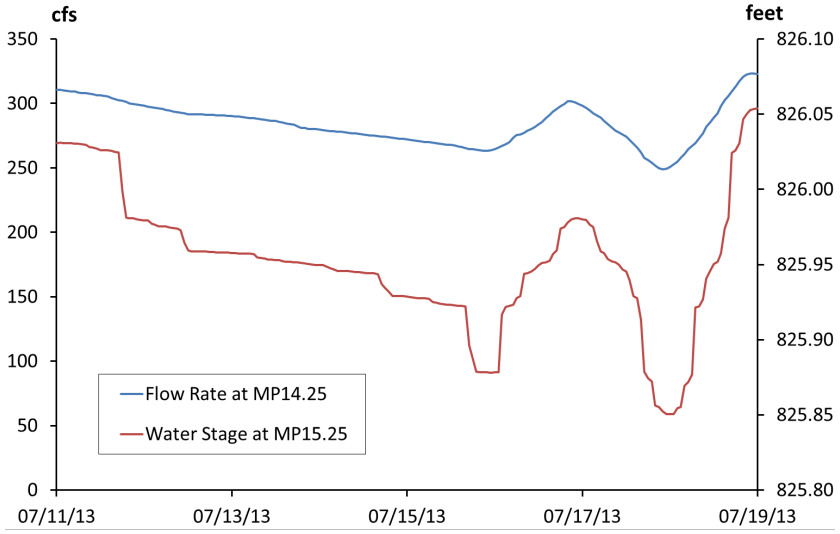

Figure 3.12: Boundary Conditions of July 11-19, 2013 at MP 14.75 Sediment Trap

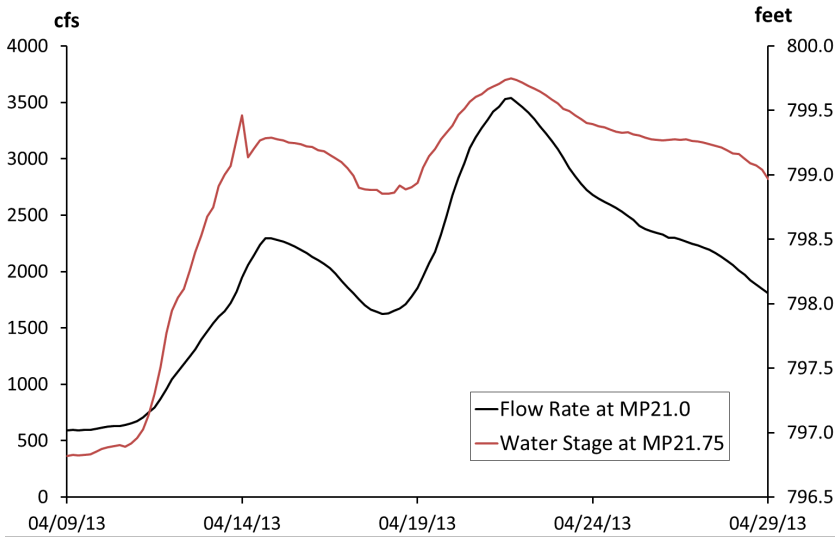

Figure 3.13: Boundary Conditions of April 9-29, 2013 at MP 21.5 Sediment Trap

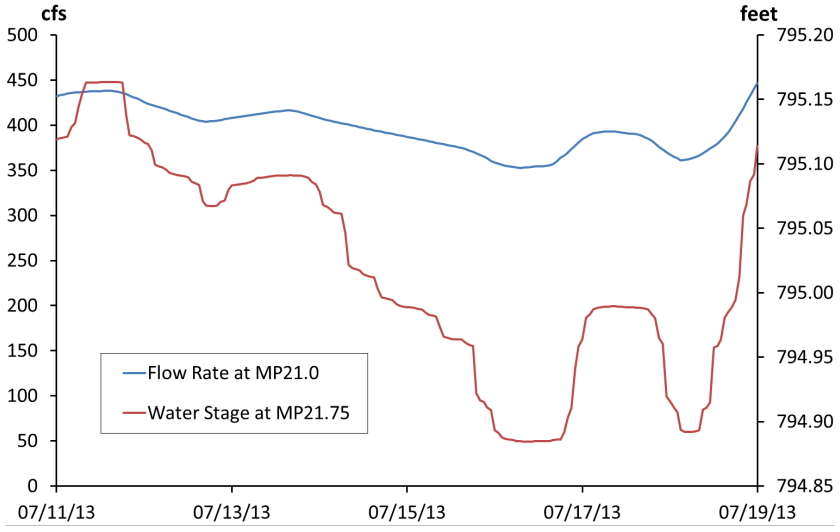

Figure 3.14: Boundary Conditions of July 11-19, 2013 at MP 21.5 Sediment Trap

a bifurcation channel along the right descending bank north of the sediment traps where velocities are low. However, under the low flow condition, water is constrained in the main channel. The absence of model results shown in the Figure 3.17 indicates that the simulated water depths were below the minimum model threshold of 10 cm or 0.3 ft. While water below this minimum depth may be present, significant new contributions of water or sediment to the sediment traps are unlikely under these very low flow conditions. The simulations showed that flows and therefore OPAs can enter the trap areas during high flow periods and remain there because of the low velocities and bed shear stress found in those depositional areas.

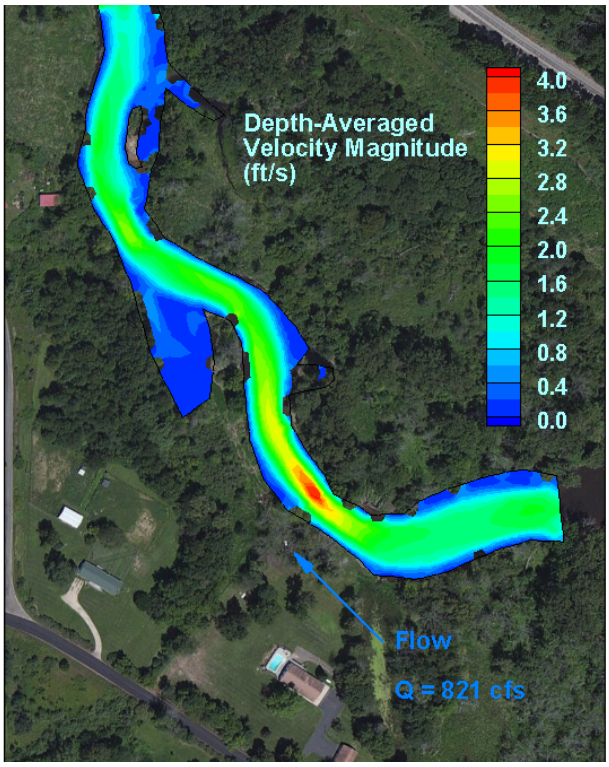

Figure 3.15: Distribution of Velocity Magnitude (MP10.4& 10.5, 20:00 April 13, 2013)

The depositional areas according to field poling results in this domain are shown in Figure 3.18 [46]. The poling results show qualitative description of oiled sediment as heavy (red), moderate (orange), light (yellow), and none (blue) in the sediment traps modeled at MP 10.5 site. The reason for deposition is flow recirculation and the loss of sediment transport capacity. The OPAs enter those recirculation zones where flow velocities are so small that

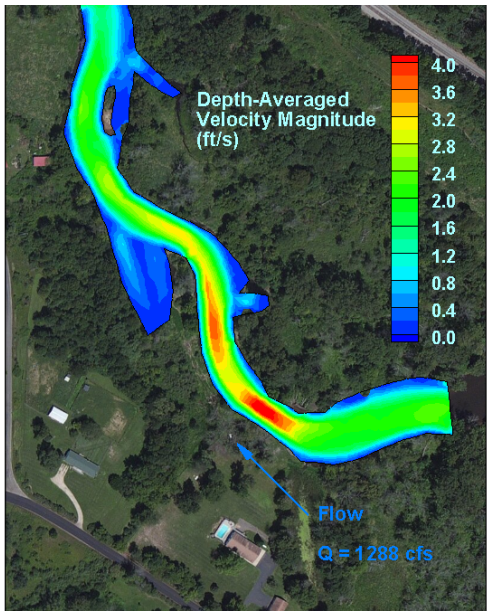

Figure 3.16: Distribution of Velocity Magnitude (MP10.4& 10.5, 8:00 April 21, 2013)

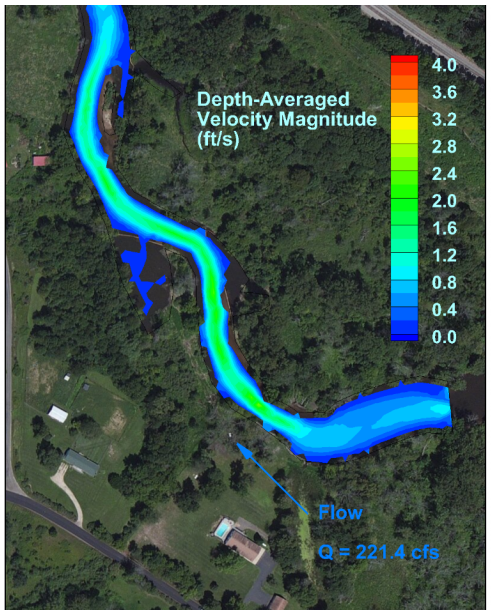

Figure 3.17: Distribution of Velocity Magnitude (MP10.4& 10.5, 20:00 July 17, 2013)

it cannot keep OPAs in resuspension. Moreover, recirculation of flow does not allow OPAs to move out of those zones so they will deposit. Figure 3.19 shows the flow path of the numerical simulation.

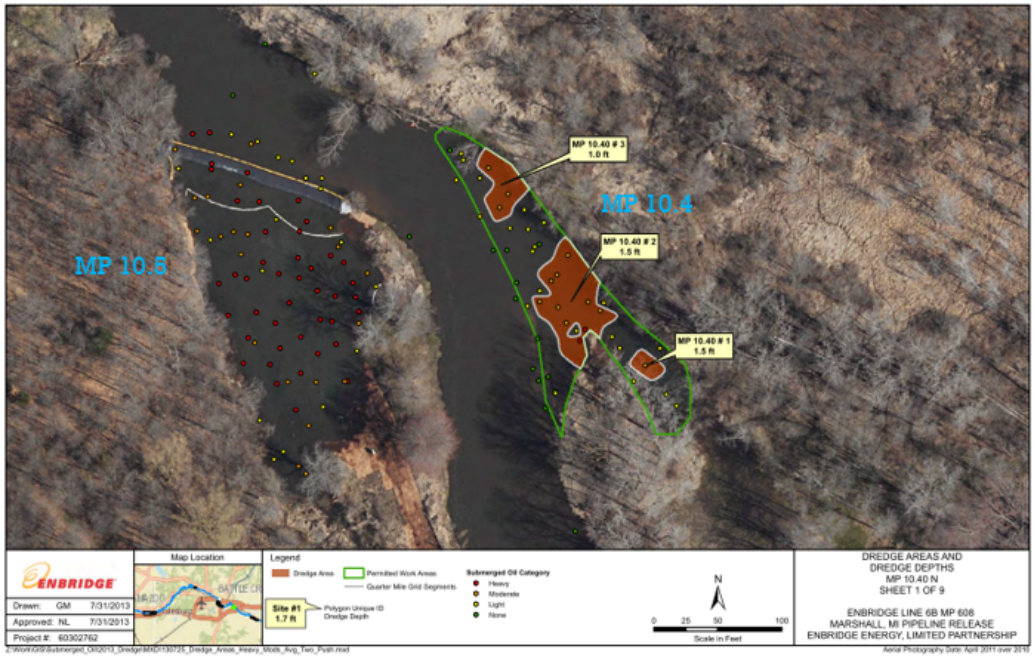

Figure 3.18: Survey of Submerged Oil in the Modeling Domain of MP 10.4& 10.5 [46]

Once the OPAs are entrained into the recirculation zone, the majority are expected to deposit before being re-entrained into the main channel. The west recirculation zone (see Figure 3.19) could be easily recognized. The east recirculation zone also has the potential to be net depositional. It is also noted that there is another recirculation zone downstream which indicates possible deposition of OPAs.

3.5.2 Distribution of Bed Shear Stress

Figure 3.20, Figure 3.21, and Figure 3.22 show distributions of bed shear stress under high and low flow scenarios, respectively. Similar to the velocity magnitude shown above, the bed shear stress in the main channel is higher than that in the sediment traps and an east side channel further downstream during high flow events.

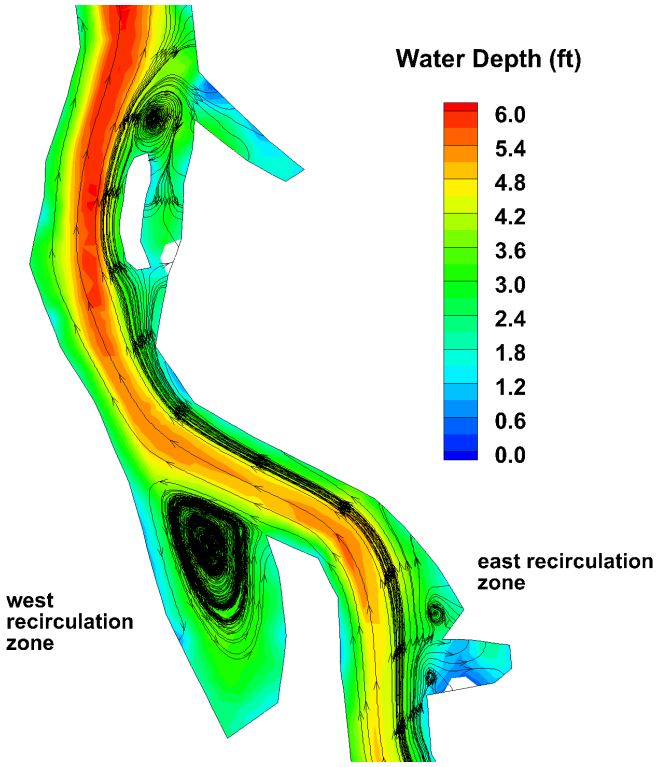

Figure 3.19: Flow Path and Recirculation Zones (MP10.4& 10.5, 8:00 April 21, 2013)

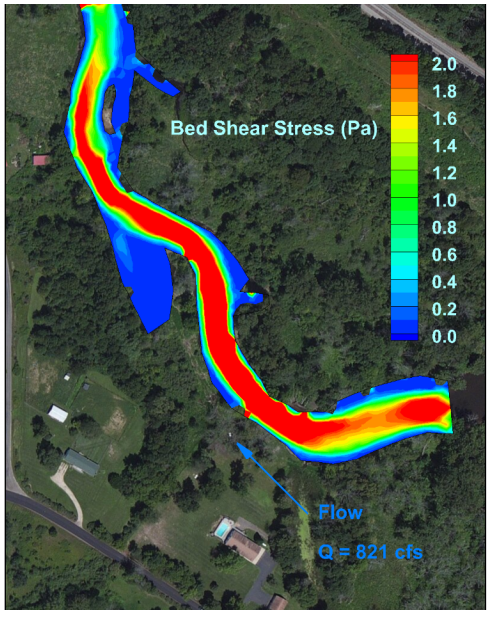

Figure 3.20: Distribution of Bed Shear Stress (MP10.4& 10.5, 20:00 April 13, 2013)

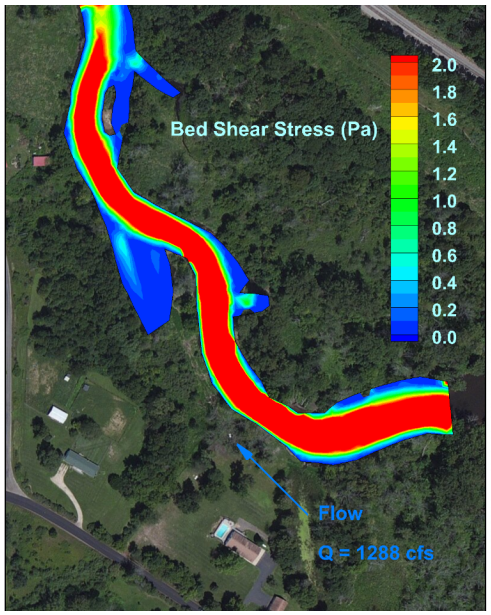

Figure 3.21: Distribution of Bed Shear Stress (MP10.4& 10.5, 8:00 April 21, 2013)

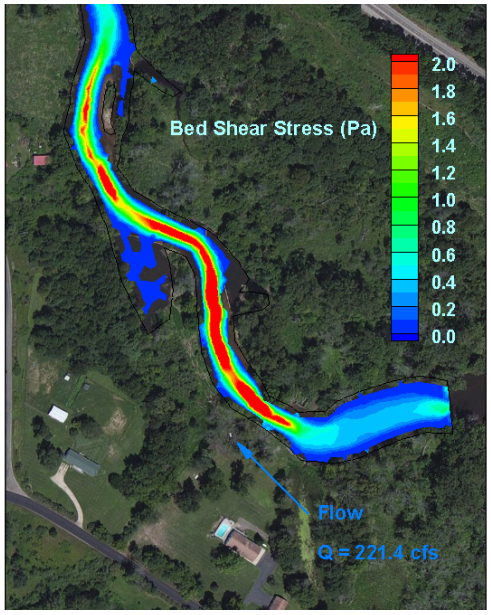

Figure 3.22: Distribution of Bed Shear Stress (MP10.4& 10.5, 20:00 July 17, 2013)

3.6 Results of MP 14.75 Sediment Trap Model

3.6.1 Distribution of Depth-Averaged Velocity Magnitude

Figure 3.23 and Figure 3.24 show the depth-averaged velocity magnitude of two flow peaks in the April 2013 high flow scenario. At the first bifurcation, more water flows into the main channel than the side channel; while at the second bifurcation velocity in the north channel is larger than that in the south channel. Figure 3.25 and Figure 3.26 show more detailed flow path at those two bifurcations with the flow discharge of 1332 cfs.

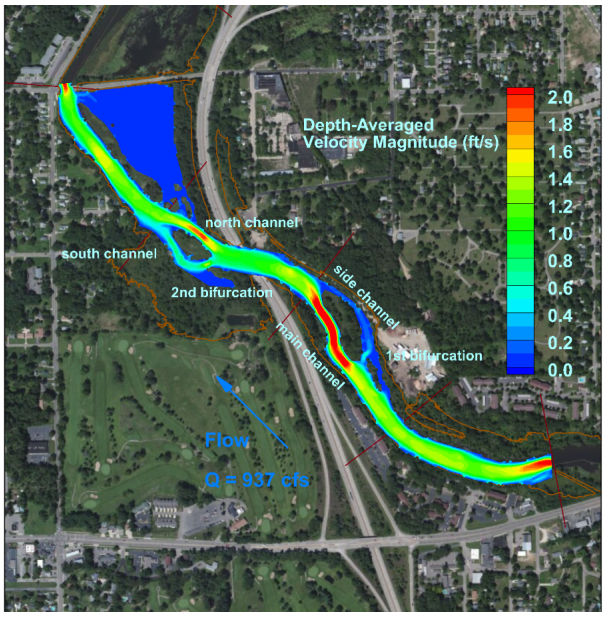

Figure 3.23: Distribution of Velocity Magnitude (MP14.75, 4:00 April 14, 2013)

Figure 3.27 shows an example of the velocity distribution in the July 2013 low flow scenario. The discharge was 298 cfs at 0:00 on July 12, 2013. The difference between the velocity magnitude and inundation areas between the two scenarios is evident. HydroSed2D model is capable of simulating wetting and drying automatically. The important characteristic of this sediment trap is the channel bifurcation (where flow separates) and confluence (where flow joins together). Sediment deposition and erosion occurs due to the distribution of flow discharge and the change of velocities as well as bed shear stress. Figure 3.27 shows that during low flows the flow follows the main channel only, so that no water and sediment can flow into the bifurcation channel.

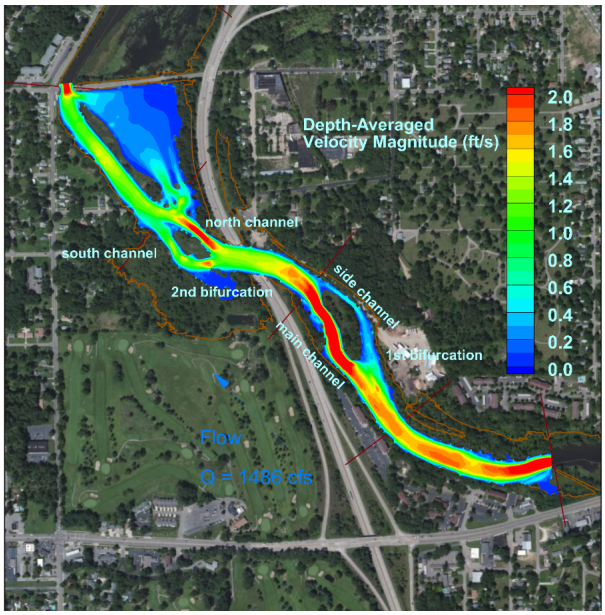

Figure 3.24: Distribution of Velocity Magnitude (MP14.75, 12:00 April 21, 2013)

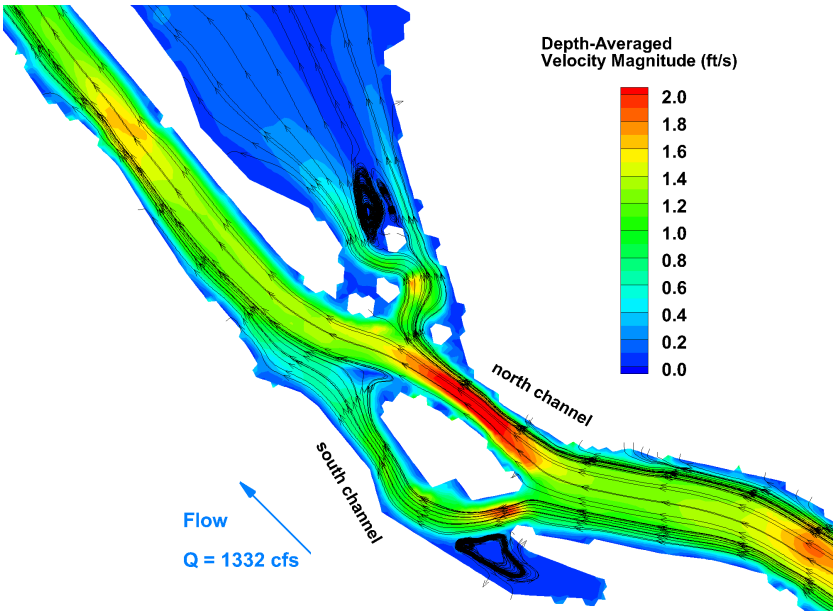

Figure 3.25: Flow Path at 2nd Bifurcation and Confluence (MP14.75, 0:00 April 20, 2013)

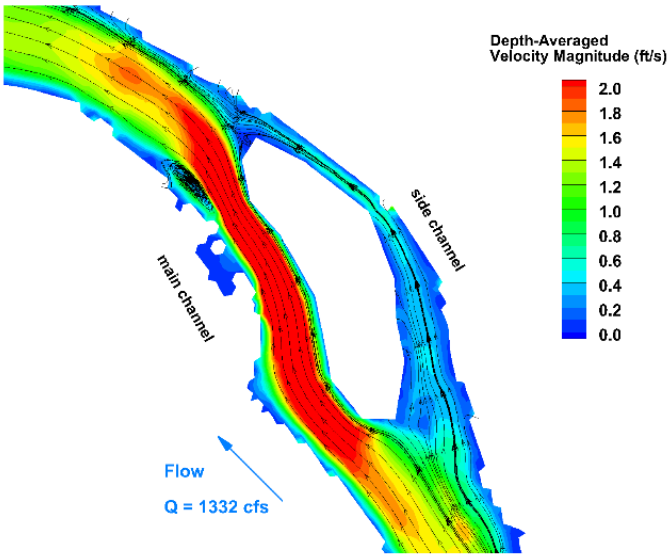

Figure 3.26: Flow Path at 1st Bifurcation and Confluence (MP14.75, 0:00 April 20, 2013)

Also, the sediment load is usually so low that not much morphological change happens.

Figure 3.24 shows that at the first bifurcation more water flows through the main channel than the side channel. Flow velocities and bed shear stress are much lower in the side channel (see Figure 3.29). Sediment can be expected to deposit due to reduced flow velocity and associated gradient in bed shear stress and sediment transport capacity. At the second bifurcation, more water flows into the north channel, but the south channel flow velocity is not reduced as much as the first bifurcation. There is a low-velocity zone at the confluence where sediment may deposit. Also, there is a dead zone at the south end of the south bifurcation channel which is also a potential deposition area. Immediately after the second confluence, there is another small side channel which bypasses some of the flow into a large floodplain, where deposition would occur due to much lower velocities.

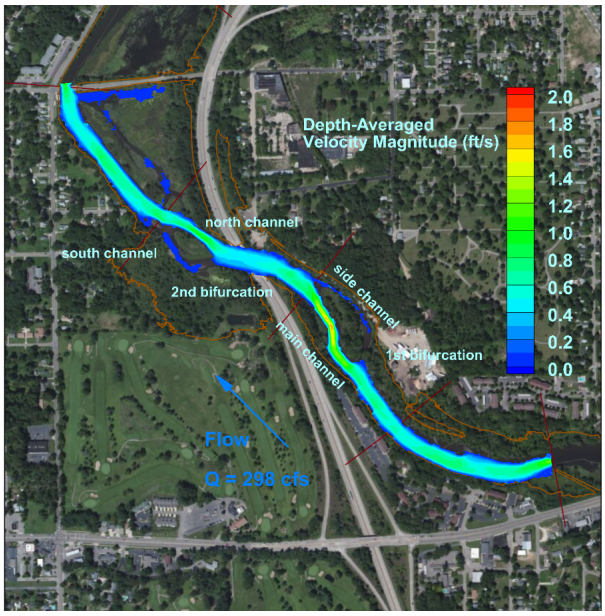

Figure 3.27: Distribution of Velocity Magnitude (MP14.75, 0:00 July 12, 2013)

3.6.2 Distribution of Bed Shear Stress

Similarly to the above depth-averaged velocity plots, Figure 3.28, Figure 3.29, and Figure 3.30 show distributions of bed shear stress under high and low flow scenarios.

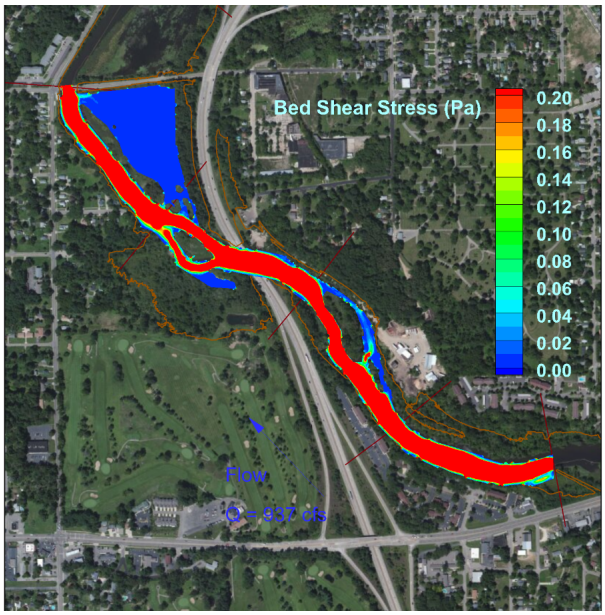

Figure 3.28: Distribution of Bed Shear Stress (MP14.75, 4:00 April 14, 2013)

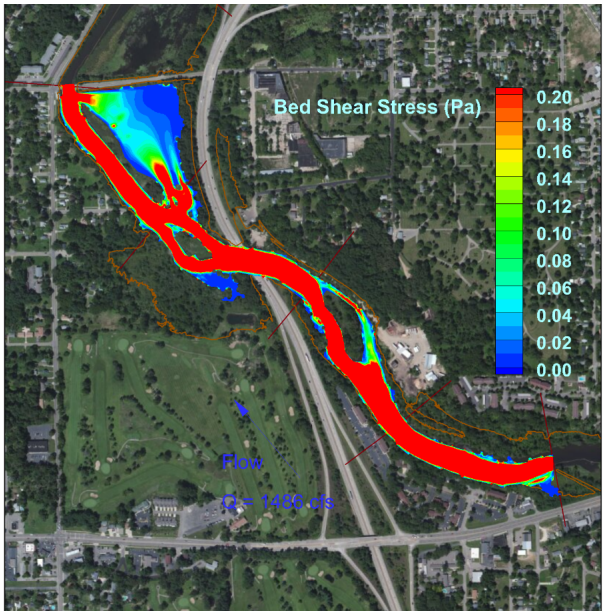

Figure 3.29: Distribution of Bed Shear Stress (MP14.75, 12:00 April 21, 2013)

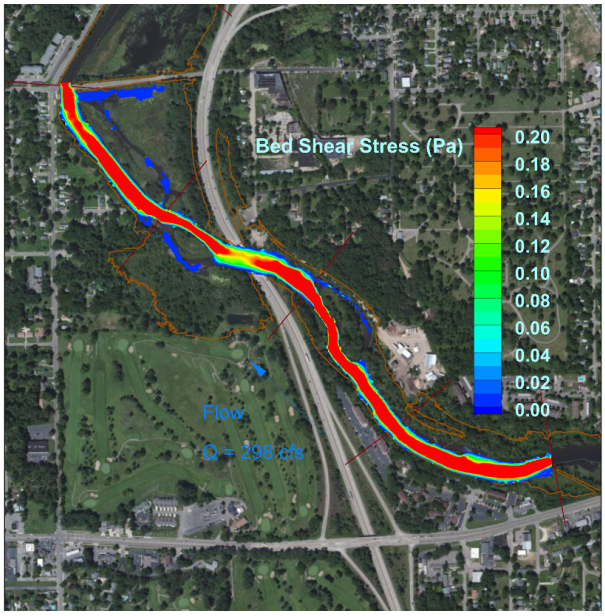

Figure 3.30: Distribution of Bed Shear Stress (MP14.75, 0:00 July 12, 2013)

Bed shear stress provides similar patterns to velocity magnitude in terms of distribution. Moreover, it is a better indicator for sediment transport, especially the fate and transport of oil-particle aggregates (OPAs). In-situ flume and lab experiments suggest that the critical bed shear stress for OPA resuspension may be as low as 0.1 Pa [31, 32]. The areas with less than 0.1 Pa bed shear stress are areas that are most likely to experience heavy submerged oil deposition.

For the high flow scenario during April 20-23, 2013, Figure 3.29 shows that bed shear stresses for the side channel area are mostly around or higher than 0.1 Pa. A downstream partial barrier was installed here. It seems that such a feature is required for the trap during high flow scenarios. While for the low flow scenario in July 2013, Figure 3.30 shows that water is flowing only in the main channels where bed shear stresses are mostly higher than 0.1 Pa.

3.6.3 Sediment Transport Simulation (100-year Flood Scenario)

A 100-year flood steady flow scenario was also simulated and sediment transport simulation was performed. This flow scenario was only done for MP14.75 and the sediment transport was only simulated for this flow at MP14.75 sediment trap. The flow discharge is 6,500 cubic feet per second. Figure 3.31 and

Figure 3.32 shows depth-averaged velocity magnitude and bed shear stress, respectively. Moreover, suspended sediment transport was modeled. The inlet sediment concentration was 130.4 mg/l (D. Soong, U.S. Geological Survey, written communication, 2014). The sediment particle size D_{84} was estimated as 0.2 mm. Figure 3.33 presents the concentration of suspended sediment. The change of concentration indicates how sediment is transported in the domain. The concentration in the sediment trap channel was found to be much lower than that in the main stream before flow separates. Therefore, the sediment carried by the flow coming into the sediment trap would deposit because of reduced transport capacity.

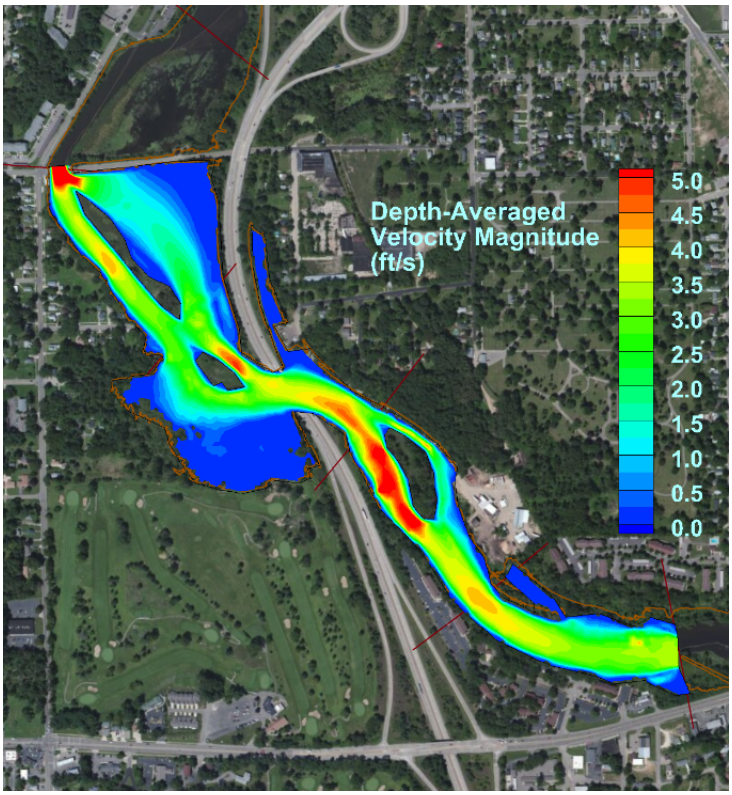

Figure 3.31: Distribution of Velocity Magnitude in 100-year Flood Scenario (MP14.75)

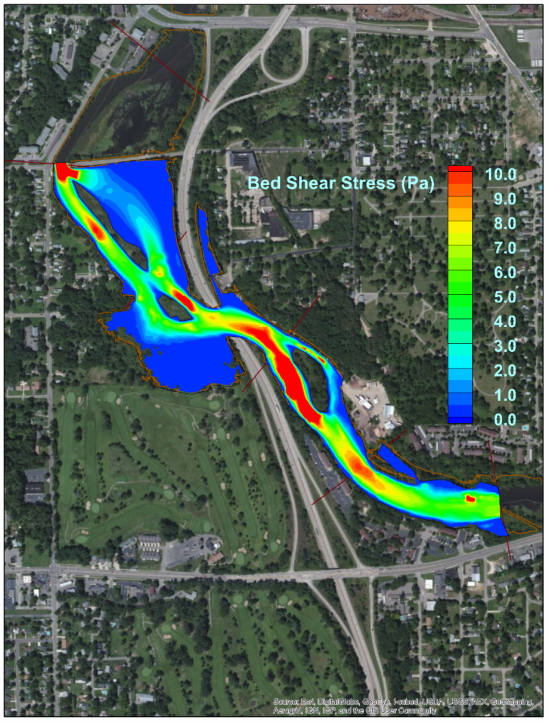

Figure 3.32: Distribution of Bed Shear Stress in 100-year Flood Scenario (MP14.75)

3.7 Results of MP 21.5 Sediment Trap Model

3.7.1 Distribution of Depth-Averaged Velocity Magnitude

Figure 3.34, Figure 3.35, and Figure 3.36 show the depth-averaged velocity magnitude under high flow and low flow scenarios.

The characteristic of this sediment trap is a cutoff channel. During the low flow period, almost no water flows into the original meandering channel. However, during high flows, some water with sediment may flow into the oxbow where sediment or OPAs would deposit as Figure 3.37 indicates.

3.7.2 Distribution of Bed Shear Stress

Figure 3.38, Figure 3.39, and Figure 3.40 show distributions of bed shear stress under high and low flow scenarios. During high flows, the bed shear stress in main stream is relatively high but once OPAs flow into the oxbow the velocities and bed shear stress become so low that they may deposit.

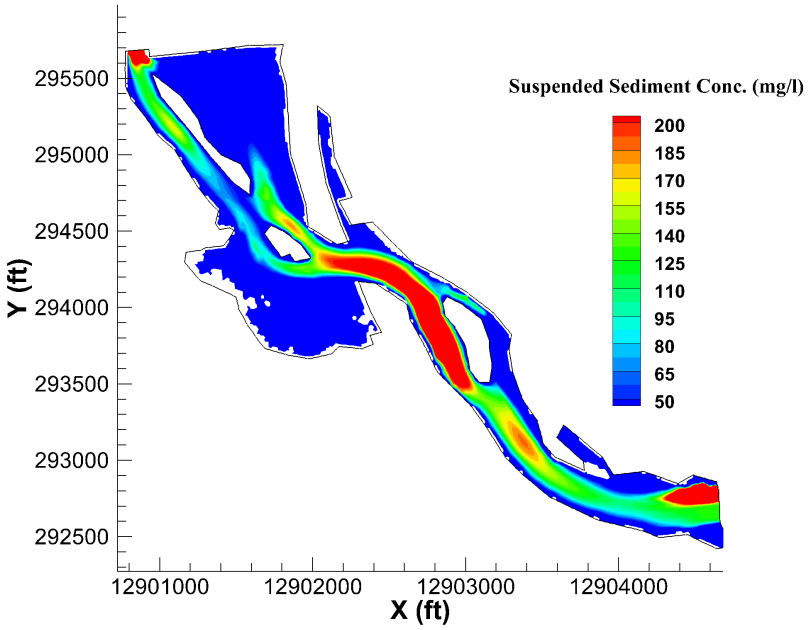

Figure 3.33: Distribution of Suspended Sediment Concentration in 100-year Flood Scenario (MP14.75)

During low flows, even the main stream has low velocities so that OPAs can deposit.

3.8 Summary

Two-dimensional hydrodynamics models were built for selected sediment traps in Kalamazoo River by applying HydroSed2D. The three natural sediment trap areas have different geometric and morphologic conditions which result in OPAs deposition in the sediment traps. The modeling results were in good agreement with the observed depositional patterns observed in the sediment traps.

The models worked well for different complex topographies and wet-dry conditions. Two flow scenarios were simulated. One was the April 2013 high flow scenario, while the other was the July 2013 low flow scenario. During low flows, no water generally flows into these sediment traps. Deposition happens during relatively high flows when water flows into sediment traps

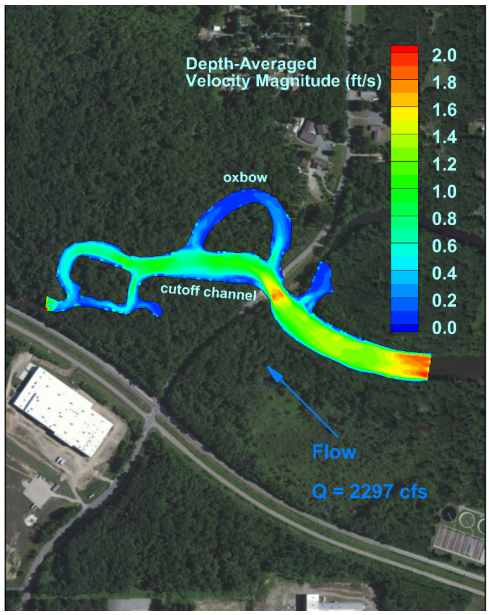

Figure 3.34: Distribution of Velocity Magnitude (MP21.5, 16:00 April 14, 2013)

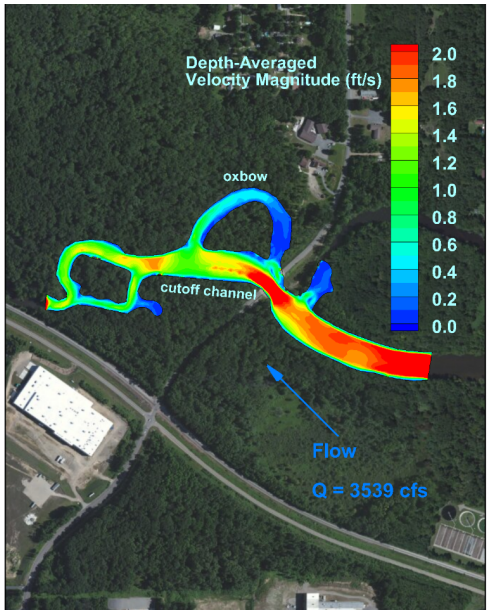

Figure 3.35: Distribution of Velocity Magnitude (MP21.5, 16:00 April 21, 2013)

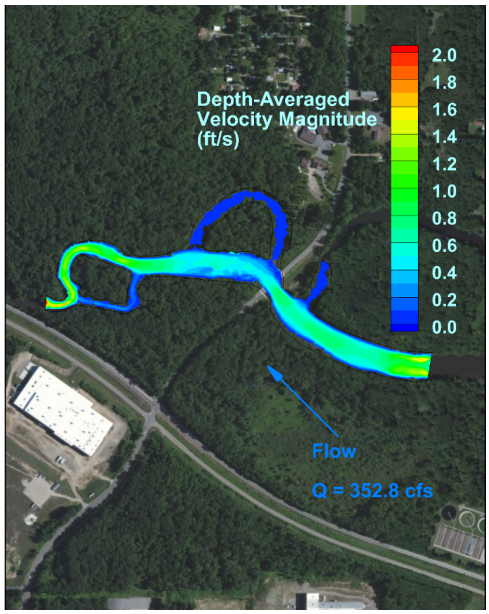

Figure 3.36: Distribution of Velocity Magnitude (MP21.5, 8:00 July 16, 2013)

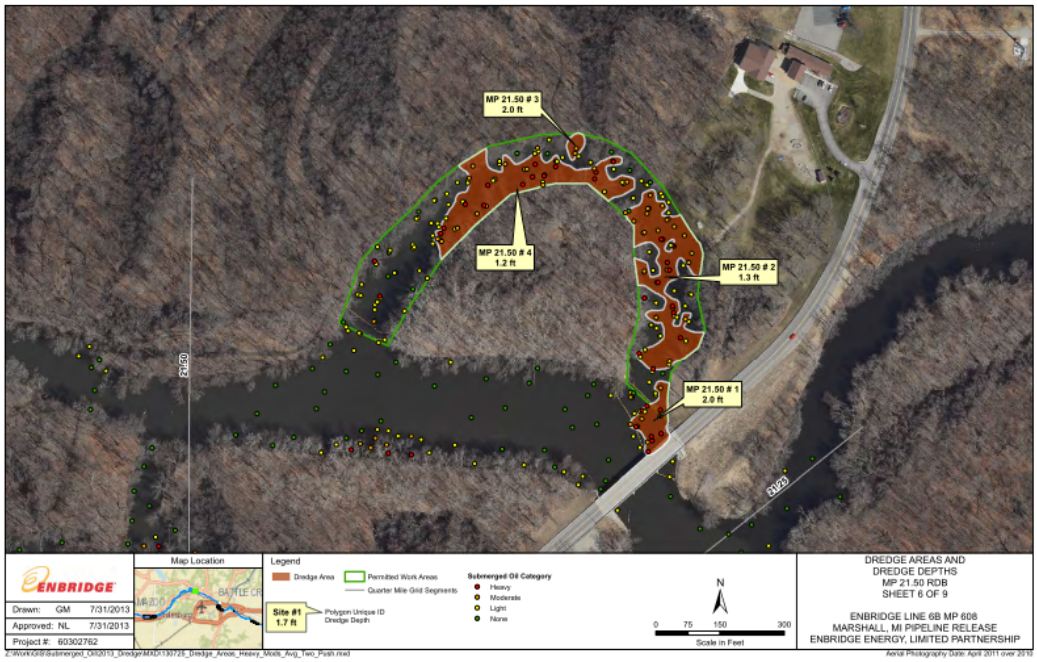

Figure 3.37: Survey of Submerged Oil in the Modeling Domain of MP 21.5 [46]

and OPAs would deposit due to gradients in sediment transport capacity associated with low velocities and bed shear stress that were captured by the model predictions.

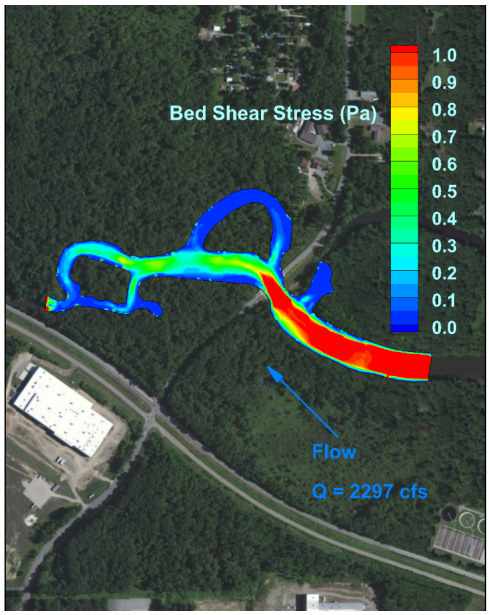

Figure 3.38: Distribution of Bed Shear Stress (MP21.5, 16:00 April 14, 2013)

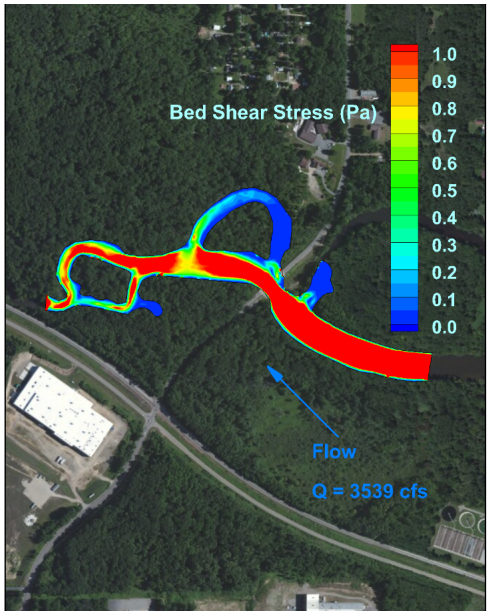

Figure 3.39: Distribution of Bed Shear Stress (MP21.5, 16:00 April 21, 2013)

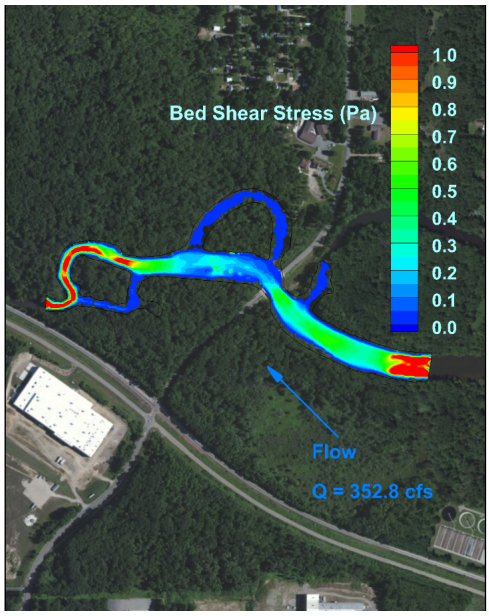

Figure 3.40: Distribution of Bed Shear Stress (MP21.5, 8:00 July 16, 2013)

The depositional areas indicated by the models agree in general with the areas of heavy submerged oil found during the field surveys. The developed models are useful tools in the ongoing cleanup work and may also be useful for future management efforts. For instance, they can be used to evaluate the effects of dredging sediment trapping areas or other engineering efforts for oil removal from the river and its floodplain. It is known that artificial sediment traps were implemented in order to either enhance the trapping efficiency of the natural sediment traps or to create additional trapping areas. The models can be helpful for evaluating the potential impact of such measures as well as in pinpointing what locations might be better suited to capture OPAs.

Computation speed is one of the main limitation of this model. It is fine for simulating selected sediment traps separately like what have been shown in this chapter. However, to simulate a whole river reach (tens of kilometers long), the computational speed is too slow unless the mesh resolution is very coarse. Parallelization techniques could help to improve the computation speed and take advantage of the more and more powerful computer clusters and workstations. Also, the implementation of turbulence model, such as the $k - \varepsilon$ model, will be useful, especially for the suspended sediment transport because it can help to know better the turbulence diffusivity. In the next

chapter, a new parallel two-dimensional hydrodynamic, sediment transport and bed morphology model, HydroSedFoam, is presented, which can address the limitations mentioned above.

CHAPTER 4

DEVELOPMENT OF A NEW PARALLELIZED TWO-DIMENSIONAL HYDRODYNAMIC, SEDIMENT TRANSPORT AND BED MORPHOLOGY MODEL

4.1 Introduction

Numerical models of river morphodynamics have become important tools for understanding process-form relationships in river channels through the computation of hydrodynamics, sediment transport and an evolving river bed morphology. Although three-dimensional (3D) models have been developed to solve for river morphological change, they require complex techniques for dealing with the interfaces between water and air, and water and sediment [47, 48, 49, 50]. Several approaches can be used for the water-air interface, such as the rigid lid approach, the volume of fluid (VOF) method [49], and approximation by two-dimensional (2D) depth-averaged continuity equation [47, 50]. The water-sediment interface is more difficult to capture when the river bed morphology is included in 3D models, though the mesh deformation method is one option for addressing this [49]. In contrast to 3D models, 2D depth-averaged models do not need meshes in the vertical direction, because the continuity and momentum equations are integrated in the vertical direction. Therefore, the water-air and water-sediment interfaces are not an issue for 2D depth-averaged models. While 2D depth-averaged models miss the information about vertical velocity distribution, they can provide appropriate hydrodynamic results for certain problems in shallow water environments where horizontal scales and velocities are dominant [51, 52, 49, 53, 54, 39].

Although 2D models are less computationally expensive than 3D models, computation speed is still a concern in many applications. Parallelization can increase computation speed by allowing models to run on multiple computation nodes on computer clusters or workstations. For example, parallelization of several 2D hydrodynamic models, with the domain decomposition method, showed good speedup and parallel efficiency [55, 56]. However, those models

did not include turbulence models or allow for an evolving bed morphology. In fact, few models that include sediment transport and bed morphology have been parallelized. A notable exception to this is TELEMAC-2D [57], which was parallelized with domain decomposition based on the Message Passing Interface (MPI) Standard.

A major drawback of the existing parallelized 2D morphodynamic models is that the source codes of these models are written in a wide variety of programming languages. Development of these existing models is limited to those developers that understand the particular programming language the model is written in. Moreover, each model can take developers significant amount of time to understand before any further development can be performed. In this thesis, a new parallelized 2D hydrodynamic, sediment transport and bed morphology model, HydroSedFoam, was developed by using Open source Field Operation And Manipulation (OpenFOAM). OpenFOAM is a C++ toolbox for the development of customized numerical solvers. The HydroSedFoam model uses MPI for code parallelization and adopts a depth-averaged $k - \varepsilon$ turbulence model. HydroSedFoam is unique compared to similar 2D morphodynamic models in that further development and modification of the model is relatively simple. Since it uses the OpenFOAM toolbox, developers do not need to write all their own code or numerical schemes. This allows researchers to focus on the scientific questions at hand, rather than the intricacies of a particular coding language.

In this dissertation, the details of the HydroSedFoam model are presented, along with the case studies used for model validation, and an analysis of the speedup and parallelization efficiency of the model. The results of hydrodynamic component of the model simulation were validated through comparison with a laboratory experiment of flow through a fixed-boundary channel with a sine-generated meandering planform. The sediment transport and bed morphology components of the model were validated through a movable-bed case study of a sine-generated "bump" of sediment on an otherwise flat mobile bed. The results of the numerical simulation of bed evolution were compared with the analytical solution for the problem. The results of HdyroSedFoam showed good agreement with both the laboratory data and the analytical solution to the movable-bed case study.

4.2 Methodology

4.2.1 Governing Equations

Two-dimensional Shallow Water Equations

The governing equations for depth-averaged continuity and momentum conservation are as follows:

$$\frac{\partial h}{\partial t} + \nabla \cdot (h\mathbf{U}) = 0 \tag{4.1}$$

$$\frac{\partial (hu)}{\partial t} + \nabla \cdot (hu\mathbf{U}) = -gh\frac{\partial h_0}{\partial x} - \frac{\tau_{bx}}{\rho} + \nabla \cdot (\nu_t \nabla (hu)) \tag{4.2}$$

$$\frac{\partial (hv)}{\partial t} + \nabla \cdot (hv\mathbf{U}) = -gh\frac{\partial h_0}{\partial y} - \frac{\tau_{by}}{\rho} + \nabla \cdot (\nu_t \nabla (hv)) \tag{4.3}$$

where h is water depth; h_0 is bed elevation; $\mathbf{U}$ represents velocity vector, (u, v) which are depth-averaged velocities in x and y directions, respectively; g is the gravitational acceleration; τ_{bx} and τ_{by} are bed shear stresses in x and y directions, respectively; and ν_t is turbulent viscosity.

Bed shear stresses are estimated using the Chezy formula.

$$\frac{\tau_{bx}}{\rho} = C_f |\mathbf{U}| u = \frac{g}{C_z^2} |\mathbf{U}| u \tag{4.4}$$

$$\frac{\tau_{by}}{\rho} = C_f |\mathbf{U}| v = \frac{g}{C_z^2} |\mathbf{U}| v \tag{4.5}$$

where C_f is the dimensionless friction coefficient; and Chezy's coefficient C_z is used to represent bed roughness.

Turbulence Model

Turbulent viscosity ν_t is modeled by a depth-averaged $k - \varepsilon$ model [58, 59].

$$\nu_t = C_\mu \frac{k^2}{\varepsilon} \tag{4.6}$$

where the empirical constant $C_\mu = 0.09$; k and ϵ respectively designate turbulent kinetic energy and its dissipation, which are given by:

$$\frac{\partial k}{\partial t} + \mathbf{U} \cdot \nabla (k) = \frac{1}{h} \nabla \cdot \left(h \frac{\nu_t}{\sigma_k} \nabla k \right) + P - \varepsilon + P_{kv} \tag{4.7}$$

$$\frac{\partial \varepsilon}{\partial t} + \mathbf{U} \cdot \nabla (\varepsilon) = \frac{1}{h} \nabla \cdot \left(h \frac{\nu_t}{\sigma_\varepsilon} \nabla \varepsilon \right) + \frac{\varepsilon}{k} (c_{1\varepsilon} P - c_{2\varepsilon} \varepsilon) + P_{\varepsilon v} \tag{4.8}$$

where the production terms can be modeled as follows:

$$P = \nu_t \left(\frac{\partial u_i}{\partial x_j} + \frac{\partial u_j}{\partial x_i} \right) \frac{\partial u_i}{\partial x_j} \tag{4.9}$$

$$P_{kv} = C_k \frac{u_*^3}{h} = \frac{1}{\sqrt{C_f}} \frac{u_*^3}{h} \tag{4.10}$$

$$P_{\varepsilon v} = C_\varepsilon \frac{u_*^4}{h^2} = 3.6 \frac{C_{2\varepsilon} \sqrt{C_\mu}}{C_f^{3/4}} \frac{u_*^4}{h^2} \tag{4.11}$$

where $u_* = \sqrt{C_f (u^2 + v^2)}$. The values of empirical constants are: $\sigma_k = 1.0; \sigma_\varepsilon = 1.3; C_{1\varepsilon} = 1.44; C_{2\varepsilon} = 1.92$.

Bed Load Transport Model

The bed load sediment transport is estimated with the help of the Meyer-Peter and Muller formula [41] (eqn. 4.12).

$$\frac{\mathbf{q}}{D\sqrt{gRD}} = 8 \left(max \left(\frac{\tau_\mathbf{b}}{\rho g R D} - \tau_c^*, 0 \right) \right)^{3/2} \tag{4.12}$$

where $\mathbf{q}$ represents the bed load fluxes; D is the sediment grain size; $R = \rho_s/\rho - 1$; ρ_s and ρ are densities of sediment and fluid, respectively; $\tau_c^* = 0.047$ is non-dimensional critical shear stress.

Suspended Load Transport Model

The suspended load sediment transport is computed with an advection-diffusion equation (eqn. 4.13) with source and sink terms in the following.

$$\frac{\partial C}{\partial t} + \nabla \cdot (C\mathbf{U}) - \nabla \cdot (\nu_t \nabla C) = \frac{v_s}{h} (E_s - C_b) \tag{4.13}$$

where C is the depth-averaged concentration of suspended sediment; v_s is the sediment fall velocity which relates to the size of the sediment particles;

E_s represents entrainment rate; and C_b represents near-bed concentration of suspended sediment which relates to settling rates, $C_b = r_o C$. r_o is a parameter to relate near-bed concentration to depth-averaged concentration. It can be estimated as 2.0, or computed by the following expression [42]:

$$r_o = 1 + 31.5\left(\frac{u_*}{v_s}\right)^{-1.46} \tag{4.14}$$

The sediment entrainment rate E_s is computed according to García and Parker formula [43, 44, 60]:

$$E_s = \frac{\mathrm{A} Z_u^5}{1 + \frac{A}{0.3} Z_u^5} \tag{4.15}$$

where the empirical constant $A = 1.3 \times 10^{-7}$.

$$Z_u = \frac{u_{*s} R_{ep}^{0.6}}{v_s} \tag{4.16}$$

where u_{*s} is the shear velocity associated with skin friction; and for fine-grained non-cohesive sediments and $R_{ep} = \frac{D\sqrt{gRD}}{\nu} < 3.5$,

$$Z_u = 0.708 \frac{u_*}{v_s} R_{ep}^{0.6} \tag{4.17}$$

The bed elevation change is computed using the Exner's equation.

$$(1 - \lambda_p) \frac{\partial h_0}{\partial t} + \nabla \cdot (\mathbf{q}) = v_s \left(C_b - E_s\right) \tag{4.18}$$

where λ_p is the bed porosity.

4.2.2 Numerical Model

The new model, HydroSedFoam, was developed using OpenFOAM (Open Source Field Operation And Manipulation) [61]. OpenFOAM is a C++ toolbox for the development of customized numerical solvers. Since the original development in the late 1980s at Imperial College, London, OpenFOAM has been used by researchers to study a variety of continuum mechanics problems, including computational fluid dynamics [49, 62, 63, 64]. It is based on the finite volume method and uses object-oriented programming to implement scalar-vector-tensor operations, which can save substantial efforts

of developers. OpenFOAM also supports automatic MPI (Message Passing Interface) parallelization for models written using OpenFOAM high-level syntax, which allows the user to take advantage of the increased computational power of computer workstations and clusters. Moreover, OpenFOAM provides pre- and post-processing utilities which help developers to focus on model development and studies.

The PIMPLE (merged PISO-SIMPLE) algorithm is used for velocity-pressure coupling. It merges the PISO algorithm (Pressure Implicit with Splitting of Operator [65]) and the SIMPLE algorithm (Semi-Implicit Method for Pressure Linked Equations), and allows the user to conveniently choose between the two schemes. The PISO algorithm was chosen for the following case studies. Many numerical schemes are supported in OpenFOAM for interpolation and discretization (for time, convective terms, diffusive terms, gradient terms and so on) [66]. Therefore, developers can focus on the high level model development and evaluate different numerical schemes in any specific study.

4.3 Case Study with Fixed Bed: Meandering Channel Laboratory Experiments

The first case study tests the hydrodynamic model in HydroSedFoam. A constant discharge was run through a laboratory flume with a fixed-boundary, sine generated meandering planform, located at the University of Illinois Ven Te Chow Hydrosystems Laboratory. The experiment was performed by Jessica Zinger of University of Illinois. Water surface elevation and flow velocity were measured in the flume and compared with the results of the numerical simulation.

4.3.1 Laboratory Experiment Methods

The flume used in the experiments consists of three meander bends with a width of $0.52m$ and a rectangular cross-section (see Fig. 4.1), located in the Ven Te Chow Hydrosystems Laboratory. The flume planform geometry (see Fig. 4.2) is a sine-generated curve given by equation 4.19. The flow depth and water surface slope in the flume were controlled by a hinged gate at the

downstream end of the flume and the discharge of the flows was monitored using a Venturi meter.

Figure 4.1: Experimental flume and ADV

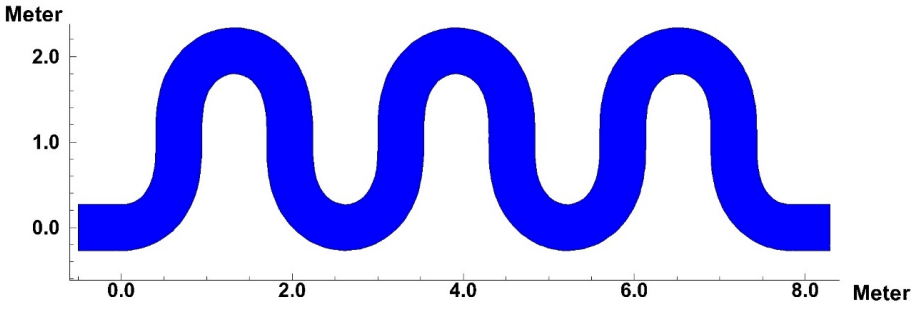

Figure 4.2: Flume planform geometry

$$\Phi = \omega sin\left(\frac{2\pi s}{M}\right) \tag{4.19}$$

where Φ is the angle of the centerline to the downstream direction at location s; s is the streamwise coordinate; ω is the maximum angle of the centerline to the mean downstream direction, $\omega = 90°$; and M is the meander wavelength, $M = 5.5m$.

Water surface elevations were measured at 34 flume cross-sections (Fig. 4.3), at a cross section located downstream of the apex of the last bend, and at a cross-section located at the end of the last bend. Three water surface were measured on each cross-section: $5cm$ from each flume wall and the flume

centerline. Flow velocities were measured using a Nortek Vectrino Profiler Acoustic Doppler Velocimeter (ADV). ADV measurements were made at sixteen cross-sections, oriented perpendicular to the local centerline. In each cross-section (except XS 21), ADV measurements were spaced horizontally by 8.67 cm and made at eight points at different heights above the bed (i.e. $0.5, 1.0, 2.0, 3.0, 4.5, 7.0, 8.5, 11.5cm$). The measurements at XS 21 were spaced every 6.5 cm in the horizontal direction and located at the same heights above the bed.

4.3.2 Numerical Simulation

A meshing software, Gambit, was used to generate a computational mesh that matches the flume geometry. The mesh has higher resolution near the wall boundaries compared to the center of the channel (see Fig. 4.4). There are totally 9,632 grid elements. The width of the channel is divided into 32 segments. Inflow discharge per width, 0.0495 m^2/s and downstream water level, 0.17 m, are applied as boundary conditions. The dimensionless friction coefficient C_f is 0.035 and a $k - \varepsilon$ model is used for modeling turbulence viscosity. As with the laboratory experiment, the numerical model was run with a fixed-boundary and no sediment transport.

Fig. 4.5 compares depth-averaged velocity magnitude between experiment measurement and numerical modeling at 87 locations. The simulated depth-averaged velocities generally match the experimental data, though the data does show some scatter. A possible explanation for this scatter is that the experimental flume did not have a perfectly flat bed, whereas the bed was perfectly flat in the numerical simulations. Another reason could be that a 2D depth-averaged model misses velocity distribution in the vertical direction. The mean absolute difference between the depth-averaged velocity measured in the experiment and simulated by the model is $0.033m/s$. Numerical results of the spatial distribution of velocity magnitude, turbulence kinetic energy and dissipation rate are shown in Fig. 4.6. With a flat-bedded, meandering channel, higher velocity occurs at inner bank of the flume, as shown by the seminal experiments of Abad and Garcia [67] and confirmed in the flume experiment described above.

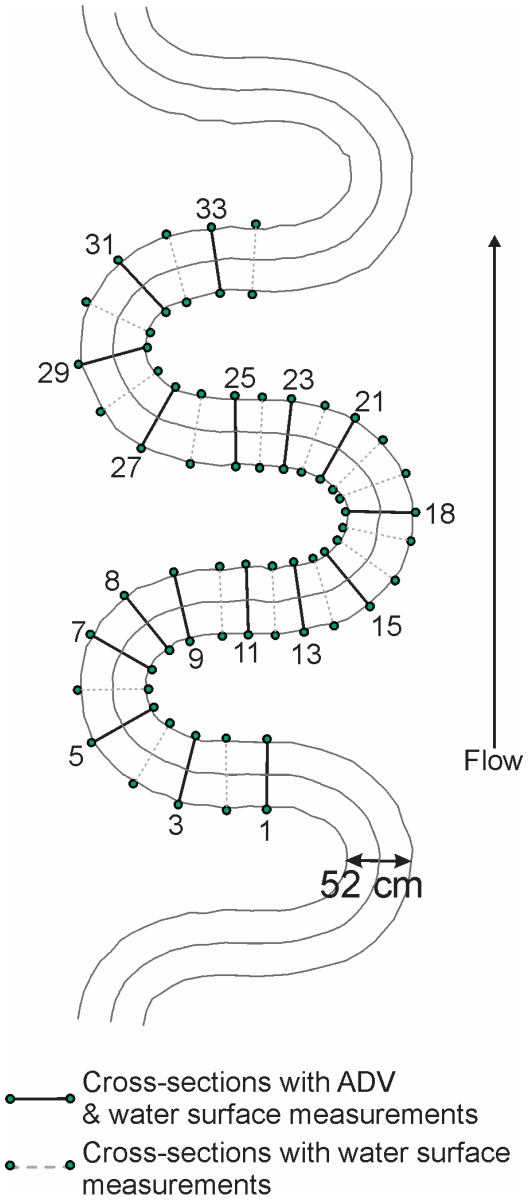

Figure 4.3: Solid grey lines show flume banklines and centerline, numbered solid black lines show cross-sections with ADV and water surface elevation measurements, and dotted grey lines show cross-sections with only water surface elevation measurements (figure by Jessica Zinger, unpublished work)

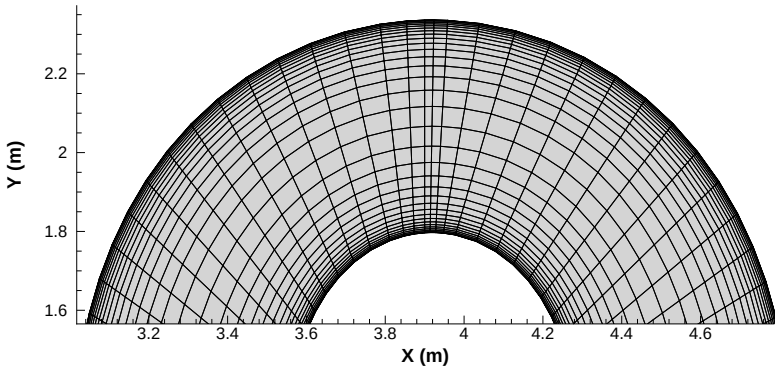

Figure 4.4: Computational mesh for the laboraotry sine channel

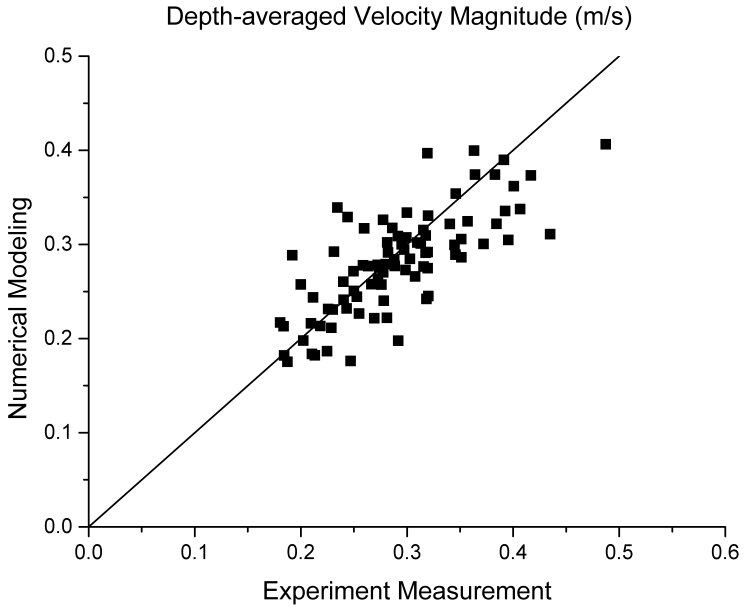

Figure 4.5: Comparison of depth-averaged velocity magnitude between experiment measurement and numerical modeling

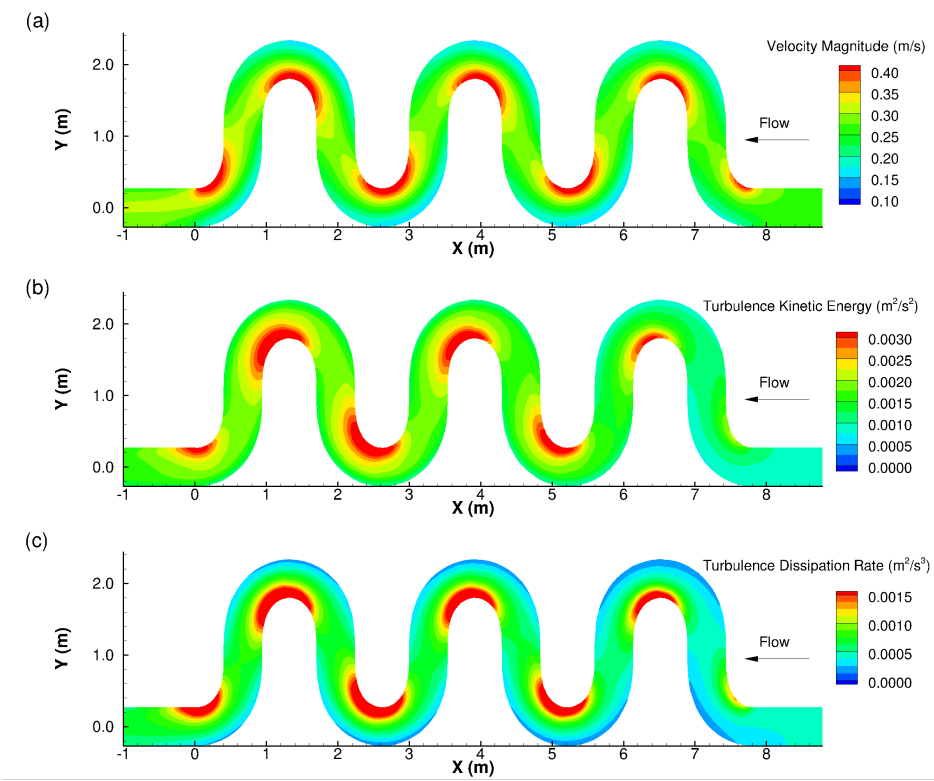

Figure 4.6: Numerical results of the sine-shape flume test

4.4 Case Study with Movable Bed: Sediment Transport and Bed Morphology

A case study of a movable bed simulation was done to validate the sediment transport and bed morphology components of the model. The test problem investigated in this case study was first proposed by Hudson [68] and used by Castro Díaz et al. [53]. The setup of this case study is a 1000 meter long and 100 meter wide rectangular channel (Fig. 4.7). The bed of the channel consists of a layer of erodible sediment overlying a flat, non-erodible bottom located at vertical coordinate zero. The layer of erodible sediment is of constant thickness, with the exception of a 200 meter long symmetrical, sine-generated bump. The initial sediment layer thickness (in meters) is defined by

$$h_0 = \begin{cases} 0.1 + \sin^2\left(\frac{\pi(x-300)}{200}\right) & \text{if} \quad 300 \leq x \leq 500, \\ 0.1 & \text{otherwise.} \end{cases} \tag{4.20}$$

The initial water surface elevation is 10.1 m. At the upstream boundary,

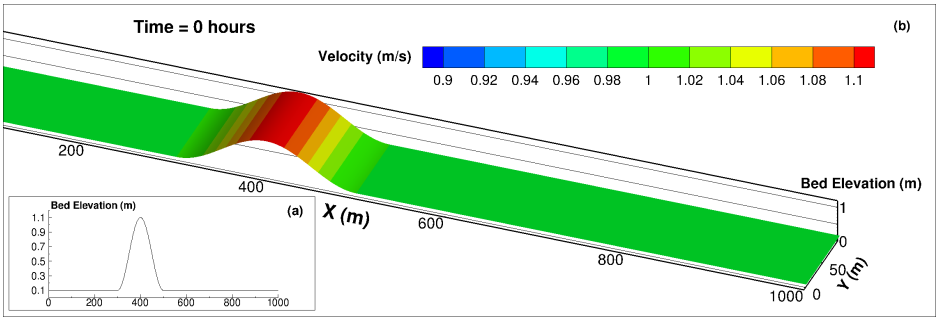

Figure 4.7: Initial conditions of the case study for bedload sediment transport: (a) shows the initial sediment layer thickness along the channel; (b) shows the velocity magnitude at hydrodynamic equilibrium state

the discharge per width is 10 m^2/s and the sediment layer thickness is 0.1 m. For the downstream boundary, the water surface elevation is 10.1 m and a free boundary is used for sediment transport. Table 4.1 summarizes the geometry configurations and boundary conditions for the movable bed case study. Since this test problem is essentially a one-dimensional problem, the mesh size is $\Delta x = 1m$ and $\Delta y = 100m$, which results in 1,000 mesh cells. The bed porosity is assumed to be 0.64 and the dimensionless friction coefficient C_f is 0.01.

Parameters	**Values**
Channel length	1000 m
Channel width	100 m
Flow per unit width	10 m^2/s
Dimensionless friction coefficient C_f	0.01
Downstream water surface elevation	10.1 m

Table 4.1: Settings of movable bed case study

Prior to running sediment transport model, the hydrodynamic model was run to equilibrium over the initial bed geometry. Once the flow model reached equilibrium, morphodynamic evolution of the bed was initiated. At each time step, the hydrodynamic model was first allowed to reach equilibrium, then sediment transport rates were calculated and the bed was evolved according to the equation 4.18. Only sediment moving as bedload was considered in this study; suspended load was neglected. The non-dimensional critical shear stress was assumed to be equal to zero in order to compare with the approximate analytical solution given in [68]. The solution is derived by assuming that the water surface elevation and the discharge is constant throughout the

domain. Fig. 4.8 shows numerical results of bed elevation and velocity after 70 hours. Fig. 4.9 shows the comparison between simulation results and the analytical solution. The numerical simulation and analytical solution agree very well, and the difference can only be seen in the close view figure on the right side of Fig. 4.9.

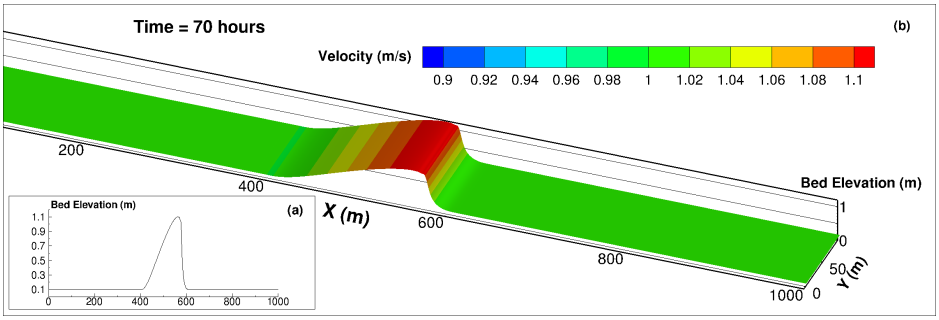

Figure 4.8: Results of the case study for bedload sediment transport after 70 hours: (a) shows the sediment layer thickness along the channel after 70 hours; (b) shows the velocity magnitude

4.5 Parallelization Efficiency

Parallelization efficiency of the model was evaluated by using the same geometry of the second case study. Only hydrodynamic simulation was performed. The model is paralleled with domain decomposition method. The model domain is divided into a number of subdomains, which are simulated on separate computation nodes. The subdomains communicate information about their boundaries with neighbouring subdomains. Therefore, there is a tradeoff between the computational speed gained by simultaneously simulating smaller subdomains and the speed lost to communicating information between subdomains. The speedup of the model S and the parallel efficiency E are used to evaluate the parallel performance of the model.

$$S = \frac{T_{seq}}{T} \tag{4.21}$$

where T_{seq} is the run time of the sequential algorithm and T is the run time of the parallel algorithm.

$$E = \frac{S}{P} \tag{4.22}$$

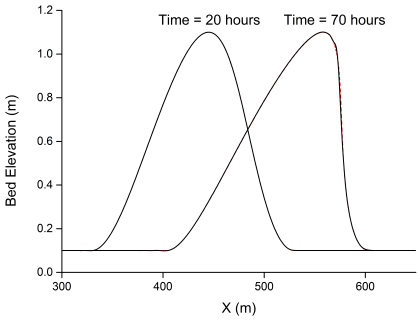

(a) Comparison at 20 hours and 70 hours

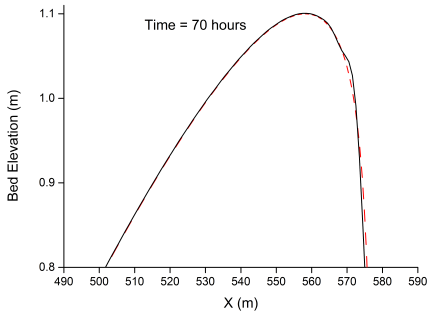

(b) A close view of results at 70 hours

Figure 4.9: Comparison between numerical results (solid line) and analytical solution (dash line) for a bedload case study of sediment dune evolution

where P is the number of computation nodes.

Fig. 4.10 shows the speedup and parallel efficiency in the test problem of rectangular channel. The domain was uniformly decomposed in the streamwise into a number of subdomains equal to the number of processors for each test. Four tests were conducted with different mesh grids. Because domain decomposition requires extra computation time in data communication between subdomains, parallel efficiency increases as the number of grid cells increase. When only 1,000 computational grids are used, parallel efficiency decreases dramatically with more than two computation nodes. The speed even slows down when more than 10 computation nodes are used due to the communication time. Also, when the total number of grid cells is the same, parallel efficiency is better when fewer cells are shared by two subdomains. The test case of $100,000 \times 1$ cells (case A) uses 100,000 grid cells in x direction and one cell in y direction; while the one of $1,000 \times 100$ cells (case B) uses 1,000 grid cells in x direction and 100 cells in y direction. Case B has more information to communicate between subdomains, so the parallel performance is worse than case A. The difference in parallel performance between case A and case B is bigger when more computation nodes are used. It is worth mentioning that the parallel performance depends on the computing hardware. In this study, the analysis was done on a Dell workstation with Dual 2.5 GHz Intel Xeon Processor E5-2680 v3 (each has 12 cores). Tests were done by using up to 24 cores.

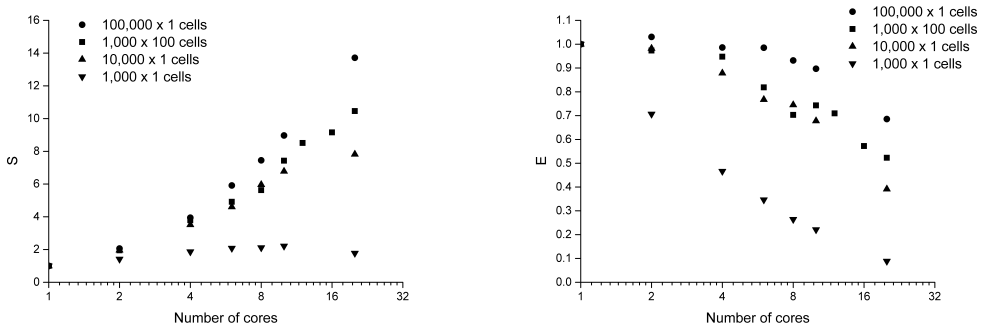

(a) Speedup performance (b) Parallel efficiency performance

Figure 4.10: Speedup and parallel efficiency in a rectangular channel test problem on a Dell workstation with Dual 2.5 GHz Intel Xeon Processor E5-2680 v3

4.6 Application to Kalamazoo River MP21.5 sediment trap

HydroSedFoam was applied to a case study of the MP21.5 sediment trap. The description of MP21.5 sediment trap can be found in last chapter. A steady case of bankful flow condition was simulated. The inflow discharge used in this simulation was 100 m^3/s. Fig. 4.11 shows the velocity magnitude when simulation reached equilibrium state. Flow direction is from right to left. At cutoff channel, most flow followed main channel, while a small portion of water flowed into cutoff channel. Velocity at cutoff channel was small so sediment particles or OPAs entering with flow would likely deposit. At downstream of the cutoff channel, river bifurcates into two sub-channels. Under bankful flow condition, velocity at both sub-channels was high so deposition might not occur here.

4.7 Summary and Conclusions

A new 2D depth-averaged hydrodynamic, sediment transport, and bed morphology model was developed with the open-source platform of OpenFOAM. A depth-averaged $k - \varepsilon$ model was implemented for the turbulence closure. The domain decomposition method was used to parallelize the model. Case studies were conducted for model validation. The hydrodynamic component

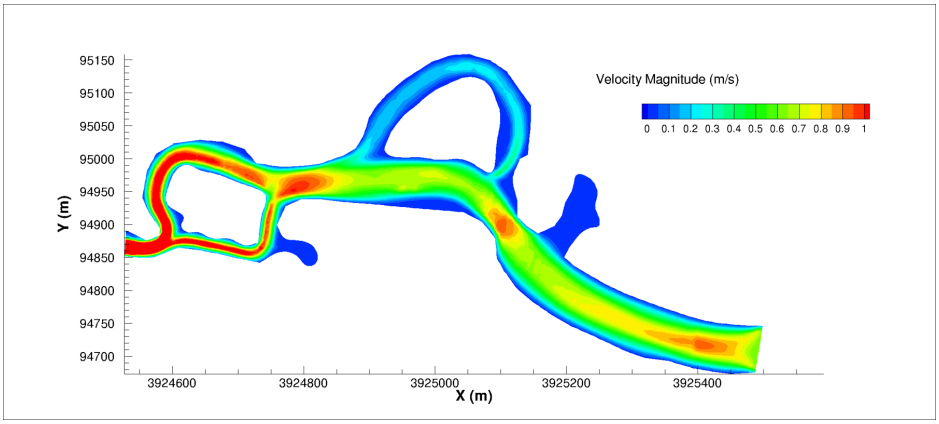

Figure 4.11: Application of HydroSedFoam to Kalamazoo River MP21.5 sediment trap (flow direction: from right to left)

of HydroSedFoam was validated through comparison with laboratory experiments that were performed with a meandering flume channel at the Ven Te Chow Hydrosystems Lab at University of Illinois at Urbana-Champaign. Flow velocities were measured using ADV at selected cross sections. The measurements and numerical results showed good agreement. The sediment transport and bed morphology components of HydroSedFoam were validated with a case study of a rectangular straight channel with a mobile bed. The mobile bed was initially flat with a single sine-generated bump. Numerical results matched well with the approximate analytical solution for this case study. The parallel performance of the model was tested on a workstation with Dual Intel Xeon Processor E5-2680. The parallel efficiency is good up to the maximum cores of the computing hardware. The HydroSedFoam model represents a significant contribution to the available 2D depth-averaged morphodynamic models due to its use of the OpenFOAM platform. Further development and modification of the HydroSedFoam are relatively easy because of the toolbox provided by OpenFOAM. Developers can focus on the research problems rather than writing all codes or implementing numerical schemes from scratch. Future work with 2D depth-averaged models should include an evaluation of the performance of the turbulence models, especially their effects on sediment transport modeling. Moreover, the parallel efficiency with complex geometry and for larger number of computing nodes needs to be evaluated.

CHAPTER 5

CONCLUSIONS AND DISCUSSION

5.1 Summary

This dissertation presents the studies of the transport and fate of OPAs resulting from an oil spill in a freshwater environment, Kalamazoo River. OPAs can deposit on the bed of rivers or lakes, which makes cleanup very difficult. For the Kalamazoo River oil spill, the cleanup of submerged oil had continued for more than three years after the spill [17]. The main questions addressed were: where does submerged oil deposit, when can it be resuspended and whether it can be transported towards Lake Michigan.

5.1.1 Modeling the transport and fate of oil-particle aggregates in Morrow Lake

A three-dimensional Euler/Lagrangian algorithm was developed for the transport and fate of OPAs and applied to the Morrow Lake. The carefully calibrated and validated model enabled consideration of hydrodynamic effects of the dam operational rules and wind effect. With the help of field and laboratory experiments, the properties of OPAs in Morrow Lake were investigated and implemented into the model. The main objectives of the modeling were:

1. To investigate whether and under which scenarios OPAs can be resuspended and transported through the Morrow Dam and then towards Lake Michigan.

2. To locate highly oil-contaminated areas in Morrow Lake and its delta.

3. To help decision makers in dredging efforts and management.

This study found that OPAs could potentially be transported towards Lake Michigan. The model can complement field poling activities to locate where OPAs heavily deposit, which can provide better spatial resolution and save money and efforts. In the two applications shown in this dissertation, the model has shown its usefulness to managers in their dredging and management efforts.

5.1.2 Modeling of Selected Sediment Traps in Kalamazoo River, Michigan

2D models were built for selected sediment traps in Kalamazoo River by applying an in-house code, HydroSed2D. The three natural sediment trap areas have different geometric and morphologic conditions which result in OPAs deposition in the sediment traps. The main objectives of the modeling were:

1. To understand where and when OPAs mostly deposit in Kalamazoo River.

2. To evaluate the applicability of the model for the whole Kalamazoo River reach.

The models worked well for different complex topographies and wet-dry conditions. During low flows, no water generally flows into these sediment traps. Deposition happens during relatively high flows when water flows into sediment traps and OPAs would deposit due to gradients in sediment transport capacity associated with low velocities and bed shear stress that were captured by the model predictions. The depositional areas indicated by the models agree in general with the areas of heavy submerged oil found during the field surveys.

Computational speed is one of the main limitation of this model. It is fine for simulating selected sediment traps separately. However, to simulate a whole river reach, the computational speed is too slow unless the mesh resolution is very coarse. Parallelization techniques could help to improve the computational speed and take advantage of the more and more powerful computer clusters and workstations.

5.1.3 Development of a new parallelized two-dimensional hydrodynamic, sediment transport and bed morphology model

A new 2D hydrodynamic and river morphology model was developed with the open-source platform of OpenFOAM. The development of this new model was motivated by the modeling of sediment traps in this dissertation. It was found that computational speed was of high concern and parallelization would be very helpful. Domain decomposition method was used to parallel the model. A depth-averaged $k - \varepsilon$ model was also implemented for turbulence closure, which could be useful for the suspended sediment transport because it can help to know better the turbulence diffusivity. The new model was validated with the help of a laboratory experiment and a case study of sediment transport modeling. The parallel performance of the model was tested on a workstation with Dual Intel Xeon Processor E5-2680. With the OpenFOAM platform, further development and modification of the model will be relatively easy because developers can focus on the research problems other than writing all codes or implementing numerical schemes from scratch.

5.2 Future Perspectives

The studies in this dissertation could be improved in many aspects in future:

1. Studies in this dissertation focus on the transport and fate of OPAs after they are formed. The formation of OPAs is very complicated and under research [69, 8]. The modeling of the formation of OPAS can be an improvement for the current model.

2. Different engineering efforts (e.g. dredging) have been applied in order to improve the trapping efficiency in the sediment traps. The models can help to evaluate them and provide insights on how to improve the trapping efficiency.

3. Properties of OPAs are critical as model inputs. More investigation of the properties using laboratory experiments will be helpful.

4. Regarding to the new model HydroSedFoam, the performance of turbulence models, especially their effects on sediment transport modeling, needs to be further studied. The parallel efficiency with complex geometry of real rivers and larger number of computing nodes also needs to be evaluated.

REFERENCES

[1] M. K. McNutt, R. Camilli, T. J. Crone, G. D. Guthrie, P. a. Hsieh, T. B. Ryerson, O. Savas, and F. Shaffer, "Review of flow rate estimates of the Deepwater Horizon oil spill," *Proceedings of the National Academy of Sciences of the United States of America*, vol. 109, no. 50, pp. 20 260–20 267, 2012.

[2] C. A. Kontovas, H. N. Psaraftis, and N. P. Ventikos, "An empirical analysis of IOPCF oil spill cost data," *Marine pollution bulletin*, vol. 60, no. 9, pp. 1455–1466, 2010.

[3] P. F. Kingston, "Long-term Environmental Impact of Oil Spills," *Spill Science & Technology Bulletin*, vol. 7, no. 1-2, pp. 53–61, 2002.

[4] G. Yoshioka and M. Carpenter, "Characteristics of Reported Inland and Coastal Oil Spills," in *Fourth Biennial Freshwater Spills Symposium*, 2002, pp. 1–11.

[5] S. Danchuk and C. Willson, "NUMERICAL MODELING OF OIL SPILLS IN THE INLAND WATERWAYS OF THE LOWER MISSISSIPPI RIVER DELTA," in *International Oil Spill Conference Proceedings*, 2008, pp. 887–891.

[6] P. Yapa, H. Shen, and K. Angammana, "Modeling oil spills in a riverlake system," *Journal of Marine Systems*, vol. 4, no. 6, pp. 453–471, 1994.

[7] J. K. Cronk, W. J. Mitsch, and R. M. Sykes, "Effective modelling of a major inland oil spill on the Ohio River," *Ecological Modelling*, vol. 51, no. 3-4, pp. 161–192, 1990.

[8] Y. Gong, X. Zhao, Z. Cai, S. OReilly, X. Hao, and D. Zhao, "A review of oil, dispersed oil and sediment interactions in the aquatic environment: Influence on the fate, transport and remediation of oil spills," *Marine Pollution Bulletin*, vol. 79, no. 1-2, pp. 16–33, 2014.

[9] O. A. Poirier and G. A. Thiel, "Deposition of free oil by sediments settling in sea water," *AAPG Bulletin*, vol. 25, no. 12, pp. 2170–2180, 1941.

[10] the ASCE Task Committee on Modeling of Oil Spills of the Water Resources Engineering Division, "State-of-the-Art Review of Modeling Transport and Fate of Oil Spills," *Journal of Hydraulic Engineering*, vol. 122, no. 11, pp. 594–609, Nov. 1996.

[11] H. Niu, Z. Li, K. Lee, P. Kepkay, and J. V. Mullin, "Modelling the Transport of OilMineral-Aggregates (OMAs) in the Marine Environment and Assessment of Their Potential Risks," *Environmental Modeling & Assessment*, vol. 16, no. 1, pp. 61–75, 2010.

[12] U. C. Bandara, P. D. Yapa, and H. Xie, "Fate and transport of oil in sediment laden marine waters," *Journal of Hydro-environment Research*, vol. 5, no. 3, pp. 145–156, 2011.

[13] S. Pando, M. F. Juliano, R. García, P. A. de Jesus Mendes, and L. Thomsen, "Application of a lagrangian transport model to organo-mineral aggregates within the Nazaré canyon," *Biogeosciences*, vol. 10, no. 6, pp. 4103–4115, 2013.

[14] R. Mahajan, H. Rodriguez, M. Plis, J. Hamrick, and S. Davie, "Use of Sediment Transport Model to Support Remediation in River Oil Spills," in *World Environmental and Water Resources Congress 2013*, Reston, VA, 2013, pp. 1814–1826.

[15] A. Khelifa, M. Fingas, and C. Brown, "Effects of Dispersants on Oil-SPM Aggregation and Fate in US Coastal Waters," Tech. Rep., 2008.

[16] D. S. Etkin, "ANALYSIS OF OIL SPILL TRENDS IN THE UNITED STATES AND WORLDWIDE," in *International Oil Spill Conference Proceedings*, 2001, pp. 1291–1300.

[17] R. H. Dollhopf, F. A. Fitzpatrick, J. W. Kimble, D. M. Capone, T. P. Graan, R. B. Zelt, and R. Johnson, "Response to Heavy, Non-Floating Oil Spilled in a Great Lakes River Environment: A Multiple-Lines-Of-Evidence Approach for Submerged Oil Assessment and Recovery," in *International Oil Spill Conference Proceedings*, vol. 2014, no. 1, May 2014, pp. 434–448.

[18] W. A. Dew, A. Hontela, S. B. Rood, and G. G. Pyle, "Biological effects and toxicity of diluted bitumen and its constituents in freshwater systems," *Journal of Applied Toxicology*, no. April, 2015.

[19] J. Hamrick, "A Three-Dimensional Environmental Fluid Dynamics Computer Code: Theoretical and Computational Aspects," Virginia Institute of Marine Science, School of Marine Science, The College of William and Mary, Gloucester Point, VA 23062, Tech. Rep. 317 in Applied Marine Science and Ocean Engineering, 1992.

[20] G. L. Mellor and T. Yamada, "Development of a turbulence closure model for geophysical fluid problems," *Reviews of Geophysics*, vol. 20, no. 4, pp. 851–875, 1982.

[21] B. Galperin, L. Kantha, S. Hassid, and A. Rosati, "A quasi-equilibrium turbulent energy model for geophysical flows," *Journal of the Atmospheric Sciences*, vol. 45, pp. 55–62, 1988.

[22] J. Smagorinsky, "General circulation experiments with the primitive equations," *Monthly Weather Review*, vol. 91, no. 3, pp. 99–164, 1963.

[23] D. Muschenheim and K. Lee, "Removal of Oil from the Sea Surface through Particulate Interactions: Review and Prospectus," *Spill Science & Technology Bulletin*, vol. 8, no. 1, pp. 9–18, Feb. 2002.

[24] O. E. Omotoso, V. A. Munoz, and R. J. Mikula, "Mechanisms of Crude OilMineral Interactions," *Spill Science & Technology Bulletin*, vol. 8, no. 1, pp. 45–54, Feb. 2002.

[25] P. Stoffyn-Egli and K. Lee, "Formation and Characterization of OilMineral Aggregates," *Spill Science & Technology Bulletin*, vol. 8, no. 1, pp. 31–44, Feb. 2002.

[26] H. Zhang, M. Khatibi, Y. Zheng, K. Lee, Z. Li, and J. V. Mullin, "Investigation of OMA formation and the effect of minerals." *Marine pollution bulletin*, vol. 60, no. 9, pp. 1433–1441, Sep. 2010.

[27] M. C. Boufadel, K. Du, V. Kaku, and J. Weaver, "Lagrangian simulation of oil droplets transport due to regular waves," *Environmental Modelling & Software*, vol. 22, no. 7, pp. 978–986, July 2007.

[28] T. Garcia, P. R. Jackson, E. a. Murphy, A. J. Valocchi, and M. H. Garcia, "Development of a Fluvial Egg Drift Simulator to evaluate the transport and dispersion of Asian carp eggs in rivers," *Ecological Modelling*, vol. 263, pp. 211–222, 2013.

[29] F. A. Fitzpatrick, M. C. Boufadel, R. Johnson, K. W. Lee, T. P. Graan, A. C. Bejarano, Z. Zhu, D. Waterman, D. M. Capone, E. Hayter, S. K. Hamilton, T. Dekker, M. H. Garcia, and J. S. Hassan, "Oil-Particle Interactions and Submergence from Crude Oil Spills in Marine and Freshwater Environments Review of the Science and Future Science Needs," U.S. Geological Survey Open-File Report 20151076, Tech. Rep., 2015.

[30] F. A. Fitzpatrick, R. Johnson, Z. Zhu, D. Waterman, R. D. Mcculloch, E. J. Hayter, M. H. Garcia, T. Dekker, J. S. Hassan, D. T. Soong, C. J. Hoard, and K. Lee, "Integrated modeling approach for fate and transport of submerged oil an oil-particle aggregates in a freshwater

riverine environment," in *Proceedings for the 2015 Joint Federal Interagency Conference on Sedimentation and Hydrologic Modeling (SEDHYD 2015)*, 2015.

[31] D. Waterman and M. H. Garcia, "Laboratory Tests of Oil-Particle Interactions in a Freshwater Riverine Environment with Cold Lake Blend Weathered Bitumen," University of Illinois at Urbana-Champaign, Civil Engineering Studies, Hydraulic Engineering Series No 106, Tech. Rep., 2015.

[32] D. Waterman, D. Fytanidis, and M. H. Garcia, "Kalamazoo River In Situ Flume Bed Erosion Study," University of Illinois at Urbana-Champaign, Civil Engineering Studies, Hydraulic Engineering Series No 105, Tech. Rep., 2015.

[33] R. T. Cheng, C.-h. Ling, J. W. Gartner, and P. F. Wang, "Estimates of bottom roughness length and bottom shear stress in South San Francisco Bay, California," *Journal of Geophysical Research*, vol. 104, no. C4, p. 7715, 1999.

[34] R. N. Szupiany, M. L. Amsler, J. Hernandez, D. R. Parsons, J. L. Best, E. Fornari, and A. Trento, "Flow fields, bed shear stresses, and suspended bed sediment dynamics in bifurcations of a large river," *Water Resources Research*, vol. 48, no. 11, Nov. 2012.

[35] X. Liu, B. Landry, and M. García, "Two-dimensional scour simulations based on coupled model of shallow water equations and sediment transport on unstructured meshes," *Coastal Engineering*, vol. 55, no. 10, pp. 800–810, Oct. 2008.

[36] Z. Zhu, "Simulation of suspended sediment and contaminant transport in shallow water using two-dimensional depth-averaged model with unstructured meshes," M.S. thesis, University of Illinois at Urbana-Champaign, 2011.

[37] Z. Zhu, V. Morales, T. Sinha, and M. H. Garcia, "Numerical modeling study on the potential impacts of hydraulic structures in the Guayas watershed, Ecuador," in *The 7th IAHR Symposium on River, Coastal and Estuarine Morphodynamics (RCEM)*, 2011.

[38] X. Liu, G. Parker, J. a. Czuba, K. Oberg, J. M. Mier, J. L. Best, D. R. Parsons, P. Ashmore, B. G. Krishnappan, and M. H. Garcia, "Sediment mobility and bed armoring in the St Clair River: insights from hydrodynamic modeling," *Earth Surface Processes and Landforms*, vol. 37, no. 9, pp. 957–970, jul 2012.

[39] A. E. Goodwell, Z. Zhu, D. Dutta, J. a. Greenberg, P. Kumar, M. H. Garcia, B. L. Rhoads, R. R. Holmes, G. Parker, D. P. Berretta, and R. B. Jacobson, "Assessment of Floodplain Vulnerability during Extreme Mississippi River Flood 2011," *Environmental Science & Technology*, vol. 48, no. 5, pp. 2619–2625, Mar. 2014.

[40] A. Grass, "Sediment transport by waves and currents," SERC London Center for Marine Technology, Tech. Rep. FL29, 1981.

[41] E. Meyer-Peter and R. Muller, "Formulas for bedload transport," in *Proceedings of* 2^{nd} *Congress, International Association for Hydraulic Research*, Stockholm, 1948, pp. 39–64.

[42] G. Parker, M. H. García, Y. Fukushima, and W. Yu, "Experiments on turbidity currents over an erodible bed," *Journal of Hydraulic Research*, vol. 25, pp. 123–147, 1987.

[43] M. García and G. Parker, "Entrainment of bed sediment into suspension," *Journal of Hydraulic Engineering*, vol. 117, no. 4, pp. 414–435, 1991.

[44] M. H. García and G. Parker, "Experiments on the entrainment of sediment into suspension by a dense bottom current," *Journal of Geophysical Research (oceans)*, vol. 98, pp. 4793–4807, 1993.

[45] L. Tech, "Kalamazoo River Hydrodynamic and Sediment Transport Model Documentation," Tech. Rep., 2014.

[46] L. Enbridge Energy, "Sediment dredge depth and area determination addendum to the 2013 submerged oil removal and assessment work plan," Tech. Rep., 2013.

[47] W. Wu, W. Rodi, and T. Wenka, "3D Numerical Modeling of Flow and Sediment Transport in Open Channels," *Journal of Hydraulic Engineering*, vol. 126, no. 1, pp. 4–15, Jan. 2000.

[48] N. R. B. Olsen, "Three-Dimensional CFD Modeling of Self-Forming Meandering Channel," *Journal of Hydraulic Engineering*, vol. 129, no. 5, pp. 366–372, May 2003.

[49] X. Liu and M. H. Garcia, "Three-Dimensional Numerical Model with Free Water Surface and Mesh Deformation for Local Sediment Scour," *Journal of Waterway, Port, Coastal, and Ocean Engineering*, vol. 134, no. 4, pp. 203–217, 2008.

[50] D. Jia, X. Shao, H. Wang, and G. Zhou, "Three-dimensional modeling of bank erosion and morphological changes in the Shishou bend of the middle Yangtze River," *Advances in Water Resources*, vol. 33, no. 3, pp. 348–360, Mar. 2010.

[51] W. Wu, "Depth-Averaged Two-Dimensional Numerical Modeling of Unsteady Flow and Nonuniform Sediment Transport in Open Channels," *Journal of Hydraulic Engineering*, vol. 130, no. 10, pp. 1013–1024, Oct. 2004.

[52] J. D. Abad, G. C. Buscaglia, and M. H. Garcia, "2D stream hydrodynamic, sediment transport and bed morphology model for engineering applications," *Hydrological Processes*, vol. 22, no. 10, pp. 1443–1459, May 2008.

[53] M. Castro Díaz, E. Fernández-Nieto, A. Ferreiro, and C. Parés, "Two-dimensional sediment transport models in shallow water equations. A second order finite volume approach on unstructured meshes," *Computer Methods in Applied Mechanics and Engineering*, vol. 198, no. 33-36, pp. 2520–2538, July 2009.

[54] A. Canestrelli, M. Dumbser, A. Siviglia, and E. F. Toro, "Well-balanced high-order centered schemes on unstructured meshes for shallow water equations with fixed and mobile bed," *Advances in Water Resources*, vol. 33, no. 3, pp. 291–303, Mar. 2010.

[55] D. Yu, "Parallelization of a two-dimensional flood inundation model based on domain decomposition," *Environmental Modelling & Software*, vol. 25, no. 8, pp. 935–945, Aug. 2010.

[56] B. F. Sanders, J. E. Schubert, and R. L. Detwiler, "ParBreZo: A parallel, unstructured grid, Godunov-type, shallow-water code for high-resolution flood inundation modeling at the regional scale," *Advances in Water Resources*, vol. 33, no. 12, pp. 1456–1467, Dec. 2010.

[57] J.-M. Hervouet, "A high resolution 2-D dam-break model using parallelization," *Hydrological Processes*, vol. 14, no. 13, pp. 2211–2230, Sep. 2000.

[58] A. K. Rastogi and W. Rodi, "Predictions of heat and mass transfer in open channels," *Journal of the Hydraulics Division*, vol. 104, no. 3, pp. 397–420, 1978.

[59] J. J. Mcguirk and W. Rodi, "A depth-averaged mathematical model for the near field of side discharges into open-channel flow," *Journal of Fluid Mechanics*, vol. 86, no. 04, pp. 761–781, 1978.

[60] M. H. García, Ed., *Sedimentation Engineering Processes, Measurements, Modeling and Practice*. Reston, Va: Am. Soc. Civ. Eng., 2008.

[61] H. G. Weller, G. Tabor, H. Jasak, and C. Fureby, "A tensorial approach to computational continuum mechanics using object-oriented techniques," *Computers in Physics*, vol. 12, no. 6, pp. 620–631, 1998.

[62] X. Liu and M. García, "Computational fluid dynamics modeling for the design of large primary settling tanks," *Journal of Hydraulic Engineering*, vol. 137, no. 3, pp. 343–355, 2010.

[63] C. Biscarini, S. Di Francesco, and P. Manciola, "CFD modelling approach for dam break flow studies," *Hydrology and Earth System Sciences*, vol. 14, no. 4, pp. 705–718, Apr. 2010.

[64] N. D. Badano, M. S. Gerbec, M. Re, and A. N. Menéndez, "A coupled hydro-sedimentologic model to assess the advance of the Parana River Delta Front," in *River Flow*, 2012, pp. 557–564.

[65] R. I. Issa, "Solution of the implicitly discretised fluid flow equations by operator-splitting," *Journal of Computational Physics*, vol. 62, no. 1, pp. 40–65, Jan. 1986.

[66] "OpenFOAM User Guide: 4.4 Numerical schemes," http://cfd.direct/openfoam/user-guide/fvschemes/, Accessed: 2015-08-26.

[67] J. D. Abad and M. H. Garcia, "Experiments in a high-amplitude kinoshita meandering channel: 1. implications of bend orientation on mean and turbulent flow structure," *Water Resources Research*, vol. 45, no. 2, 2009, w02401.

[68] J. Hudson, "Numerical Techniques for Morphodynamic Modelling," Ph.D. dissertation, University of Reading, 2001.

[69] L. Sørensen, A. G. Melbye, and A. M. Booth, "Oil droplet interaction with suspended sediment in the seawater column: influence of physical parameters and chemical dispersants." *Marine pollution bulletin*, vol. 78, no. 1-2, pp. 146–152, Jan. 2014.